Mechanism of Clinical Complication of Metal-on-Metal Total Hip Replacement: Nanoparticle Characterisation, Nanotoxicity, and Biological Metal Corrosion

Liu, Zhao

Mechanism of Clinical Complication of Metal-on-Metal Total Hip Replacement: Nanoparticle Characterisation, Nanotoxicity, and Biological Metal Corrosion

A Dissertation Submitted to The Swansea University in Fulfilment of the Requirements for the Degree of Doctor of Philosophy

Swansea University

Prifysgol Abertawe
Swansea University

Zhao Liu
600854

Supervisors: Dr. Zhidao Xia,
Prof. Marc Clement

31/12/2018

Abstract

Metal-on-Metal total hip arthroplasty (MoM THA) has undergone a recent resurgence as an important treatment for patients with end stage osteoarthritis. Despite the satisfactory short-term survivorship of the implant, revision surgeries caused by metal wear particles involved clinical complications are increasingly reported. Metal wear particles produced from failed implants have caused significant adverse local tissue reactions (ALTR) such as abnormal periprosthetic soft-tissue (pseudotumours). There are limited understandings of the potential mechanisms involved. The broad aim of this thesis was therefore to characterise metal wear nanoparticles recovered from tissue during revision, and to create in vitro modules to study the mechanism of nanotoxicity of the of metal wear nanoparticles and cell mediated corrosion.

Metal wear products retrieved from three common types of hip replacements, including metal-on-metal resurfacing (MoM HRA), metal-on-metal large head total hip arthroplasty (MoM LHTHA) and non-metal-on-metal hip dual modular neck total hip arthroplasty (Non-MoM DMNTHA) were characterised. The shape, size and number of metal wear nanoparticles were quantified by Transmission electron microscopy (TEM) and 'ImageJ' analysis. The element composition of the retrieved tissue samples was detected through energy dispersive x-ray spectrometry (EDS). The results showed that the physical properties such as size, shape and number of metal wear nanoparticles were dependent on the type of hip replacement. The element composition of metal wear products retrieved were different due to different configuration of prostheses.

Subsequent research focused on the cytotoxicity with Neutral Red assay and mechanism of different metallic nanoparticles interaction with THP-1 macrophages. The in vitro experiment demonstrated that metal nanoparticles induced cytotoxicity and cell death. Moreover, siRNA knock out study proved that HIF1α is likely to involve in cobalt nanoparticles (CoNPs) induced cellular cytotoxicity.

The metal corrosion by macrophages was also studied by scanning electron microscopy (SEM) and white-light interferometry (WLI). In addition, macrophages involved extra cellular metal corrosion was detected with an in-house developed biosensor. The results showed that THP-1 macrophages were likely to corrode metal surface directly and produce electrochemical reaction at the cell-metal interface.

In conclusion, clinical complication of MoM THA is closely related to metal wear nanoparticles; the clinically relevant metal nanoparticles are toxic to cells in vitro; metal corrosion by macrophages may release metal ions to contribute to the toxicity and ALTR.

This study has created in vitro models to investigate the mechanism of clinical complication of MoM THA. Further work is required to reveal the molecular pathways and electrochemical reaction at the interface between cells and metal implants, which will benefit the improvement of total hip replacement technology.

Key words: metal-on-metal total hip arthroplasty (MoM THA), THP-1 macrophages, cytotoxicity, metal wear nanoparticles, metal corrosion

DECLARATION

This work has not previously been accepted in substance for any degree and is not being concurrently submitted in candidature for any degree.

Signed ..... (candidate)

Date .....

STATEMENT 1

This thesis is the result of my own investigations, except where otherwise stated. Where correction services have been used, the extent and nature of the correction is clearly marked in a footnote(s).

Other sources are acknowledged by footnotes giving explicit references. A bibliography is appended.

Signed ..... (candidate)

Date .....

STATEMENT 2

I hereby give consent for my thesis, if accepted, to be available for photocopying and for inter-library loan, and for the title and summary to be made available to outside organisations.

Signed ..... (candidate)

Date .....

Table of Contents

Acknowledgement

I would like to express special appreciation to my supervisor Dr Zhidao Xia and Prof Marc Clement who have provided guidance, encouragement and support through my PhD study. I would like to thank Dr John Evans and Dr Alex Lord for their knowledge and training of SEM and EDS; Dr Christopher Von Ruhland for his knowledge and training on tissue sample processing and TEM observation; Dr Wendy Francis for her knowledge of molecular biology and the supervision with patience in my HIF-1α experiments; Gareth Blayney, Dominic Fung and Dr Andy Wain for their supports in the design of biosensor; Mr. Mark Roberts for the contributions of training and supporting for tissue culture; and Dr. Yadan Zhang for the support and advices at the laboratory. Special thanks go to Prof James Sullivan and Yin Cheung Lau's group for their valuable comments and supports in my biocorrosion experiments.

I owe many thanks to everyone in Scientia group, in particular Jenny Child and all the colleagues who have been a great support to me. Thanks to my fellow PhD students especially Mr. Yunsong Shi and Miss Raha Rahbari who are great companions during my PhD study.

Finally, I would like to thank my mother for all her supports and encouragements during my research. I would also give special thanks to all my friends who supported me during my PhD life.

List of Figures

List of Tables

Abbreviation

ADAM	Animated Dissection of Anatomy for Medicine
ALTR	Advers local tissue reaction
ARMD	Adverse reactions to metal debris
BSE	Back-scatter electron detector
BAC	Bicinchoninic acid kit
BHR	Birmingham hip resurfacing
CoNPs	Cobalt nanoparticles
Cr	Chromium
EDS	Energy dispersive spectroscopy
EDX	Energy dispersive X-ray Spectroscopy
FBS	Foetal bovine serum
FDA	Food and Drug Administration
HIF-1α	Hypoxia inducible factorα
HMWP	High molecular weight polyethylene
Image J	Image Processing and Analysis in Java
MoM	Metal-on-metal
MoM RES	Metal-on-metal resurfacing system
MoM HRA	Metal-on-metal hip resurfacing arthroplasty
MoM LHTHA	Metal-on-metal large head total hip arthroplasty
Non-MoM DMNTHA	Non-metal-on-metal hip dual modular neck total hip arthroplasty
OA	Osteoarthritis
OC	Osteoclast
PBS	Phosphate buffered saline
PMA	Phorbol-12-myristate-13-acetate
P/S	Penicillin/ streptomycin
RPMI	Roswell park memorial institute medium
RFU	Relative fluorescence units
ROS	Reactive oxygen species
SEM	Scanning electron microscopy
TEM	Transmission electron microscopy

THA	Total hip arthroplasty
THR	Total hip relacement
WLI	White-light interferometry

Chapter 1 Introduction

1.1.Overview

Osteoarthritis (OA) is the most common type of arthritis affecting more than 190 million people in the world (Mendez et al., 2003; Tortorella & Malfait, 2003). In 2012, it was found that more than 10% of adults had this kind of disease in America (nearly 27 million) (Murphy & Helmick, 2012). The number of people who have been diagnosed with osteoarthritis in Australia and the UK is 1.9 million (Felson, Lawrence, Dieppe, et al., 2000) and 8.75 million (UK, 2013) respectively. The major symptoms of osteoarthritis include pain, stiffness, swelling and producing cracking or clicking noises in the joint, which will increase with exercise and age (Kim et al., 2011).

Total Hip Arthroplasty (THA) is one of commonly used treatments for late stages of osteoarthritis (J., B., & W., 2004; Learmonth, Young, & Rorabeck, 2007). Two metal-on-metal (MoM) types which are metal-on-metal hip resurfacing arthroplasty (MoM HRA) and metal-on-metal large head total hip arthroplasty (MoM LHTHA), and one non-metal-on-metal hip dual modular neck total hip arthroplasty (non-MoM DMNTHA) are most commonly used hip replacements.

MoM HRA account for the highest proportion among the three widely used designs, as resurfacing has the advantage of cost-effectiveness, greater implant stability, bone conservation, high clinically successful surgical rate and assumed easier revision surgery (H. C. B. et al., 2007; Shimmin, Beaulé, & Campbell, 2008). In 2008, the National Joint Registry for England and Wales Annual Report showed that in 2008, the National Joint Registry for England and Wales Annual Report showed that hip resurfacing procedures made up 46% (1585 of 3471) of all the primary hip arthroplasty procedures undertaken in patients under 55 years old (Smith, Dieppe, Vernon, Porter, & Blom, 2012). In Australian patients of the same age, 29% of the primary hip arthroplasty operations carried out were hip resurfacing procedures (Buergi & Walter, 2007). In 2006 the Food and Drug Administration (FDA) in the United States estimated an annual increase in hip resurfacing procedures approaching 100% (Karas, 2012).

However, it has been reported that metal on metal hip resurfacing arthroplasty implants release a large amount of tiny metallic debris (around 50nm) and metal ions (Zhidao Xia et al., 2011), which can lead to adverse local tissue reactions (ALTR) or adverse reaction to metallic debris (ARMD) in the patient's body (Perino et al., 2014). The number of nanometer-sized particles that are generated from MoM bearing surfaces is 500 times more than the particles generated from conventional metal-on-Polyethylene (MoP) bearings, although the bearing rates of MoM bearings is considered as lower than conventional MoP bearing systems (C. Delaunay, Petit, Learmonth, Oger, & Vendittoli, 2010).

More and more researches have already focused on the risks of the metal nanoparticles produced from MoM hip resurfacing procedures as this arthroplasty has been increasingly used in the patients which are young and active (P. T. C. B., P., J., & C., 2006). The adverse biological reactions caused by these metal nanoparticles include two parts, systemic and local. The common systemic adverse biological responses, such as risks of hypersensitivity reactions and cancer, have been reported in previous researches (Brewster et al., 2013; Teo & Schalock, 2016).

As for the local adverse reactions, pseudotumour is one of the most common ALTRs, which has increasingly been reported in recent researches (Ayers, 2018; Hjorth et al., 2018). This local adverse reaction draws a lot of attention in the orthopedic surgical area including large numbers of orthopedic centres in both the United Kingdom (Laughton et al., 2009) and the United States (Board, Mohan, Gambhir, & Porter, 2009). Pseudotumour, also called inflammatory mass (Glyn-Jones et al., 2009), cyst (Vogel et al., 2005) or bursa (Campbell, Shimmin, Walter, & Solomon, 2008), is a symptomatic soft-tissue mass occurring around the hip joint (Tamaki et al., 2017). The proportion of patients requiring revision surgery caused by the local damaging of these pseudotumours is around 70% (Matthies, Skinner, Osmani, Henckel, & Hart, 2012). According to previous researches, metallic debris was identified in extensive necrotised macrophages which have been regarded as the reason for pseudotumours occurring (Pandit et al., 2008; Zhidao Xia et al., 2011).

As there are increasing reports of ALTR, it has become one of the most serious problems which affect the development of metal-on-metal hip resurfacing arthroplasty and the health of patients. It is necessary for more and more related research centres to investigate the mechanisms of these metallic wear and corrosive particle-induced ALTRs. However, published researches to provide the related studies are limited. The existing studies of the characteristic of the nanoparticles produced, such as their physical properties and chemical composition in patients with MoM HRA are important but currently largely unknown. In addition, it is necessary to understand the biological reaction between metal nanoparticles and human tissue in order to find out how these particles interact with human tissue to cause clinical complications such as pseudotumours; to date, the reason has still not been completely understood.

It is believed that these metal corrosion products are produced by the wear and corrosion occurred in the bearing surface of hip replacements, but the mechanisms of wear and corrosion are yet to be fully recognised. A better and comprehensive understanding of the metal nanoparticles produced and the mechanism for implant failure is urgently required as it will be of benefit in many related aspects such as the improvement of the design for future hip replacements and surgical techniques which can improve the quality of the patient's life.

1.2. Specific objective

The specific objectives of this study were:

- to characterise the physical properties and chemical compositions of these metal nanoparticles from retrieved implants of total hip-replacement;
- to investigate the cytotoxicity and potential mechanisms of metal nanoparticles on macrophages
- to explore the electrochemical process of THP-1 macrophage mediated metal corrosion.

1.3. Structure of this thesis

The structure of this thesis is shown below:

- Chapter1 gives an introduction and an overview of the structure of the thesis.

- Chapter2 presents the literature review of the introduction of commonly used hip replacements, including the developments, structures and current clinical complications. In addition, literature about the cell-mediated metal corrosion is also discussed in this chapter.

- Chapter3 describes the nano-analytic characterisation of nanoparticles retrieved from MoM total hip-replacement. This chapter reports the physicochemical properties of the nanoparticles produced from different types of hip replacement after implanting.

- Chapter4 reports metal nanoparticle-induced cytotoxicity. This chapter investigates the toxic reactions between human THP-1 macrophages and nanoparticles.

- Chapter5 reports the potential role of hypoxia inducible factor 1 α in cobalt nanoparticle induced cytotoxicity of human THP-1 macrophages.

- Chapter 6 presents a macrophage mediated metal corrosion experiment. This experiment initiated a new method to investigate the bio-metal corrosion between cells and the metal surface.

- Chapter 7 is the conclusion of the thesis and discussion of limitations of the study. In addition, future work in this research area is proposed.

Chapter 2 Literature Review

2.1. Hip osteoarthritis

Osteoarthritis is one of the most common joint diseases with large numbers of patients (nearly 3.8%) in the world (Fig. 2.1) (Mendez et al., 2003). It has been defined as the degenerative illness within a joint. Continual wear and tear of the underlying bone and cartilage will give a high chance of getting this disease. (Tibor & Ganz, 2015)

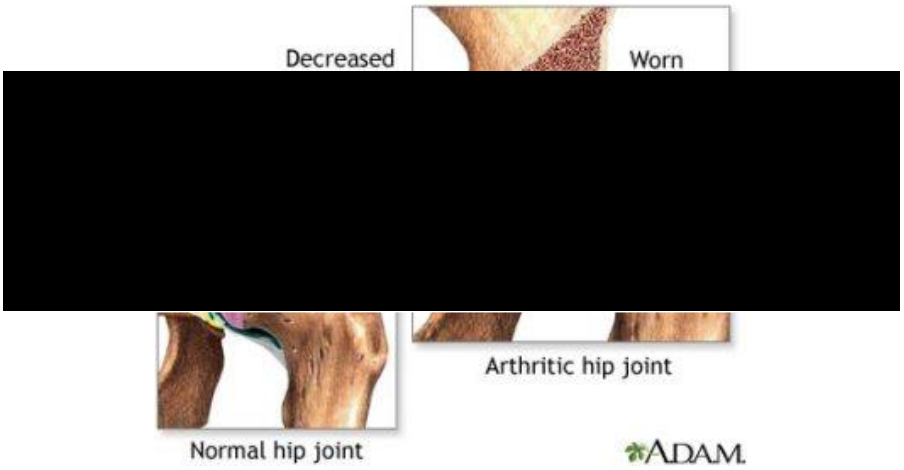

Figure 2.1. Comparison of Arthritic Hip Joint and Normal Hip Joint
Figure obtained from Animated Dissection of Anatomy for Medicine (ADAM), http://www.joint-pain-solutions.com/hip-osteoarthritis.html

Patients who get osteoarthritis will show a variety of symptoms, which will seriously affect their daily lives. A sharp aching pain inside the joint is one of the most typical symptoms. What is even worse is that doing exercise will not improve the symptom, in fact it will make it worse. Another typical symptom which affects people's daily movement is stiffness of the joint, which is often found in the morning. Moreover, symptoms such as the production of clicking or cracking noises, and swelling in the joint also affect general movement and the quality of the patients' lives. (Kim et al., 2011).

There are a variety of causes which may lead to osteoarthritis. One of the most important reasons is being overweight. The joints of overweight people will take much more mechanical stress which means more continual wear and tear will occur in the underlying bone and cartilage, as mentioned before (Felson, Zhang, Anthony, Naimark, & Anderson, 1992). Another main factor which may cause osteoarthritis is age, as the intensities of muscles and the recovery abilities of injured tissues become weaker with increased age. This increases the chance of causing weaker shock absorption capabilities and other instability between joints. Therefore older people are more likely to suffer with osteoarthritis (Nüesch et al., 2011). In addition, men and women have different probabilities of being affected by osteoarthritis. It is reported that women have more chance of getting osteoarthritis than men, in people over 55 years old (Paradowski, Bergman, Sundén-Lundius, Lohmander, & Roos, 2006). In addition, people who have had injuries to their joints earlier in their lives are more likely to have osteoarthritis as the age (Nüesch et al., 2011).

2.2. The treatment of hip osteoarthritis

Treatments for the early stages of osteoarthritis aim at reducing symptoms such as pain and stiffness caused by this disease. These initial treatments include applying drugs and physical therapies. Drugs such as pain relief creams or tablets and non-steroidal anti-inflammatory drugs (NSAIDs) can reduce symptoms associated with early stages of osteoarthritis after long-term use. Physical therapies such as joint splinting and suitable physical exercises are applied as supporting therapies for this disease. If the osteoarthritis related symptoms still haven't been improved after the initial treatments, further therapy such as steroid injection is recommended to lessen pain or other symptoms. For the late stage of osteoarthritis, patients with significant joint damage and severe pain no longer have good responses to the initial treatment or further treatments. Thus, surgical treatments such as total joint arthroplasty or hemi-arthroplasty are highly recommended to be carried out. (Felson, Lawrence, Hochberg, et al., 2000)

2.3. Total hip arthroplasty

Total hip arthroplasty, also called total hip replacement, is a widely used surgical treatment for late stage osteoarthritis. Prosthetic implants will replace both the femoral head and acetabulum of the patient during this treatment, as Fig 2.2. A metal stem can either be cemented or fitted through pressure into the channel in the femur's centre. The damaged femoral head is replaced with a metal or ceramic ball which is located on the top of the metal stem. The damaged cartilage surface of the socket is replaced by a metal or polyethylene acetabular component (socket). In order to provide a smooth gliding surface between the new femoral head and socket, a liner (spacer) made with metal, ceramic or plastic is placed on the surface to improve the environment for movement. (Mallory, 2003)

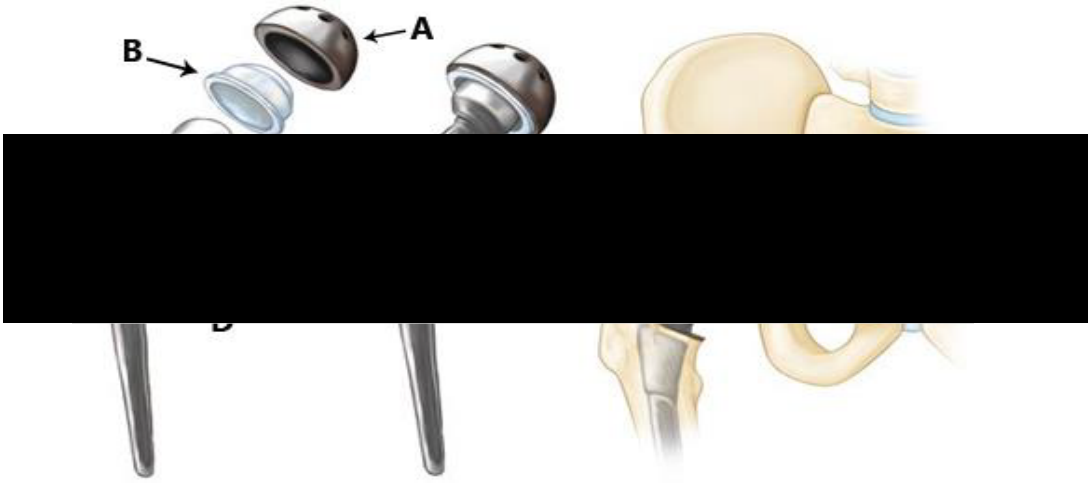

Figure 2.2 The structure of a common type of total hip arthroplasty

A. Acetabular component (socket), B. Liner (spacer), C. Femoral head, D. Metal femoral stem
Figure obtained from https://www.drltomar.com/hip-replacement-surgery-in-delhi/

At present, total hip arthroplasty is still the most cost-effective treatment for disability caused by rheumatism or arthritis, with a high clinical success rate. Reports showed that, in 2011, the rate of hip replacement surgeries in Organisation for Economic Co-operation and Development (OECD) countries is 3/1000. Moreover, this rate in Switzerland, Austria, Germany and the United States had already exceeded 200/100,000 inhabitants (Pabinger & Geissler, 2014). The most hip replacement

surgeries were performed in the United States. The number of the procedures performed annually as of 2003 was 202,500, and this number is expected to reach 572,000 per year in 2030 (Liao et al., 2011). According to the records of the National Joint Registry of England and Wales, 76,759 hip replacement surgeries (68,907 primary procedures and 7,852 revision surgeries) were performed in 2010, The rate has increased by 6% when comparing with the number of replacement procedures in 2009 (11).

2.4. Development of hip replacement

Arthritides have defied the effectiveness of many interventions for several thousand years (MacLennan, 1999). Joint pathologies have been evidenced in Homo sapiens from Saxon (Rogers, Watt, & Dieppe, 1981), medieval (Rogers et al., 1981) and Roman (Thould & Thould, 1983) excavations. And also, the pathological marks of articular disease have been detected in the bones of Homo sapiens neanderthalensis (Trinkaus, 1985).

2.4.1. Early hip arthritis surgery in the 1800s

During the first half of the eighteenth century, identifying the physiology of the skeletal tissues made significant progress, which led to orthopaedics making a great deal of progress toward the end of that century (P. F. Gomez & J. A. Morcuende, 2005).

Excision of the joints was undertaken widely as a treatment for joint disease in Europe and America. In the United Kingdom, Liverpool was noted for its skilled surgeons as it was a large commercial port. These types of injuries required radical treatment which, in the late 1700s, meant amputation (Park, 1733). Because of the outbreak of warfare in parts of Europe, amputation was much used by military surgeons as the speed of a procedure was most valued during the pre-anaesthesia era (Leonardo, 1943).

The first credited excision arthroplasty was carried out by Anthony White (1782-1849) in 1821, London. The patient survived for twelve years after the surgery and finally died because of consumption. However, White did not make a personal report of the operation. This procedure preserved mobility and reduced pain but did not provide stability. (P. F. Gomez & J. A. Morcuende, 2005).

In 1826, the earliest recorded osteotomy on an ankylosed hip was performed by John Rhea Barton (1794-1871) in Philadelphia. The intertrochanteric osteotomy was performed without anaesthesia and the whole procedure only lasted seven minutes. Twenty days after the operation, a fibrous reaction was provoked at the ends of the severed bone through manipulating the joint. This surgery was reported in the Surgical and North American Medical Journal. (Barton, 1827) The patient had lost all the motion six years later. After that, bony ankylosis was treated with this popularised hip osteotomy as a rational plan. However, the outcome was generally unpredictable; most of the joints eventually became ankylosed after the operations. What is worse, the mortality rate of this surgery was approximately 50 percent. (Stanley, 2003)

In 1860, soft tissue hip interpositions had been performed by Auguste Stanislas Verneuil (1823–95), from Paris. (Pablo F Gomez & Jose A Morcuende, 2005). After that, surgeons used a variety of interpositional materials to test the result of this surgery, but none of them were successful. Among the wide variety of materials, they used were silver plates, muscle, rubber struts, celluloid, zinc, decalcified bones, glass, wax and celluloid. Some materials, such as magnesium, even consolidated the bone osteotomies or fractures, so they formed exactly the opposite of what they were supposed to do (P. F. Gomez & J. A. Morcuende, 2005).

2.4.2. The interpositional hip arthroplasty in the 1900s

The first credited attempts at hip implant fixation were carried out in Germany by Berliner Professor Themistocles Glück (1853-1942). In 1891, Glück designed an ivory ball and socket joint which could be fixed to bone with nickel-plated screws. The idea of using ivory to replace the femoral head introduced a new way of developing hip implant fixation (Rang, 1966). Among some of the famous approaches were hip cheilotomy ("The surgical clinics of john b. murphy, m.d., at mercy hospital, chicago," 1912), pig bladder interpositional hip arthroplasty and gold foil interpositional hip arthroplasty, which had the longest follow-up report recorded in the history of arthroplasty. This surgery was carried out by Sir Robert Jones (1855-1933) in 1918, and the patient still retained effective motion at the joint twenty-one years later (P. F. Gomez & J. A. Morcuende, 2005).

2.4.3. The prosthetic hip arthroplasty in the 1900s

The first total hip arthroplasty (THA) was recorded by Philip Wiles (1899-1966) of the Middlesex Hospital In 1938. He mentioned that precisely fitted stainless steel components were used and were fixed to the bone with bolts and screws during the surgery. Unfortunately, he did not achieve results which were sufficiently satisfactory (Wiles, 1958).

The first widely distributed hip arthroplasty product was designed by Frederick Röeck Thompson (1907-1983) in 1950. He developed a Vitallium prosthesis which contains a distinctive flared collar below the head and a vertical intramedullary stem. (Thompson, 1952). Böhlman and Moore refined the implant and described a model that featured ‘a fenestrated stem to allow bone ingrowth’ (Moore & Bohlman, 2006) in 1952. These designs were eventually widely-accepted and are still often used today for replacing the femoral head and neck, particularly for hip fractures in the elderly. After this, THA was on the rise and more remarkable prostheses, with surprisingly good results, were produced based on these designs (McKee & Watson-Farrar, 1966). One of the most famous designs was produced by Peter Ring (b. 1922) in Redhill, Surrey. In 1964, he experimented with cementless components with a metal-on-metal (MoM) articulation developed according to his clinical experience and achieved very successful results. Up to 97% patients survived at follow-ups 17 years later (Ring, 1971).

In the 1970s Sir John Charnley, working in the field of tribology, introduced a new model that had almost replaced the other designs by the 1970s. This was the High Molecular Weight Polyethylene (HMWP) model, which featured a titanium hip prosthesis with a ceramic head and a polyethylene acetabular cup (Waugh, 1990). Nevertheless, the metal on metal implants were "rediscovered" by Swiss and British surgeons in the1980s as they continued working extremely well. some reports even showed that the wear of appropriately metal-on-metal implants is much lower than that of metal on polyethylene (Eswaramoorthy, Moonot, Kalairajah, Biant, & Field, 2008).

In 1988, the Metasul bearing couple was developed and widely used in clinical

treatment. This was the beginning of a new generation of metal-on-metal articulation for THA. The Metasul module was described as using wrought high-carbon (>0.2%) CoCr alloys which are much smoother than traditional cast alloys. The first generation of this module was designed with a liner rim edge and a head sleeve, but both of them were removed for the second design in 1995 (C Delaunay, 2006). The Metasul design was proved, with low wear rates, improved joint stability and an increased range of motion in many clinical reports at that time (Anissian, Stark, Gustafson, Good, & Clarke, 1999; C. P. Delaunay, 2004).

In 1997, British orthopaedic surgeon McMinn introduced the Birmingham hip resurfacing (BHR) system using CoCr-molybdenum alloy with 5% carbide content (Reito, Puolakka, & Pajamäki, 2011). Only a few centimetres of bone around the femoral head were removed during the procedure, which means that this method was expected to minimise the damages to the bone during the surgery and maximise the patients' movements after the impaling surgery (Narvani, Tsiridis, Nwaboku, & Bajekal, 2006). It is reported that the BHR system is one of the best treatments for men under 55 years with osteoarthritis as it has excellent performance when compared with other types of metal-on-metal hip resurfacing implants. (the most commonly used device with the longest follow-up and the lowest revision rate) (Corten & MacDonald, 2010). Moreover, the application of BHR system has been approved by the United States Food and Drug Administration (FDA) in 2006 and still been used at present (Della Valle, Nunley, Raterman, & Barrack, 2009; Ford et al., 2018).

2.5. Current popular hip replacements

Nowadays, different materials are used in the design of hip replacements, some popular designs include the metal-on-metal (MoM) bearing system, ceramic-on-metal (CoM), metal-on-polyethylene (MoP), metal on cross linked polyethylene (MoXP), ceramic-on-ceramic (CoC) and ceramic-on-polyethylene (CoP) (Gioe; Perino et al., 2014). For the designs of the structures of hip replacements, there are three types are most commonly used: metal-on-metal hip resurfacing arthroplasty (MoM HRA), metal-on-metal large head total hip arthroplasty (MoM LHTHA) and non-metal-on-metal hip dual modular neck total hip arthroplasty (non-MoM DMNTHA). The MoM resurfacing system (MoM RES) is the most attractive and popular design among these

designs, being expected to exhibit better stability and wear characteristics in order to improve the restoration of anatomic hip mechanics and minimise debris-associated failures (Guillaume Mabilleau, Kwon, Pandit, Murray, & Sabokbar, 2008).

2.5.1. Metal-on-metal hip resurfacing arthroplasty (MoM HRA)

MoM HRA has been developed as a surgical alternative to THR as its potential advantages when compared with traditional total hip replacements (THR) such as less bone removal, easier revision surgery and reduced chance of hip dislocation (Mont, Ragland, Etienne, Seyler, & Schmalzried, 2006). Despite the potential risks such as femoral neck fractures, aseptic loosening and metal wear, MoM HRA has been reported as the best choice for young men with osteoarthritis as it showed the best performance of all kinds of hip replacements (van Dijk, Groothuis-Oudshoorn, Marshall, & IJzerman, 2016). Furthermore, many athletes with resurfaced hips have achieved excellent performances at the professional level competitions. Kay Glenn received gold medal in high jump at the National Senior Olympics in 2007 (Middleton, 2013); Ron Noreman won the Masters Division of Bodybuilding Championships in 2010 ("Beyond The Spotlight with Ron Noreman," 2015). It is reported that this method accounted for 46% of all primary hip arthroplasty surgeries for patients with osteoarthritis under 55years in the United Kingdom and one-third of 250,000 primary hip arthroplasty surgeries in the United States each year (Zhidao Xia et al., 2011).

However, the MoM HRA system has not been recommended for patients who have osteoporosis or poor bone stock as the occurrence of cysts were observed close to the femoral head neck junction during revision surgery of patients with severe bone loss in their femoral head (Mont et al., 2006). Furthermore, women of child-bearing age are been reported unsuitable for the MoM HRA system due to related unknown effects on the foetus caused by the released metal ions (Halawi, Brigati, Messner, & Brooks, 2017).

2.5.2. Metal-on-metal large head total hip arthroplasty (MoM LHTHA)

Large metal-on-metal (> 36-mm) femoral head arthroplasties (MoM LHTHA) is another frequently used device. It is reported by the National Joint Registry for England, Wales and Northern Ireland (NJR) that 31,335 MoM LHTHA surgeries have been applied from 2003 to 2014, accounting for nearly 15% of all total hip arthroplasty

surgeries. (Lehil & Bozic, 2014). The application of MoM LHTHA is increased in part as the expected advantages such as enhanced joint stability and admirable wear characteristics in vitro (Mertl et al., 2010).

Whereas, the high revision rate and high incidence of pseudotumors are increasingly been reported in recent year. A research reviewed the results of 1235 patients and reported that the revision rate of MoM LHTHA was 87% after 12 years follow-up. The common reasons for revision surgeries include adverse reactions to metal debris (ARMD), which account for 48% of revision surgeries, and loosening or failure of ingrowth (31% of revision). The report therefore suggested the patients with MoM THA return for clinical and radiographic follow-up (Lombardi, Berend, Morris, Adams, & Sneller, 2015). Another research reported pseudotumor were detected in 35% of 626 patient after median follow-up of 3 years and the occurrence of pseudotumor formation significantly increased after prolonged follow-up (Bosker et al., 2015).

2.5.3. Hip dual modular neck total hip arthroplasty (DMN THA)

Hip dual modular neck total hip arthroplasty (DMN THA) is also called "exchangeable femoral neck" or "dual taper" total hip arthroplasty (Colas et al., 2017). This design was expected to reduce the risk of dislocation and improve restoration of joint biomechanics, but it has been reported as having a poorer performance than other designs (Traina et al., 2011). According to the French national health-insurance databases, 8,931 (3%) of the 324,108 French patients with a mean age of 77 years received the DMNTHA between 2009 and 2012 and 59% of these have since been replaced with other THA in revision surgeries (Colas et al., 2017).

It is reported that DMN THA has been associated with implant failures due to corrosion at the modular junction, although it demonstrates a low dislocation rate and low neck fracture (Gofton, Illical, Feibel, Kim, & Beaulé, 2017). A recent research has reported the poor early survivorship of this hip arthroplasty design (37% of hips had been revised at a mean follow-up of 2 years) and assessed the catastrophically high rates of the ultimate failure rate (Nawabi et al., 2016). Another report showed the additional neck-stem taper interface of the DMN THA is vulnerable to mechanical failure and bio-metal corrosion, subsequently produce metal particles and release metal ions which lead to ALTR (Baxmann, Pfaff, Schilling, Grupp, & Morlock, 2017).

2.6. Implant survivorship

The implant survivorship of different hip replacements is one of the most concerned topics in the orthopaedic literature recently. Statistical analyses are normally used in these researches to compare the failure rates or survival rates of different prostheses procedures (Schätzle, Männchen, Zwahlen, & Lang, 2009). The vast majority of these implant survival analyses usually begin with an assumed time that all patients received their operations in that day or year, and end with the time of revision surgeries (Murray, Carr, & Bulstrode, 1993). Any better analyses at most reported the number of procedures followed, lost followed and failures, such as the life-time table reported by Kaplan and Meier (Lie, Engesæter, Havelin, Gjessing, & Vollset, 2004). However, more detailed information such as assessment of pain or function are rare in recent studies. Furthermore, 21% of unexplained failure cases for the MoMHRA failures have been recorded by the National Joint Registry for England and Wales (Smith et al., 2012). This suggests that more detailed studies for the understanding of implant failures are needed.

According to recent research, all other FDA approved HRA devices, except the BHR system, have been recalled due to higher than anticipated revision rates (Laaksonen, Donahue, Madanat, Makela, & Malchau, 2017). Furthermore, DMN THA and MoM LHTHA has largely been abandoned from the market (Seppänen et al., 2018) as a result of poorer survivorship than other designs (Colas et al., 2017).

2.7. Metallic wear particle-associated adverse tissue reactions

Millions of hip replacements are performed worldwide for patients with end stage osteoarthritis (A. V. Lombardi, Jr. et al., 2012). However, wear or corrosive metal particle-related adverse tissue reactions have raised wide concerns recently due to chronic inflammation and failure of implants, which require early revision (Xia et al., 2017). These failures can lead to significant patient morbidity, injury to abductor muscles, extensive tissue necrosis and increased revision complications (Beaver & Fehring, 2012; Kayani et al., 2012; J. T. Munro, B. A. Masri, C. P. Duncan, & D. S.

Garbuz, 2014; Wyles, Van Demark, Sierra, & Trousdale, 2014). The revisions for MoM hip implants caused by wear or corrosion related complications are increasingly reported by the National Joint Registry for England, Wales and Northern Ireland (NJR) (Haddad et al., 2011).

2.7.1. Metallic wear nanoparticles and metal ions

Previous research shows that both MoM and MoP bearing systems will generate nanometre-sized particles after implanting procedures. Moreover, MoM bearings produce 500 times more nanometre-sized metallic particles than MoP bearings, although MoM bearings have lower wear rates (Sieber, Rieker, & Köttig, 1999). Another research has calculated the volume of a single particle and the average volume of single particles, and then inferred that one MoM bearing surface is estimated to produce 6.7×10^{12} to 2.5×10^{14} nanoparticles per year. This number is much more than the number of nanoparticles generated by a metal-on-polyethylene bearing per year (Doorn et al., 1998).

Some researches mention that the metals prosthesis will undergo corrosion by body fluid and release metal ions after being implanted into the patient's body, as body fluid is comprised of electrolytes (G Mabilleau et al., 2006). What is worse, these released metal ions can be circulated around the body which is much more dangerous than the metal particles themselves (Wang, Wicklund, Gustilo, & Tsukayama, 1997). Some metal ions have already been detected during corrosion of metal implants such as Co^{2+} and Cr^{3+}. These metal ions can form serious complexes such as inorganic metal oxides and organometallic complexes (Catelas, Medley, Campbell, Huk, & Bobyn, 2004). It is reported that most of the metallic wear nanoparticles and generated metal ions are released from the bearing surfaces, as with the wear and corrosion in previous research, but the rate of corrosion is affected by the environment of the local tissue; thus the definite value is still unknown (Cobb & Schmalzreid, 2006). Many reports about the modern MoM bearings have recorded that Co and Cr levels in serum are higher than the pre-operative levels and that the peak levels occurred within the first year after the procedures (6 months for Co, 9 months for Cr) (Daniel, Ziaee, Pradhan, Pynsent, & McMinn, 2007; Germain et al., 2003).

2.7.2. Adverse systemic tissue reactions

Adverse biological responses to the metallic wear nanoparticles and generated metal ions can be either systemic or local as mentioned in chapter 1. It has been reported that the systemic adverse biological responses are associated with carcinogenesis, hypersensitivity and chromosomal abnormality in patients (G. Keegan, Learmonth, & Case, 2007; Willert et al., 2005). Furthermore, some researchers have mentioned that the resulting chromosomal problems risk being passed to the next generation (Brodner et al., 2004; Ziaee, Daniel, Datta, Blunt, & McMinn, 2007).

Researchers have already demonstrated the cancer risks of Co and Cr wear particles in animal models in the past (Heath, Freeman, & Swanson, 1971). However, the available data are not enough to support the association between the carcinogenetic potential and MoM THA. Some researches have even demonstrated the opposite result, that no apparent increased relative risk of cancer following MoM THA has been shown in this epidemiological study (Visuri, Pukkala, Paavolainen, Pulkkinen, & Riska, 1996). The relationship between increased cancer risk and MoM THA is still an on-going concern as researchers are still looking for better plans to overcome the limitations of this study, such as short follow up and a small patient group (Tharani, Dorey, & Schmalzried, 2001).

Metal hypersensitivity, also called metal sensitivity, has been found in 25% of patients with well-functioning implants and 60% of patients with failed or poor-functioning implants (N. Hallab, Merritt, & Jacobs, 2001). Increasingly researches have focused on the adverse metal hypersensitivity reactions in patients with MoM THA because of their high risk of occurrence and serious consequences (Benson, Goodwin, & Brostoff, 1975). Recent researches report that T-lymphocytes related to antigen-specific or acquired immune response will be induced by metal particles and lead to autoimmune disease (Benson et al., 1975; Willert et al., 2005). Chronic inflammatory response will be sustained by the T-lymphocytes and these T-lymphocytes will be activated and begin to proliferate. At same time, various cytokines will be released by these T-lymphocytes and result in the activation and accumulation of specific antigens (Nadim J Hallab, Mikecz, & Jacobs, 2000).

Macrophages, in many researches, are supposed to be the 'specific antigen' in this type of hypersensitivity reaction because metal particles have been observed in related periprosthetic tissue analyses (Davies, Willert, Campbell, Learmonth, & Case, 2005; Doorn, Mirra, Campbell, & Amstutz, 1996; Witzleb, Hanisch, Kolar, Krummenauer, & Guenther, 2007). However, there is a limited understanding of the relationship between the metal hypersensitivity histological features and MoM implant failures. This because studies for the adverse metal hypersensitivity reaction are not fully established, with limited clinical data available at present (Korovessis, Petsinis, Repanti, & Repantis, 2006; Milošev, Trebše, Kovac, Cör, & Pišot, 2006; Shahrdar, Campbell, Mirra, & Dorr, 2006).

2.7.3. Adverse local tissue reactions (ALTR)

Periprosthetic soft tissue mass is one of the most serious local adverse biological response in patients with MoMHRA. The occurrence of soft tissue masses has been increasingly reported in recent researches and is causing a growing concern for periprosthetic surgeries (Boardman, Middleton, & Kavanagh, 2006; Campbell et al., 2008; A. Hart et al., 2009). According to the published cases from several orthopaedic centres across the United Kingdom, the periprosthetic soft tissue masses relating to the hip joint have been described by different names such as inflammatory mass (Boardman et al., 2006), cysts (Gruber, Böck, Trattnig, Lintner, & Ritschl, 2007), bursae (Campbell et al., 2008) and 'pseudotumour' (Scully & Teeny, 2013) which is the most commonly used name in related studies.

Research shows that the proportion of patients with pseudotumours and requiring revision surgery is extremely high at approximately 70% (Grammatopolous et al., 2009). Pseudotumours have been histologically characterised by extensive necrotized macrophages and T-lymphocytes (Kwon et al., 2009). Moreover, the pseudotumours have been described as locally highly destructive soft tissue masses, and produce various symptoms such as dislocation, rash, pain, the presence of a lump and femoral nerve palsy (Kwon et al., 2011).

A study has reported that 75% of patients with pseudotumours required revision surgeries after using conventional no-MoM bearings hip replacement such as MoP, CoP and CoC bearings (Pandit et al., 2008). The magnetic resonance imaging (MRI) method has started to be used in the study of soft-tissue masses such as pseudotumours in recent years. In 2008, researchers in Leeds characterised the soft-tissue disease in these patients with the help of MRI examination (Toms et al., 2008). They collected the radiographic findings in 19 patients following CoCr on CoCr alloy THA and reported that 8 hips had shown the presence of corrosion and pittings of the femoral stems. 12 cases were found with occurrences of necrosis (4 of proximal femoral diaphyseal necrosis and 8 of soft tissue necrosis) following histological examination. In addition, studies of soft-tissue masses in patients following MoM hip resurfacing procedures have also been reported on recently. In recent research, soft tissue periprosthetic hip lesions causing unexplained pain were reported in 15 of 26 patients with MoMHRA (A. Hart et al., 2009). In another report, high concentrations of metal particles have been detected in the solid psoas masses after a successful BHR procedure (Boardman et al., 2006).

2.8. Cell-mediated metal corrosion

Corrosion can be defined as a chemical or electrochemical process that converts materials such as metals to their oxide, hydroxide or sulphide. The structures and useful properties of materials such as appearance, strength and stability will undergo gradual destruction during the whole corrosion process. (Revie, 2008) The main types of corrosion, such as high-temperature corrosion (Khanna, 2016), microbial corrosion (Videla & Herrera, 2004) and galvanic corrosion (Oldfield, 1988), have already been reported in various research areas.

Another kind of corrosion, called cell-mediated corrosion (Kolatat et al., 2015), has raised wide concerns in the surgical and biomaterial community as it has already caused serious problems to the biomaterials increasingly used in such procedures as hip replacements (Nadim James Hallab, Anderson, Stafford, Glant, & Jacobs, 2005; Singh & Dahotre, 2007). Cell-mediated corrosion is defined as "an immune system related electrochemical process which occurs on the metallic surfaces of implants inside the human body". The gradual destruction of the structures and qualities of implants occurring in the patient's body, and the degradation products which may harm the host have been generated at same time (Sansone, Pagani, & Melato, 2013).

It is believed that wear and corrosion of hip prostheses are the major reason for the production of bio-reactive particles such as metallic debris which may lead to implant failure and revision surgery (Perino et al., 2014; Wedemeyer et al., 2007). Some reports mention that osteoclasts (bone-resorbing cells) and macrophages have been involved in the cell mediated metal corrosion process (Mediero et al., 2015). In the case-series reports, adverse local tissue reactions (ALTR) such as bone lyses, inflammation, cytotoxicity and generation of pseudotumours are caused by the production of metallic nanoparticles from osteoclasts and macrophages with digestion, mediated uptake processes (Junnila et al., 2015; O. Lainiala et al., 2014; D. J. Langton et al., 2011; Z. Xia et al., 2011)

Macrophages are “a type of white blood cells which are differentiated from phagocytes and can differentiate into osteoclasts” (Gamblin et al., 2014). Substances coming from outside of the body, such as microbes and biomaterials, will be attacked by macrophages as one of their functions for defending against foreign substances (another important function of macrophages is engulfing cell debris or effete cells) (Goodman, Ma, Chiu, Ramachandran, & Smith, 2006). A recent research study reported that some resorption bits have been observed on the surface of surgical stainless steel (one of the most common biomaterials) following SEM examination, and proved that human cells involved the biomaterials degradative processes (Cadosch, Chan, Gautschi, Simmen, & Filgueira, 2009). Therefore, human cells mediated biocorrosion is suggested to be involved in the generation of metal wear particles and subsequently leads to adverse biological reactions.

2.9. Summary

- Hip osteoarthritis is one of the most common form of joint disease which affecting the quality of patients' life, hip replacement is one of commonly used treatments for late stages of osteoarthritis.

- Total hip replacements are increasingly being used in patients with end staged osteoarthritis and significantly improved quality of life

- The design of hip replacements has been developed for more than hundred years and MoM hip replacement were "rediscovered" science 1980s and this technology is still in use today.

- Despite the widespread application of hip replacements and satisfied short-term performances after implant surgeries. There are heightened concerns over the unknow risks of increased implant failures and adverse biological response.

- It is reported that the generation of metallic nanoparticles and ions from hip replacements are one of the key factors causing adverse biological response and clinical complications. The adverse biological response includes adverse systemic tissue reactions such as metal hypersensitivity and adverse local tissue reactions such as pseudotumours.

- Human cells mediated biocorrosion is suggested to be involved in the biomaterials (metal) degradative processes and producing metallic ions and nanoparticles which leads to adverse biological responses.

- There is limited understanding of the potential mechanisms involved in the generation of metallic nanoparticles from hip replacements and the cytotoxic effects of these nanoparticles. Definitive evidences are required in related researches.

- Therefore, further studies designed to explore potential mechanisms of metal nanoparticles involved cytotoxicity and human cells involved bio-corrosion to provide evidence-based recommendations to contribute to the development of hip replacement and minimise implant failure related clinical complications.

Chapter 3 Nano-Analyses of Metal Wear Particles from Failed Hip Prostheses

3.1. Introduction

Total hip arthroplasty (THA) or hip resurfacing arthroplasty (HRA) are the most successful treatment for end staged osteoarthritis (Chapter 2). The numbers of applications of THA or HRA are recently increasing in the majority of treatment cases (J. Lombardi, AV et al., 2012). However, more and more revision surgeries of failed implants have been reported which already became a serious problem that affect both public health and the majority of patients with implant operations (Matharu, Mellon, Murray, & Pandit, 2015).

These failures can result in the occurrence of the adverse biological responses caused by metallic particles involved severe inflammatory reactions (Cooper, Urban, Wixson, Meneghini, & Jacobs, 2013; Jacob T Munro, Bassam A Masri, Clive P Duncan, & Donald S Garbuz, 2014; Witt et al., 2014). It is reported that the rates of adverse biological responses across diverse implant configurations are increased with growing risk of wear and, corrosion and wear (Mao, Tay, Godbolt, & Crawford, 2012). The occurrence of implant failures has been increasingly reported in both MoM THA and non-MoM THA configurations (Cooper et al., 2013; McMinn, Daniel, Ziaee, & Pradhan, 2011; Jacob T Munro et al., 2014; Witt et al., 2014). Metal products produced from these implant prostheses are reported as one of the main reasons which cause the adverse local tissue reaction (ALTR) and implant failures according to Chapter 2.

Three typical classes of implant configurations which are widely used have been selected for study in this chapter. The configurations and the areas that potentially produce metal wear particles are shown in Figure 3.1.

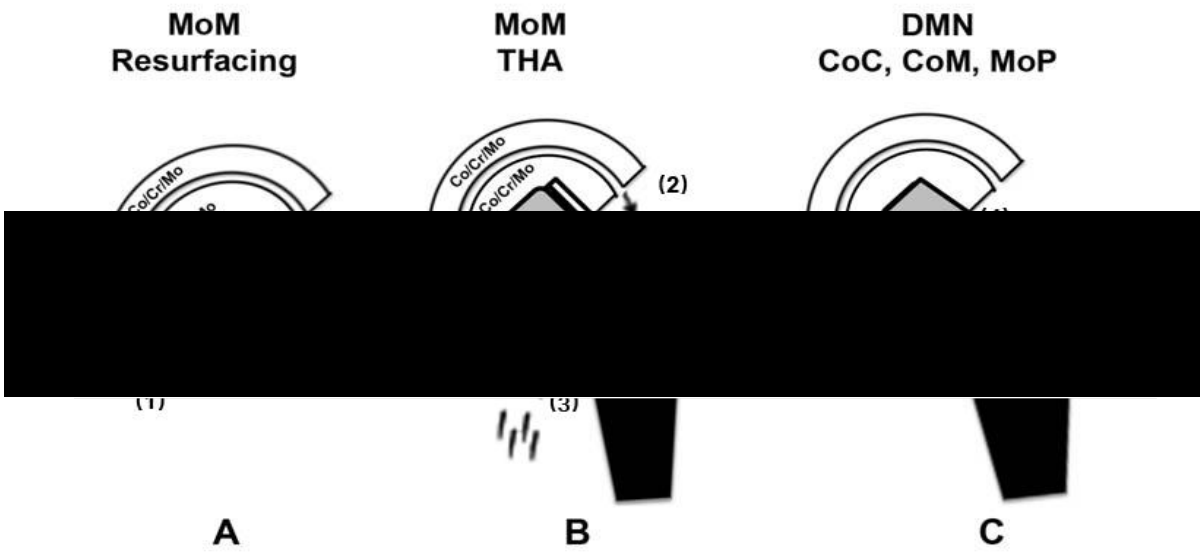

Figure 3.1. Configurations of three common types of hip replacement associated with ALTR.

A indicates the structure of metal-on-metal hip resurfacing arthroplasty (MoM HRA).
B indicates the structure of metal-on-metal large head total hip arthroplasty (MoM LHTHA).
C indicates the structure of non-MoM bearing surface (ceramic-on-polyethylene or metal-on-polyethylene) total hip arthroplasty with Co/Cr/Mo metallic dual modular neck (Non-MoM DMNTHA)

According to Figure 3.1, we can find that both femoral head and cup of the MoM HRA implants are composed of Co/Cr/Mo alloy (Fig 3.1-A). Metal nanoparticles are possibly generated at the bearing surface as the cause of either sliding tribocorrosion (Fig 3.1-A-1) or edge loading (Fig 3.1-A -2) (Catelas et al., 2004).

Both femoral head and cup of the MoM LHTHA implants are composed of Co/Cr/Mo alloy. In addition, a Co/Cr metallic adapter sleeve has been designed to connect the Ti metal stem with the Co/Cr/Mo femoral head (Fig 3.1-B). Likewise in Fig 3.1-B-1, metal nanoparticles are possibly produced similarly shown in Fig 3.1-A-1 and Fig 3.1-A-2, or even at the Ti metal stem and the metallic adapter sleeve interface as the cause of possibly abrasion, by fretting and crevice corrosion (Fig 3.1-B -3) (Meyer et al., 2012).

Non-metal on metal alternatives are selected as the bearing surface of the non-MoM DMNTHA implants, a Co/Cr metal modular taper is placed between the Ti steam and femoral head to connect with each other (Fig 3.1-C). The materials selected for the bearing surface can be various such as metal-on-polyethylene (MoP), ceramic-on-metal (CoM) or ceramic-on-ceramic (CoC). The majority of metal nanoparticles are likely created at interface of Ti steam and Co/Cr metal modular taper by fretting and crevice corrosion (Fig 3.1-C-4) (Di Laura et al., 2017).

Metal products produced from these mentioned implant prostheses are reported as one of the main reasons which cause the adverse local tissue reaction (ALTR) and implant failures in previous studies. However, the mechanisms of particle generation are yet to know. Furthermore, few researches are focusing on the characterization of these generated particles in the tissue of failed implants, although the European Union and HOC scientific committee have advocated comprehensive studies of these wear particles and emphasized the importance of understanding the wear particles such as shape, size and chemical properties (G. M. Keegan, Learmonth, & Case, 2008).

One of the main limitations is because the wear products are nano-sized, and it is difficult to be analysed by the conventional light microscopy experiments. Another difficulty is that it is hard to collect high quality tissue samples from revision surgeries with the authorization of patients. The application of new techniques has successfully provided the characterization information of these metallic particles and contribute to the understanding of the ALTR mechanism in this study.

3.2. Hypothesis

- The physical properties such as shape, scale and Feret ratio of metal wear particles which are generated from three classes of hip replacements are different.
- The chemical components and element distributions of these formed particles are different.
- The reasons of producing these metal wear particles are different and related to the design of configurations and materials used for each type of hip replacement.

3.3. Aim of study

The aim of the study in this chapter is to compare the physiochemical properties of metallic nanoparticles produced from three common classes of hip replacement to find out the mechanism of cells such as macrophages involved in the corrosion of implant prosthesis subsequently lead to ALTR and implant failures.

3.4. Materials and Method

3.4.1. Samples preparations

Periprosthetic tissues were collected at surgery from January 2013 to December 2014 undergoing revision surgery for adverse local tissue reaction (ALTR) at New York Hospital for Special Surgery. All patients were provided with informed and written consent regarding participation in this study. Ethical committee approval was obtained prior to this study (Institutional Review Board, Protocol Number 26085).

Three groups of prostheses have been studied here, which are 6 MoM HRA (BHR, Smith and Nephew, London, UK), 6 MoM LHTHA (femoral head >36 mm diameter) with metallic CoCrMo sleeve adapter and 6 Non-MoM DMNTHA with CoCr dual modular neck.

The collected tissues were fixed in 4% glutaraldehyde in 0.1 M PBS and delivered to Swansea University. The samples were then selected for serial dehydration followed by resin embedding, and undergone routine ultrathin sections.

3.4.2. TEM analysis and TEM EDS mapping

18 out of 52 samples were selected from three different groups (6 samples in each group) of failed prostheses as mentioned above (MoM-HRA, MoM-LHTHA and non-MoM DMN THA). The selected samples were examined by TEM at the University Hospital of Wales.

Energy dispersive x-ray spectrometry (EDS) was applied to identify the particular elements and their relative proportions (Goldstein et al., 1981). In this study, the EDS analysis for retrieved samples was processed by an Oxford Instruments 80 mm^2 EDX Silicon Drift Detector (SDD) and running INCA x-ray analysis system (Oxford Instruments, Abingdon, United Kingdom), which was performed with support from Leeds University.

Nine samples have been selected for the micrographs of TEM EDS element mapping (three samples for each type of configuration). Photoshop software were applied for processing the elements distribution mapping for each tissue sample. The achieved EDS images have been added to the scale bars and dyed with different colours according to corresponding elements by using Photoshop software to process elements distribution mapping different type of hip replacement.

3.4.3. ImageJ analysis

The collected TEM images were analysed through the 'ImageJ' software. ImageJ is a Java-based public domain image processing software, which can be downloaded through the 'ImageJ' official website. The information on the program states that it "can be utilized to develop user-coded plugins to suit the specific requirements of any conceived application" (Mazzoli & Favoni, 2012). The general process procedure was as followed:

i. 'Scale' setting, the dimensions of the images were set as the real physical dimensions based on the scale bar showed on the collected TEM image. (Fig 3.2-A)

ii. 'Brightness/Contrast' adjusting, the sharpness of TEM images were adjusted via 'Brightness/Contrast' function to show the particles clearer on the images as acquired images have distractions in the background in our cases. Some particles were important but mixed with background or other particles that the software could not identify them automatically. ImageJ's command 'Magic wand' function was used to highlight these particles manually.

iii. ‘Threshold…’ setting, after all the particles were obvious on the image. TEM images were transformed into binary images which display 2^8 grey levels with ImageJ's command “Threshold…”, it is as shown in Fig 3.2-B.

iv. ‘Analyse particles’ function, the accurate measurement of the size of particles have been generated with removing the distractions of background (setting the size over 100nm^2). Meanwhile the selected areas (particles) in the image have been observed through selecting “Show Outlines” option. (Fig 3.2-C).

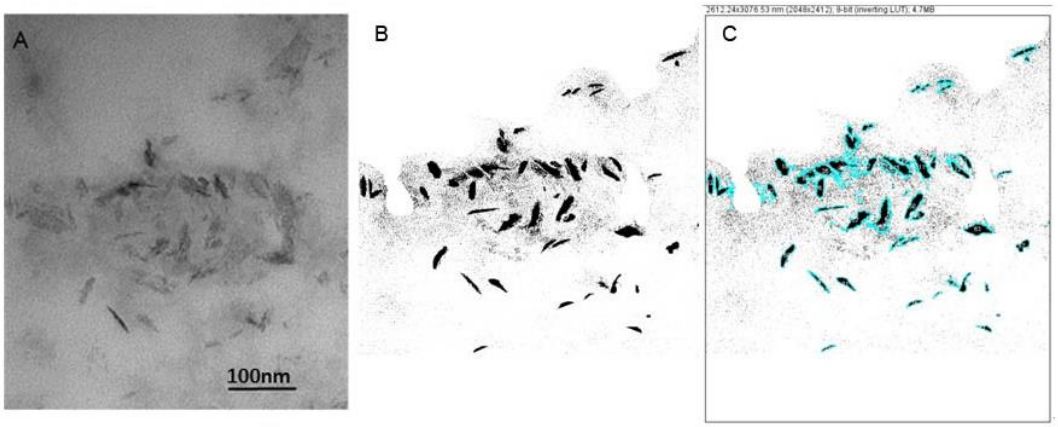

Figure 3.2. The process of nanoparticle measurement using ImageJ

After all settings were completed, the physical information such as the area, size of shape (Feret diameter) of each particle were generated automatically by ‘ImageJ’. The achieved data can provide a better understanding of these metallic particles.

3.4.4. Feret diameter

Feret diameter, also known as the calliper diameter, is defined as “the distance between the two parallel planes restricting the object perpendicular to that direction”(Mazzoli & Favoni, 2012). The maximum distance between any two points along the selection boundary of the particles is defined as the maximum Feret diameter or Feret Max. On the contrary, the minimal distance after calculating is defined as the minimal Feret diameter or Feret Min as shown in Fig 3.3. The shape of objects (particles) can be roughly described with a value which is called the Feret ratio. The Feret ratio can be

calculated by using the minimal Feret diameter then divide the maximum Feret diameter (Feret Min/ Feret Max) (Warchomicka, Stockinger, & Degischer, 2006). Thus, if the shape of a particle is close to a circle (the Feret Min close to the Feret Max), which means that the Feret ratio of this particle is close to 1.

Figure 3.3. Definition of Feret diameter

3.4.5. Statistical analysis

The TEM images of 18 selected samples were refined by 'ImageJ', the achieved data from 'ImageJ' have been well organised and processed against statistical knowledge with GraphPad software to compare the histological variables between each type of hip-replacement. One-way ANOVA method has been chosen for the continuous variation of analyses (nanoparticles). The Kruskal-Wallis test was used to treat the data as non-parametric. Significance level was set at 0.05 (95% confidence intervals). T-test and f-test were used for assessing the discontinuous variation (tissue samples).

3.5. Results

3.5.1. TEM Observation:

Figure 3.4 shows the selected TEM images of retrieved tissue samples for three types of hip replacement, each image represents corresponding type of configuration (MoM HRA, MoM LHTHA and Non-MoM DMNTHA). More achieved TEM images are shown in Appendix 3.

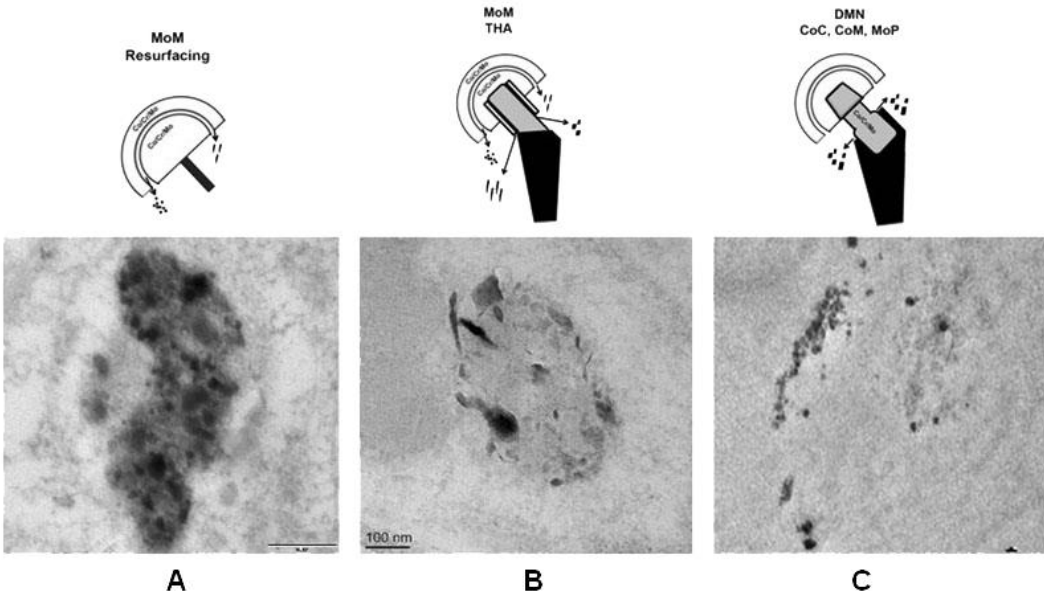

Figure 3.4. Three selected images from acquired TEM images

The TEM images indicate the brief shapes and distribution of nanoparticles in retrieved tissue samples in three types of configuration. A indicates metal nanoparticles which are generated from MoM HRA sample; B indicates metal nanoparticles which are generated from MoM LHTHA sample; and C indicates metal nanoparticles which are generated from Non-MoM DMNTHA sample. Scale bars: A, C=500nm; B=100nm

As it can be seen from Figure 3.4, the shapes of metal particles which are generated from each types of hip replacements have represented a significant difference. The TEM image of MoM HRA samples, the shapes of produced metal particles are either circular or needle like (Fig 3.4-A). MoM LHTHA samples, some spindly needle like and some irregular metal particles which are produced from bearing surface and the metal stem with metal sleeves (Fig 3.4-B). Non-MoM DMNTHA, tribological corrosive particles are produced with virtually circular shapes (Fig 3.4-C).

3.5.2. TEM/EDS elements distribution mapping

The analysis of the chemical components of detected nanoparticles has been supported by the micrographs of TEM EDS elements mapping as shown in figure 3.5. Three samples have been selected for each class of configuration.

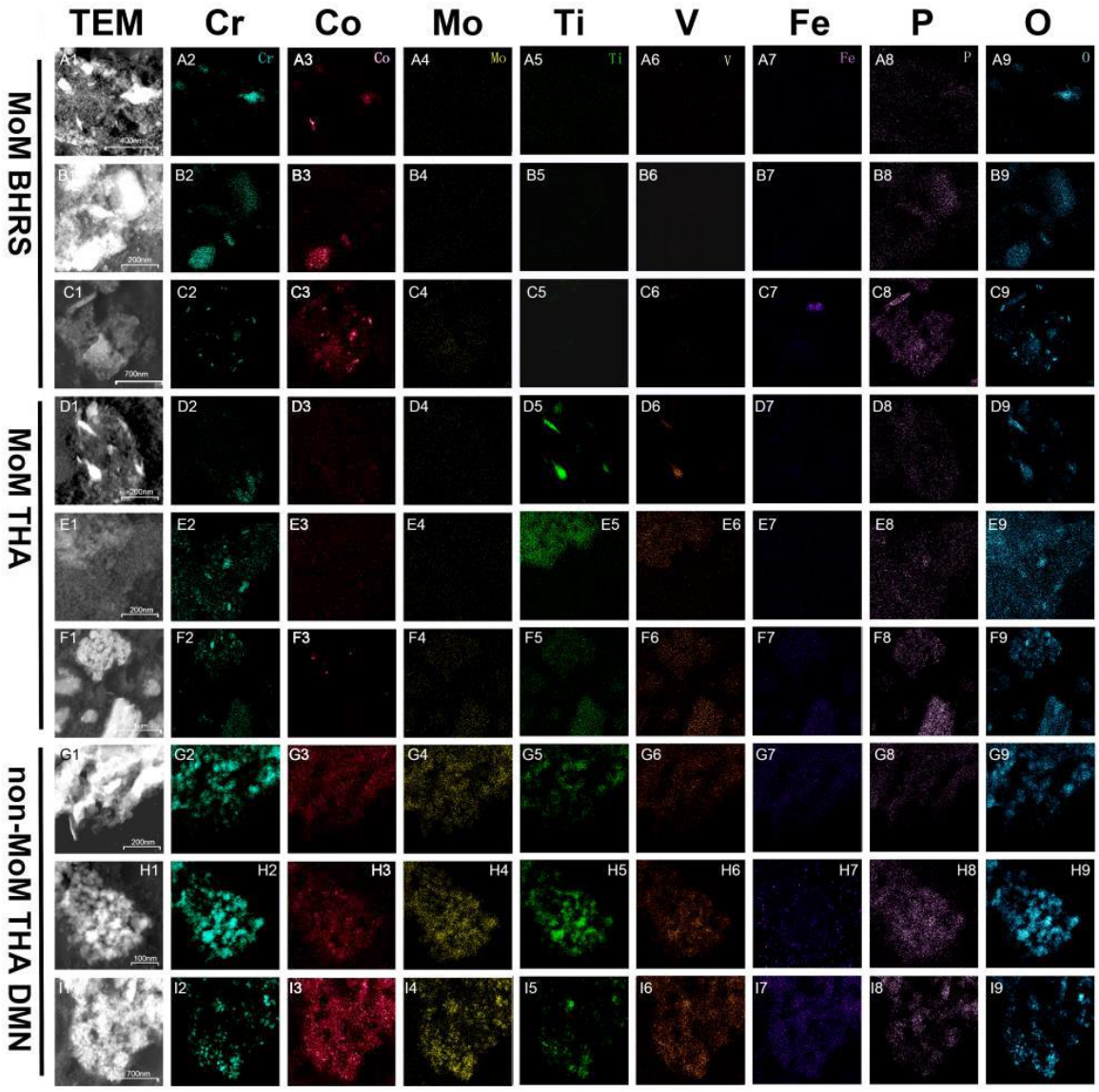

Figure 3.5. The elements distribution within nanoparticles from three types of hip replacement (MoM HRA, MoM LHTHA and Non-MoM DMNTHA).

Images in the first column are the 9 selected original TEM images for element mapping (A1-I1), and the remaining images are the corresponding EDS analysed images. Each column indicates one kind of element and each row indicates one selected sample. Each element mapping is filled with specific colour and listed behind the corresponding original TEM image.
Scale bar: A1=400 nm; B1, D1, E1 and G1=200nm; C1, I1 =700nm, F1=1000 nm

It is clearly to compare the distribution and proportion of each element in the tissue samples of different type of configuration by using this elements mapping shown in figure 9. As stated by the mapping, we can find that, three elements are found in larger amounts in all samples, which are Cr (A2-I2), P (A8-I8) and O (A9-I9). Both MoM HRA (B1-B3) and MoM LHTHA (B4-B6) groups contain a small number of high electron density particles, and Co have been observed in the particles in the Non-MoM DMNTHA group (G3-I3). Non-MoM DMNTHA groups contain High concentration of Mo (G4-I4). Ti and V are barely detectable in MoM HRA groups (A5-C5, A6-C6), but they are detected co-existing in the MoM LHTHA (D5-F5, D6-F6) and Non-MoM DMNTHA (G5-I5, G6-I6). Some samples, such as C7, H7 and I7 contain Fe which are not co-localize with other metal particles. The concentration of P is lower than oxygen, but P and O co-existed with each other.

3.5.3. Physical properties analyses

After the selected TEM images are processed by the 'ImageJ' software, the data of three samples for each class of configuration have been organised by Excel software to compare the Feret Ratio distributions of three classes of configuration.

A table that represent the Feret Ratio distributions in each type of hip replacement is shown in Table 3.1. the values of Feret Ratio were classified into 8 ranges with every 0.5 changing space (1.0-1.5, 1.5-2.0 to >4.5). The proportion of the Feret Ratio of nanoparticles located in each classified range was calculated by the 'Frequency' equation of Excel software.

Table 3.1 Percentage Feret Ratio distributions of nanoparticles in each type of hip replacement

Feret Ratio Range	MoM HRA	MoM LHTHA	Non-MoM DMNTHA
1.0-1.5	31.49%	34.32%	50.33%
1.5-2.0	37.92%	36.25%	35.31%
2.0-2.5	14.85%	16.24%	10.54%
2.5-3.0	4.65%	7.69%	2.72%
3.0-3.5	2.14%	2.39%	0.28%
3.5-4.0	0.53%	1.26%	0.41%
4.0-4.5	0.19%	0.24%	0%
>4.5	0%	1.61%	0.42%

The first column represents different range of Feret Ratio, the rest 3 columns are studied three types of hip replacement. The percentage values in the table indicates the proportion of Feret Ratio located in related area.

Both bar chart and pie chart were plotted in Figure 3.6 according to the obtained results in Table 3.1. to compare the Feret Ratio distribution of nanoparticles in three configurations

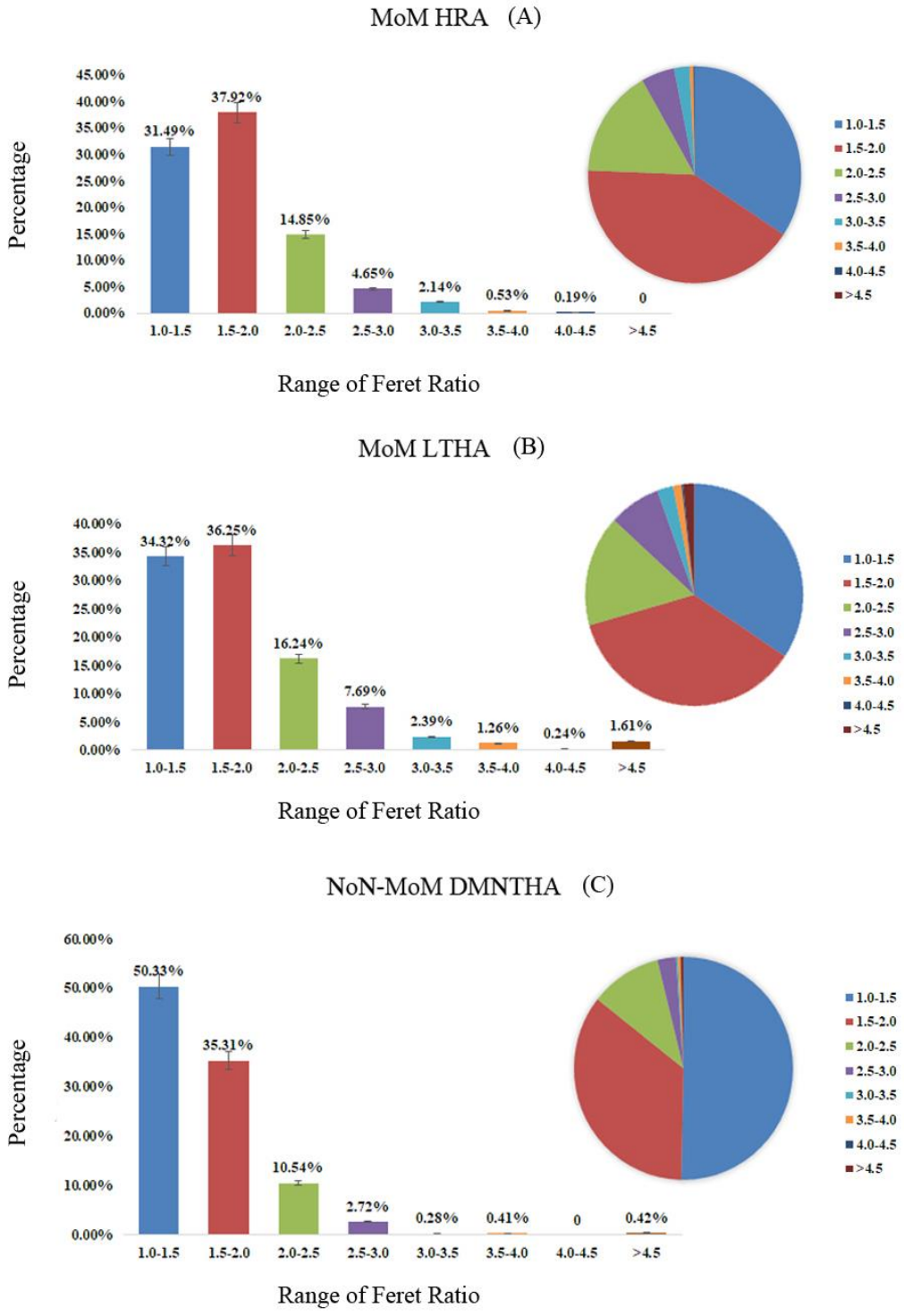

Figure 3.6. The Feret Ratio distribution for Three classes of configuration (MoM HRA, MoM LHTHA and Non-MoM DMNTHA)

The X-axis indicates the values of Feret Ratio ($Feret_{max}/Feret_{min,}$), Y-axis indicates the proportion of different Feret Ratios. Different colours were applied to distinguish the values of Feret Ratio in varied ranges.

As it can be seen from Figure 3.6-A, the majority number of Feret Ratios of nanoparticles observed in the MoM HRA group are in the range of 1.5 to 2, which account for 37.92% of total nanoparticles. This indicats that large numbers of nanoparticles produced in the MoM HRA group demonstrate rectangular or oval shapes.

Fig 3.6-B represents the distribution of the Feret Ratios of particles from MoM LHTHA as irregular. Various shapes of nanoparticles exist in the tissue sample. in addition, needle like nanoparticles (Ratio > 4.5) also exist in this group with the proportion of 1.61%.

50.33% of Feret Ratios for Non-MoM DMNTHA groups (Fig 3.6-C) are located between 1 to 1.5 area and account for more than half of total nanoparticles, which demonstrated that the majority shapes of metal nanoparticles generated from the DMNTHA are close to the shape of circle or square.

3.5.4. Statistical analyses of observed nanoparticles in TEM images

After the 'ImageJ' process, the achieved data such as Feret Max, Feret Mini and Feret Ratio of all nanoparticles observed in selected TEM images (3 images for 1 of 18 samples) are analysed through 'Graph Pad' software. It only selected particles which have at least one Feret diameter larger than 10 nm, and the total analysed number is 3850 (1493 of MoM HRA, 1200 of MoM LHTHA and 1157 of non-MoM DMNTHA). One-way ANOVA analysis and Tukey–Kramer test with $p<0.05$ significance have been applied to compare the difference of nanoparticles from three types of hip replacements. The results are shown in Figure 3.7:

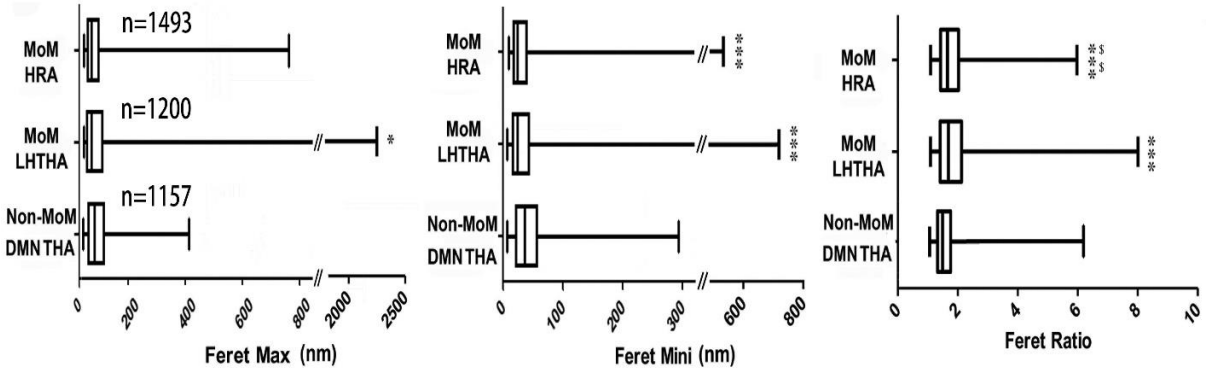

Figure 3.7. Comparison of the nanoparticles produced from three types of hip replacements against statistical knowledge

'*' indicates the level of significant difference ($p<0.05$) when LHTHA and MoM HRA compared with DMNTHA respectively; '$' indicates the level of significant difference ($p<0.05$) when LHTHA and MoM HRA compared with each other. (Error bar: mean±stand deviation)

Figure 3.7 shows a range of particle sizes (Feret Max and Feret Min) and shapes (Feret ratio) distribution of three major types of hip implants from the smallest (the end of left bars) to the largest (the end of right bars). The boxes of the bars show the 25% (the left edge of the box), medium (the vertical line in the box) and 75% (the right edge of the box). According to the collected data, the Feret Max of MoM LHTHA group presents significant difference (*) when compared with non-MoM DMNTHA group; the Feret Mini of both MoM LHTHA and MoM HRA represent significant difference (***) when compared with those in the non-MoM DMNTHA group. Both the MoM LHTHA and MoM HRA represent significant difference (***) when compared with non-MoM DMNTHA group for the Feret Ratio comparison and the Feret Ratio of MoM HRA group represent significant difference ($$) when compared with those in the MoM LHTHA group.

The T-test and F-test were applied to compare the variances of all tissue samples (patients) between three common classes of hip implants with ‘Excel’ software. The T-test is a univariate hypothesis test, that is applied in order to compare the averages of two small groups (Rouder, Speckman, Sun, Morey, & Iverson, 2009). The F-test is a statistical test, which is used during the process of obtaining the result of the T-test (Erdfelder, Faul, & Buchner, 1996).

The average values of the selected 18 tissue samples (patients) have been calculated and classified into the three common classes of hip implants. The T-test and F-test were applied to compare the variances between each class of hip implants with 'Excel' software. The obtained results are organised and shown in Table 3.2 and Figure 3.8

Table 3.2 The T- and F-test analysed comparison of three common classes of hip implants

	(A) Feret Max			(B) FeretMini			(C) FeretRatio		
	Non-MoM DMN vs MoM HRA	MoM HRA vs MoM LHTHA	Non-MoM DMN vs MoM LHTHA	Non-MoM DMN vs MoM HRA	MoM HRA vs MoM LHTHA	Non-MoM DMN vs MoM LHTHA	Non-MoM DMN vs MoM HRA	MoM HRA vs MoM LHTHA	Non-MoM DMN vs MoM LHTHA
F-Test	0.470935617	0.052789	0.448758687	0.266971	0.128341	0.948762	0.59863	<u>0.025552</u>	0.033864
T-test	0.065474258	0.087601	0.775454138	<u>0.024389</u>	0.309114	0.221008	<u>0.028367</u>	0.067469	<u>0.012627</u>

The comparing groups which have significant difference ($p<0.05$) were highlighted with underline in the table.

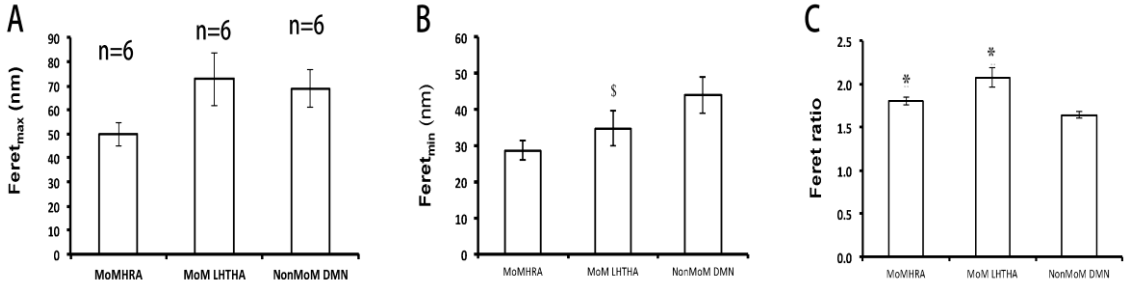

Figure 3.8. Comparison of three common classes of hip implants

'*' indicates the level of significant difference ($p<0.05$) when LHTHA and MoM HRA compared with DMNTHA respectively; '$' indicates the level of significant difference ($p<0.05$) when LHTHA and MoM HRA compared with each other. Error bar: mean±stand deviation

According to the obtained results above, the comparison of Feret Mini (Table 3.1-B and Fig 3.8-B) represent significant difference ($) when LHTHA and MoM HRA are compared with each other. The Feret Ratio in non-MoM DMNTHA group also shows significant difference (*) when compared with LHTHA and MoM HRA respectively (Table 3.1-C and Fig 3.8-C). Whereas no significant difference has found in the comparison of Feret Max between each group (Table 3.1-A and Fig 3.8-A).

3.6. Discussion

According to previous research, the metallic particles in biopsies retrieved from MoM HRA were analysed, it is found that both needle-like particles (high density) and smooth-surfaced particles (low density) have been detected in both living and dead macrophages (Zhidao Xia et al., 2011). The results of this report are consistent with what we obtained in this study. Furthermore, many other studies have reported the hypothesis that metal wear particles generated from failed hip prosthesis is one of the main reasons that cause ALTR and implant failures. However, these reports remain uncertain, such as characterizing the particle properties is limited from the results obtained from light microscopy (Fang et al., 2008).

The physical properties such as size, shape, number of metal wear particles in selected tissue samples have been studied by using TEM nano-analytical tools such as 'ImageJ' in this research. The results denote that the physical properties of these analysed particles of three common classes of hip implants are different with each other.

Most of the wear particles in the MoM HRA group are circular shapes with the size smaller than 50 nm (A. J. Hart et al., 2010). These particles were produced from the bearing surface with the occurrence of sliding tribocorrosion (Catelas et al., 2004). Moreover, these particles possibly produce secondary particles after they have been phagocytized and then released by necrotic macrophages (Ricciardi et al., 2016). Besides, some needle-like small particles were also detected in this group. The possible reason for this formation is perhaps the edge loading or some other unexpected cases of the implant components such as gross dislocation or migration.

The majority of the wear particles in the MoM HRA group include two types. The first type of particles was generated from the bearing surface which are similar to those in the MoM HRA group. The second type of particles are irregular shape with larger Feret Ratio and scale (nano or micron size). These particles were generated from the adapter sleeve-male neck taper interface by either the abrasion of the titanium particles as described in other research or the occurrence of some mechanical effects such as crevice corrosion and fretting (Meyer et al., 2012). The secondary particles released

from a large amount of necrotic macrophages, possibly accelerate the wear process of the lubricating tribolayer and increase the risk of ALTRs (Ricciardi et al., 2016).

In the Non-MoM DMNTHA group, most of the detected particles are irregular nano-size particle aggregates. Some large detected particles are regarded as the agglomeration of circular corrosion particles. These particles were caused at the femoral stem female taper interface with the neck distal taper by mechanically fretting and inflammatory cell induced biochemical corrosion (Gilbert et al., 2015).

The majority of detected particles in the MoM HRA group are principally composed of oxidized chromium and cobalt; most of detected particles in the MoM LHTHA group are composed of cobalt and chromium with the addition of vanadium and titanium; the majority of detected particles in the Non-MoM DMNTHA group are composed of co-localized titanium, cobalt, chromium, and molybdenum. Although the element components of wear particles from both MoM-LHTHA and Non-MoM DMNTHA groups are similar, the element distributions of these two groups are distinctively different. For instance, the Cr/Co particles from the MoM LHTHA groups are separated from those containing of titanium and vanadium, whereas the Cr/Co particles from the non-MoM DMNTHA group are fused with the Ti/V particles. Figure 3.9 represents the comparison of the distribution of two major metallic particles (Cr and Ti) by overlay of Cr with Ti maps.

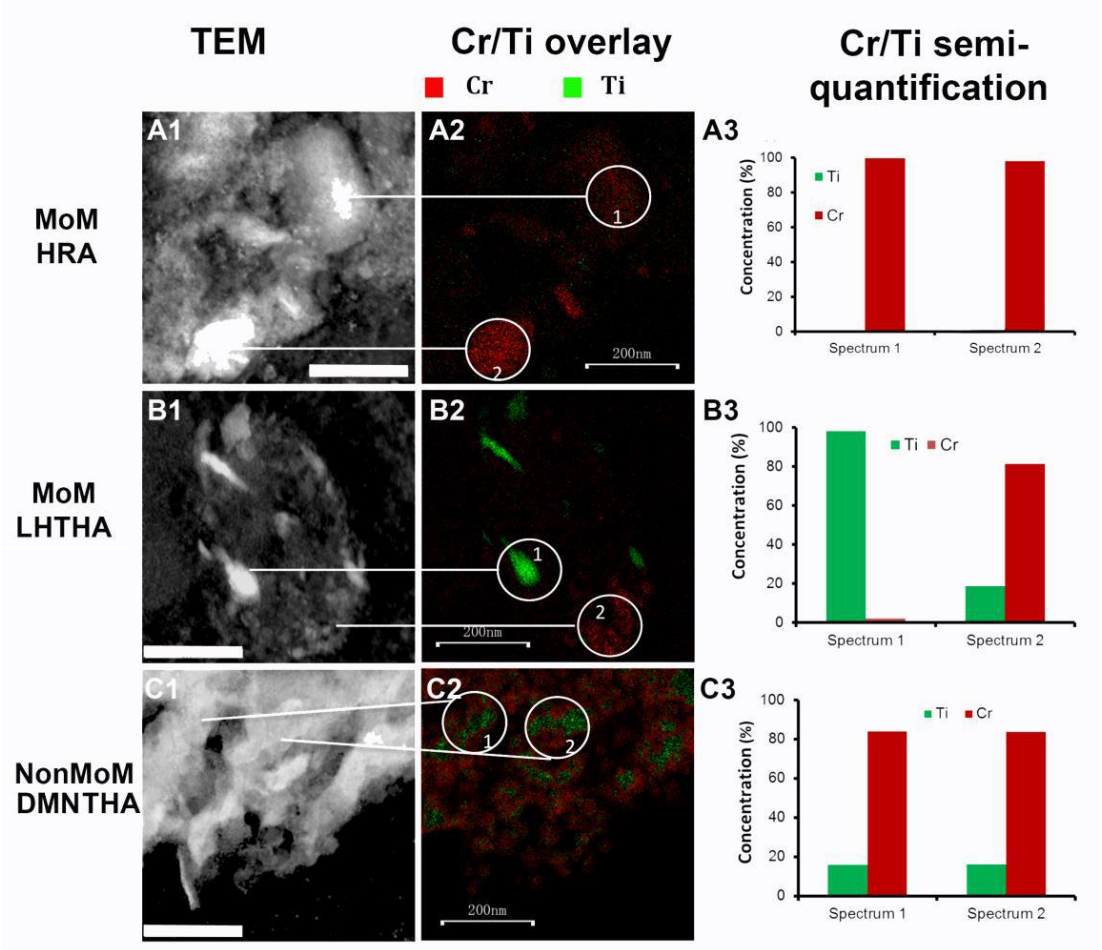

Figure 3.9. Characterization of the distribution of two major metal particles (Cr and Ti) by of TEM EDS mapping

A1-C1 indicates the original TEM image of three analysed implant groups (MoM HRA, MoM LHTHA and Non-MoM DMNTHA).
A2-C2 indicates the overlay maps of two major metallic particles (Cr and Ti) with two selected area (in circles) from A1-C1.
A3-C3.is the semi-quantitative analysis of Cr and Ti concentration (%) in the selected areas.
Scale bar = 200 nm

As it can be seen in Figure 3.9, Cr particles have been observed in the MoM HRA group, but Ti is barely detectable in select area of the MoM HRA group (Fig 3.9-A1-A3). Two types of particles have been observed in the MoM LHTHA group (Fig 3.9-B1-B3). First type is the large needle-like particles which almost exclusively composed of Ti (98.04%) with very low chromium (Fig 3.9-B2-1 and B3 spectrum 1). Another type is the particles containing Cr (81.31%) with minor component of Ti (Fig 3.9-B2-2 and B3 spectrum 2), the compositions of this type of particles are very similar to those in the Non-MoM DMNTHA group. In the Non-MoM DMNTHA group (Fig 3.9-C1-C3), both Cr and Ti have been detected with a similar composition with predominant Cr element in both selected area (Cr 84.14% for Fig 3.9-C3 spectrum1

and Cr 83.72% for Fig 3.9-C3 spectrum 3). Thus, the characterizations of this overlay EDS maps contributes the support of exploring mechanism of generating these metal wear particles which have mentioned above.

In conclusion, the study of this chapter has provided the physiochemical properties of these wear products in three common types of implants, also introduced a better understanding of the mechanism of generating nanoparticles from failed hip replacement. Further analysis is suggested to focus on the nanoparticle induced cytotoxicity study to assess the biological response of metal nanoparticles effect on cells. In vitro or in vivo toxicological analysis will be necessary to explore how these metallic interacted with cells or tissue and subsequently cause ALTR and implant failures.

Chapter 4 Metal Nanoparticles Induced Cytotoxicity on THP-1 Human Macrophages

4.1. Introduction

Element analysis of metallic particles in retrieved tissue samples (Chapter 3) has confirmed that large amount of Co, Cr and Ti nanoparticles and their mixture are appeared in tissues. Moreover, recent reports indicated Co and Cr levels in the median serum of patients with pseudotumours were considerably higher when comparing with patients without pseudotumours (up to twelve folds) (Back, Young, & Shimmin, 2005; Daniel et al., 2007). Hence, the presence of extensive necrosis and granuloma-like collections of macrophages would demonstrate a local metal-induced cytotoxic effect. Furthermore, the local metal-induced cytotoxic effect is assumed to lead a vicious cycle that may release resultant metal particle and cause further repetition of the cell death process which includes macrophage recruitment, particles phagocytosis and subsequent apoptosis or necrosis (Campbell et al., 2010). However, limited researches have elucidated the biological response of phagocytosis of clinically relevant metallic nanoparticles on macrophages although it was hypothesised that metallic nanoparticles such as Co, Cr and Ti may play an important role in the generation of pseudotumours. Thus, the study of this chapter is designed to investigate the biological mechanisms of metal nanoparticles (Co, Cr and Ti) induced cellular cytotoxicity study with the Neutral Red method in vitro.

The Neutral Red method is a sample, accurate method which has been developed by Puerner in 1985 (Hu et al., 2015). The vital dye, Neutral Red (Toluylene Red, Basic Red 5) is the key component of this method. This vital dye will be taken up by viable cells through active transport and incorporated into lysosomes. On the contrary, the dye will not be taken up by non-viable cells. The cells are briefly washed or fixed after they have been allowed to incorporate the dye. An acidified ethanol solution (Neutral Red Assay Solubilization Solution) will liberate the incorporated dye from the cells. (Jiang et al., 2016)

The amount of dye incorporated by the cells in the culture will be affected by some concomitant changes such as increasing or decreasing the number of cells or their physiological state. This shows the level of cytotoxicity which the test material produced. (Fields, Fowler, Hargreaves, Reeve, & Bombick, 2017)

4.2. Hypothesis

Base on the results from Chapter 3, the implants produce a mixture of Co, Cr and Ti are more subject to failure, we hypothesise that even though Co, Cr and Ti may be toxic to phagocyte, a combination of them may be more toxic.

4.3. Aim of Study

The aim of this research is to investigate the interaction between macrophages and metallic nanoparticles in vitro; also, whether the mixture of Co, Cr and Ti nanoparticles are more toxic than single type of them or not.

4.4. Materials and Methods

4.4.1. Cell Culture

THP-1 cell line is defined as a kind of human monocytic leukemia cell line which has become a popular model for studying the mechanisms of monocyte or macrophage. THP-1 cells can be differentiated into macrophage-like cells with the influences of phorbol 12-myristate 13-acetate (PMA) which mimic native monocyte-derived macrophages in several respects (Lund, To, O'Brien, & Donnelly, 2016). Monocyte and macrophage activities such as signaling pathways, nutrient and drug transport have been explored with the help of numerous THP-1 studies (Chanput, Mes, & Wichers, 2014; Tsuchiya et al., 1980). Recent reports show that THP-1 cells have been extensively used in estimating the immune-modulating effects on cells such as THP-1 inflammasome test (Casson et al., 2015) or cytotoxicity studies in vitro (Anantharajah et al., 2015).

THP-1 macrophage cell line was cultured in RPMI1640 culture medium with 2mM glutamine (Thermo Fisher, 11875093, UK) supplemented with 10% foetal bovine serum (FBS; Labtech International, UK) and penicillin / streptomycin (Gibco, BRL, Invitrogen Ltd, Paisley, UK) in a 10 cm diameter cell culture plate with 3-4x10^4/ml seeding density.

4.4.2. Nanoparticles

Co, Cr and Ti obtained from American Elements (purity 99.8%, a mean size 30 nm), were stored in 100% ethanol with 10^{15} particles/ml and kept at -20°C to avoid corrosion or agglomeration.

For cell culture treatments, all the particle stock solution was diluted 1:1000 in RPMI1640 with glutamine to obtain a concentration of 0.1 mg (or 1×10^{12} particles)/ml. Concentration of wear nanoparticles in the tissue from clinical report varied significantly. It is suggested that in normal condition, the annual nanoparticles produced from MoM resurfacing is around 1 mm^3or 1×10^{13} in number. A dose range 1×10^9 to 1×10^{12}particles/ml was used for the study, which is equivalent to clinical exposure.

4.4.3. Neutral Red kit

Neutral Red Solution 0.33% in DPBS purchased from Sigma-Aldrich (N-2889). The Neutral Red Assay Solubilization Solution is composed with 1% Acetic acid in 50% Ethanol 125 ml. the procedure of Neutral Red assay are shown below:

i. Remove cultures from incubator into a fume cabinet.
ii. Add 0.33% Neutral Red Solution in an amount equals to 10% of the culture medium volume, then return cultures to incubator for 2 hours
iii. At the end of the incubation period, the medium was carefully removed, and the cells have been washed in PBS pH7.4 (Thermo Fisher, 10010023, UK)
iv. After that, remove the wash solution, and the incorporated dye is then

solubilized in a volume of Neutral Red Assay Solubilization Solution equals to the original volume of culture medium (200nl/well). The cultures were stand for 10 minutes at room temperature with gentle stirring in a gyratory shaker to enhance mixing of the solubilized dye.

v. Tests performed in 96 well plates have been read by the 'FLUO star Omega' plate reader. Spectrophotometrically measure absorbance at a wavelength of 540 nm. Measure the background absorbance of multi-well plates at 690 nm and subtract from 540 nm measurement.

4.4.4. Cytotoxicity study with CoNP in different culturing time

THP-1 cells were seeded into a 96-well cell culture plate (Greiner CELLSTAR, M0812-100EA, UK) with 3 x 10^4/ml seeding density per well, the plate design is shown in Figure 4.1. 50nM PMA (Sigma Aldrich, 79346, UK) was added to each well after overnight incubation. After 72 hours of transfection, THP-1 cells were co-cultured with cobalt nanoparticles (99.8% purity, American Elements, Mereles Crop. Los Angeles, USA) at different concentrations (10^9, 10^{10}, 10^{11},10^{12}) in RPMI with 10% FBS and penicillin / streptomycin (P/S) for 8, 16 and 24 hours respectively. The Co nanoparticles were processed with a sonication water bath for 5 minutes to keep them suspended in RPMI culture medium. The relative fluorescence units (RFU) were measured with Neutral Red proliferation assay which as mentioned before.

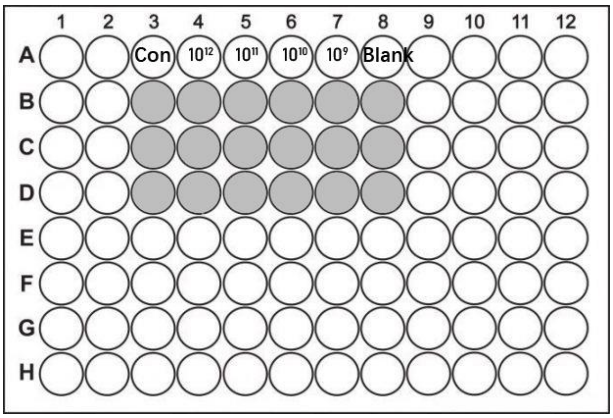

Figure 4.1. The Plate design of cytotoxicity study with CoNP in different culturing time

B3-D3: THP-1+50nM PMA in RPMI medium+10% FBS and P/S (Control)
B4-D4: THP-1+50nM PMA+10^{12}CoNP in RPMI medium+10% FBS and P/S
B5-D5: THP-1+50nM PMA+10^{11}CoNP in RPMI medium+10% FBS and P/S
B6-D6: THP-1+50nM PMA+10^{10}CoNP in RPMI medium+10% FBS and P/S
B7-D7: THP-1+50nM PMA+10^{9}CoNP in RPMI medium+10% FBS and P/S
B8-D8: RPMI medium only (Blank)

4.4.5. Cytotoxicity study with Co, Cr and Ti nanoparticles treatment

THP-1 cells were seeded into four 96-well cell culture plates with 3 x 10^4/ml seeding density per well with the same plate design in Figure 4.1. 50nM PMA was added to each well after overnight incubation. After 72 hours of treatment, three different metal nanoparticles (Co, Cr and Ti, 99.8% purity, American Elements, Mereles Crop. Los Angeles, USA) and the combined Co Cr and Ti nanoparticles, with the same amounts, were added into one of four 96-well culture plates at different concentrations (10^9, 10^{10}, 10^{11},10^{12}) respectively and co-cultured with the differentiated THP-1 cells in RPMI with 10% serum for 24 hours. The relative fluorescence units against added nanoparticles at different concentrations were measured with Neutral Red proliferation assay.

4.4.6. SEM/EDS observation

THP-1 cells were seeded onto clean and autoclave-sterilised 1cm × 1cm silicon wafers (Agar Scientific, Essex, UK), which were cultured in 12 well plates (Greiner Bio One, Stonehouse, UK) at 1×10^5 cells/cm^2. THP-1 cells were differentiated for 3 days by 50 nM PMA and incubated with CoNP (10^{12} particles/ml) for 24 hours.

After co-cultured with CoNPs, samples were fixed in 2.5% glutaraldehyde solution (Fisher Scientific BP2548-1, USA) in PBS buffer for 10 minutes in a fume cabinet. Samples subsequently been wash thoroughly in 3 changes PBS. They were then serially dehydrated in graded series of ethanol for 15 minutes (30%, 50%, 70%, 90% and 2×100%) and subsequently infiltrated in 50% hexamethyldisilazane (Fluka, 52619, UK) and then 100% hexamethyldisilazane for 20 minutes. After that, sample were replaced with fresh 100% hexamethyldisilazane, afterward it has been placed in a fume cabinet overnight to dry. The dried samples were applied for SEM/back-scatter electron detector (BSE) scanning with EDS analysis in Swansea University.

4.4.7. Statistical analysis

'GraphPad' software was used to perform the statistical analyses. One-way ANOVA method has been chosen for the Continuous variation of analyses. The Kruskal-Wallis test was used to treat the data for the inter-group comparisons. Differences at $p< 0.05$ were considered to be significant.

4.5. Results

4.5.1. Microscopy observation

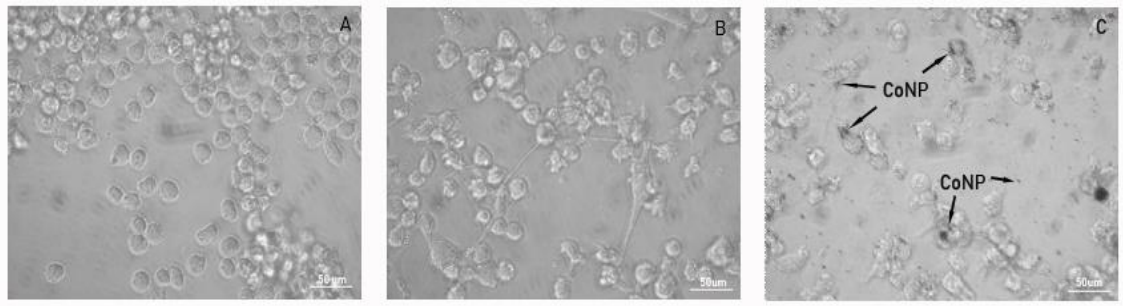

Figure 4.2. Microscopy observation of THP-1 differentiation (A, B) and phagocytosis of CoNP (C). Scale bar= 50μm

As it can be seen from Figure 4.2, Micrographs of light microscope demonstrates control THP-1 cells (A), THP-1 cells with 72 hours of differentiation by PMA (B) and differentiated THP-1 cells cultured with Co nanoparticles in vitro for 24 hours (C). The THP-1 cells have been successfully differentiated into macrophages by 50nM PMA with 72 hours of transfection (A and B). CoNPs were scattered over the whole area in Figure 4.1-C (black spots) and been observed inside some of the macrophages by phagocytosis.

4.5.2. Cellular cytotoxicity study with CoNPs in different time

Metallic particles were observed in macrophages through light microscopic examinations at all concentration range (1×10^9, 10^{10}, 10^{11},10^{12} particles/ml). The overall relative fluorescence units (RFU) of the cytotoxicity assay of co-culturing with CoNPs in different time (8 hours, 16 hours and 24 hours) were measured with the Neutral Red assay. The obtained data were processed with Excel software. A graph of RFU against 3 co-culturing times were plotted in Figure 4.3. A control group that THP-1 cells are cultured with PMA activation without adding CoNPs, and a blank group with only RPMI 1640 culture medium were designed for comparing with other groups. The error bars on the graph were set as the calculated stand deviations for each group.

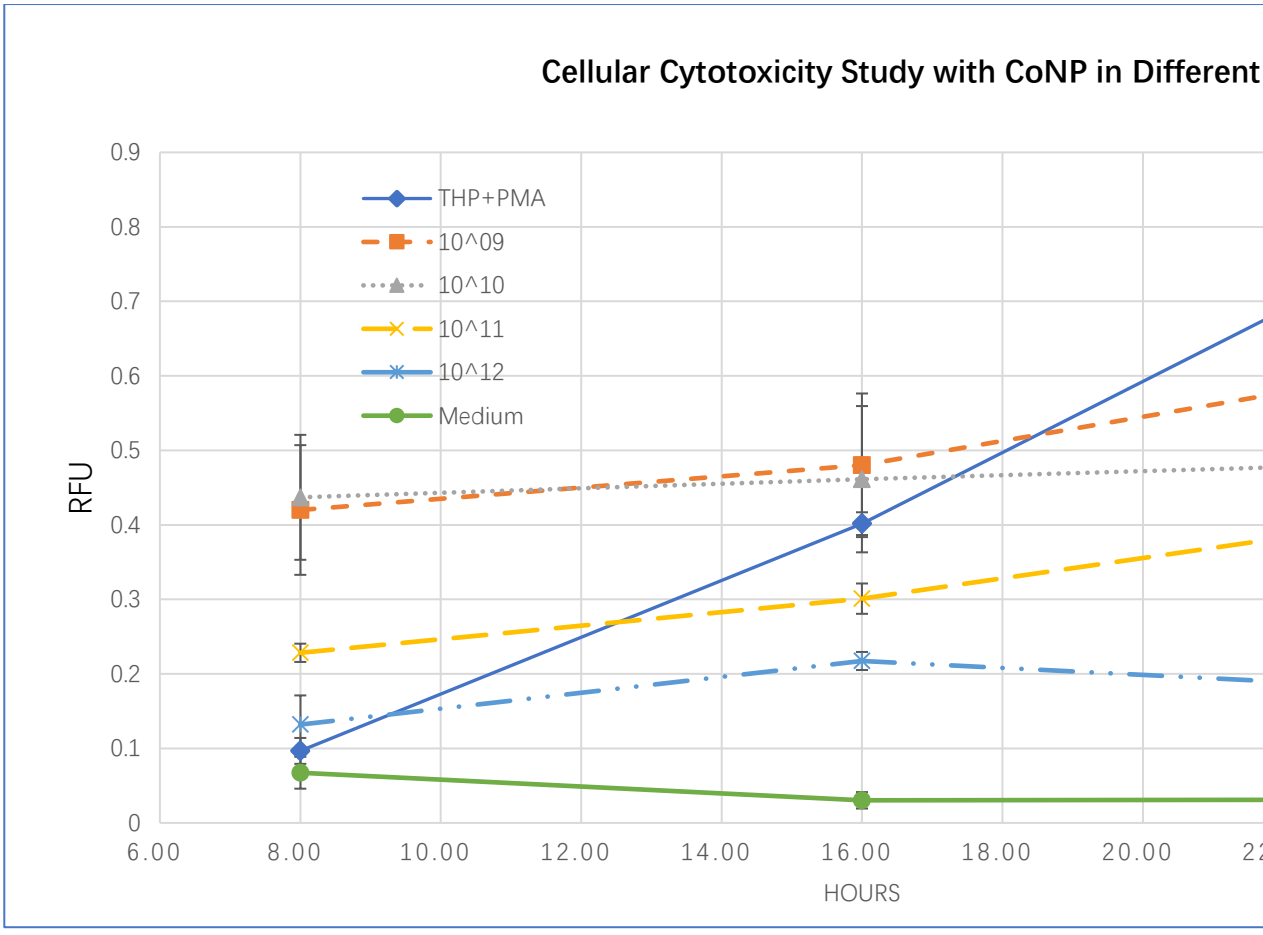

Figure 4.3 The effect of Co nanoparticles with different concentration on macrophage viability

The X-axis indicates the time of co-culturing with CoNPs (unit: hour); Y-axis indicates the relative fluorescenc
graph indicates the control group without CoNPs added (0 particles/ml). The '10^12', '10^11', '10^10' and '10
culture with CoNPs at different concentration (1 x 10^9, 10^{10}, 10^{11},10^{12} particles/ml). 'Medium' icon indicates the b

The comparisons of control group against low concentration of Co nanoparticles group (1×10^9 particles/ml) and high concentration of Co nanoparticles group (1×10^{12} particles/ml) were selected from Figure 4.4 and replotted in Figure 4.4 with statistical analysis in order to make the comparison more clearly. Two-way ANOVA method was applied to compare the difference between each group at different co-culturing time (8, 16 and 24 hours).

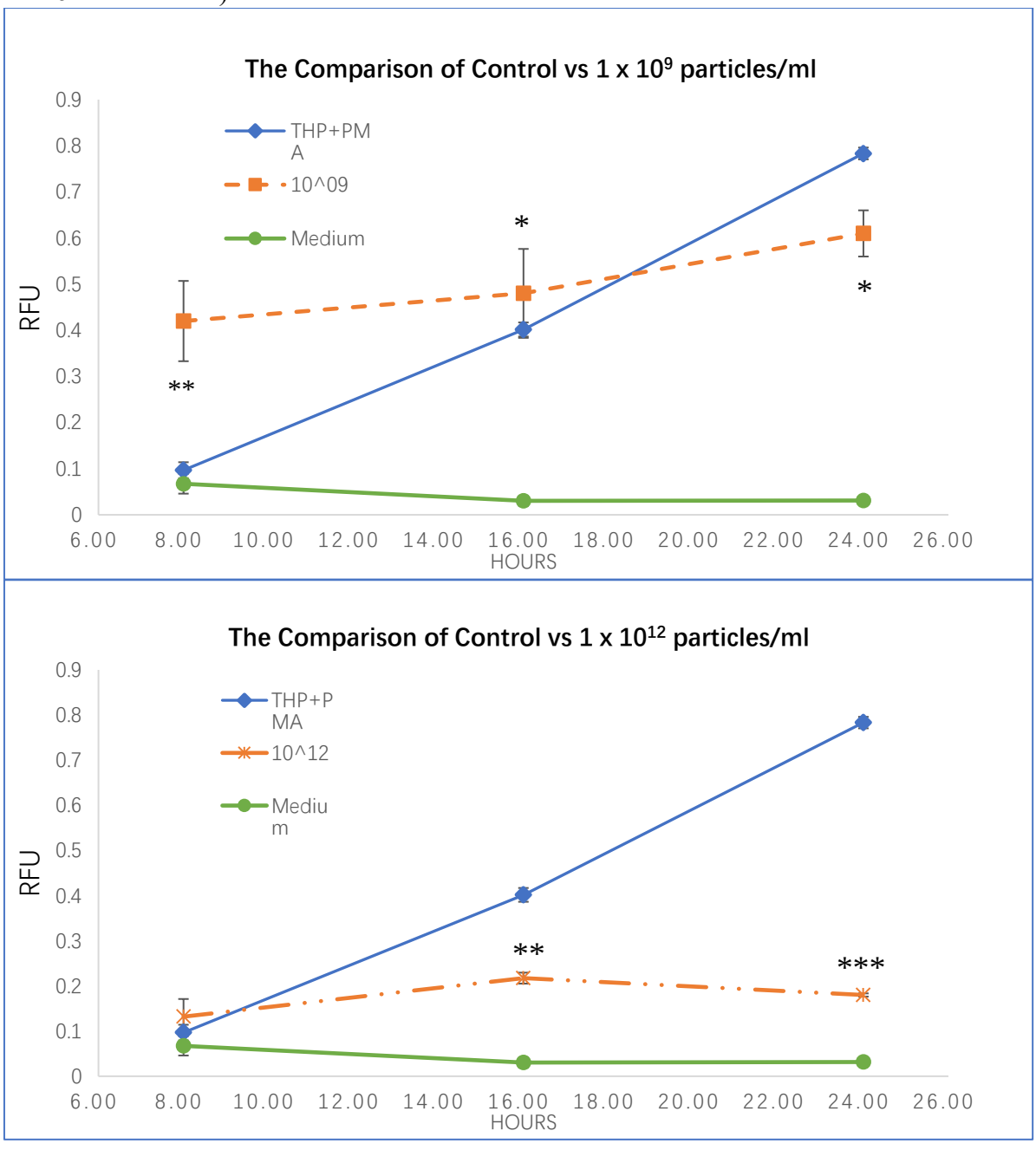

Figure 4.4. The effect of metal nanoparticles on macrophages with two concentrations (1×10^9 and 1×10^{12} particles/ml). Asterisk (*) indicates $p < 0.05$ against the control group (THP+PMA). Error bar: stand deviation.

Figure 4.4 demonstrates that the CoNP group with low concentration ($1x10^9$ particles/ml) begins to show significant difference at 8 hours (**), and the difference is decreasing with time. On the contrary, non-significant difference has been found at 8 hours in the CoNP group with high concentration ($1x10^{12}$ particles/ml), but a striking difference has been found at 24 hours (***) when comparing with control group.

4.5.3. Cellular cytotoxicity study with different nanoparticles treatment

The overall relative fluorescence units (RFU) of the cytotoxicity assay of co-culturing with three different nanoparticles (Co, Cr, Ti) and the combined Co Cr and Ti nanoparticles with same amounts (Mix) were measured with the Neutral Red assay. Altered concentrations (1×10^9, 10^{10}, 10^{11},10^{12} particles/ml) of metallic nanoparticles were applied to compare the continuously changing. The obtained data were processed with Excel software. A graph of RFU against 3 co-culturing times were plotted in Figure 4.6.

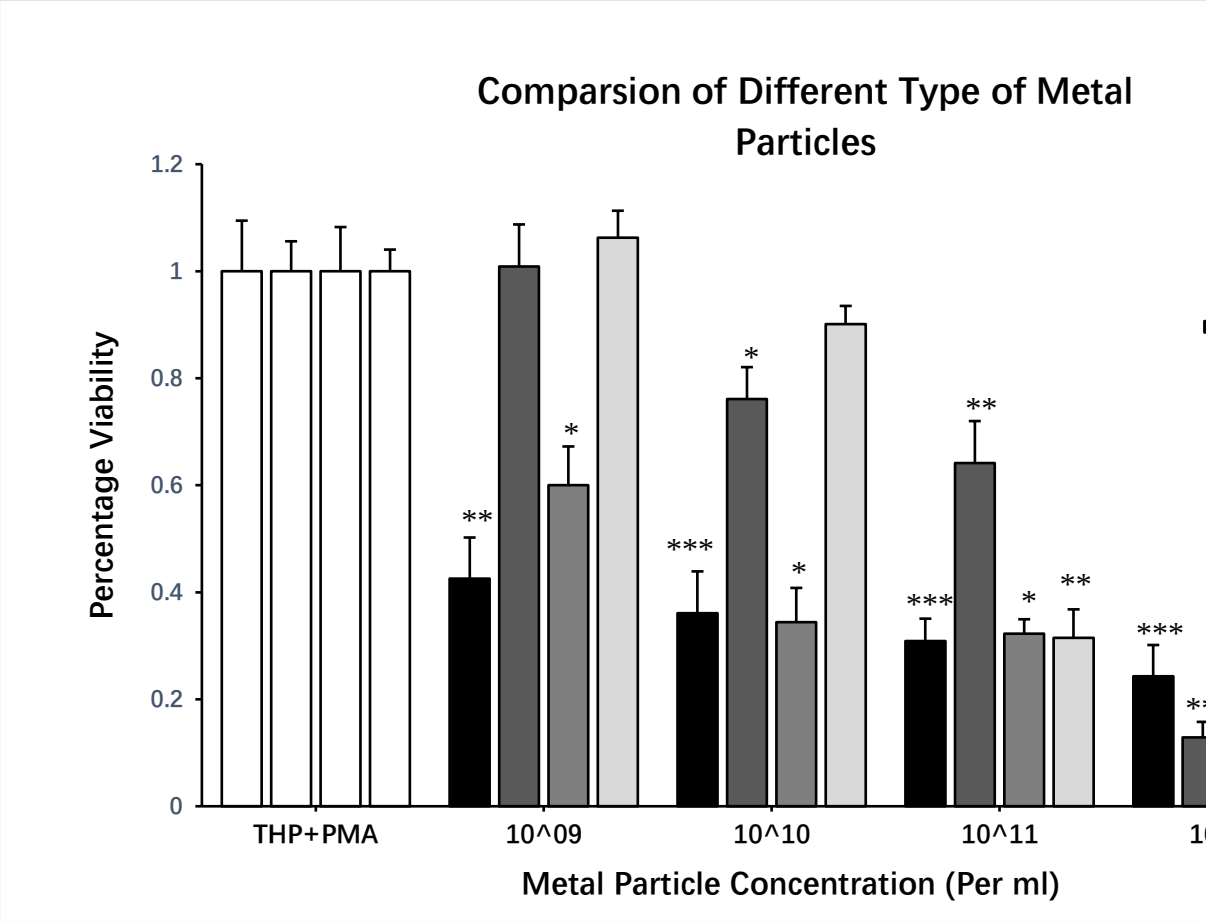

Figure 4.5. The effect of different types metal nanoparticles with different concentration

The X-axis indicates different concentrations of added metal nanoparticles; Y-axis indicates the percentage v
against the control group. Error bar: stand deviation.

A control group that THP-1 cells are cultured with PMA activation without adding CoNPs, and a blank group with only RPMI 1640 culture medium were designed for comparing with other concentrations. The '10^12', '10^11', '10^10' and '10^09' on the graph indicate the cell culture with CoNPs at different concentration (1×10^9, 10^{10}, 10^{11},10^{12} particles/ml). 'Medium' indicates the blank group. The error bars on the graph were set as the calculated stand deviations for each group. The obtained data have statistical analysed with 'Graph Pad' software to compare the difference between each group. One-way ANOVA method with Kruskal-Wallis test was applied for the inter-group comparisons. Differences at $p< 0.05$ were significant.

According to Figure 4.6, it is found that the overall trends in each metal nanoparticle group are the same when compared with control group, which is the relative fluorescence units RFU reducing with the increased concentration of metal nanoparticles. The 'Mix' group shows higher significant differences, at all particle concentrations, than other single metal groups when comparing with control group. Whereas the Cr group shows the lowest differences amongst the four metal nanoparticle groups.

Compared to the control group (no nanoparticles added group), the Neutral Red assay shows non-significant reductions in the relative fluorescence units in Cr and Ti groups at low concentration ($1x10^9$ particels/ml) and significant difference have been observed in the Co groups at low concentration ($1x10^9$ particles/ml) on the graph. The 'Mix' group starts to show significant difference （**） from the $1x10^9$ particles/ml concentrations when comparing with control group ($p<0.05$).

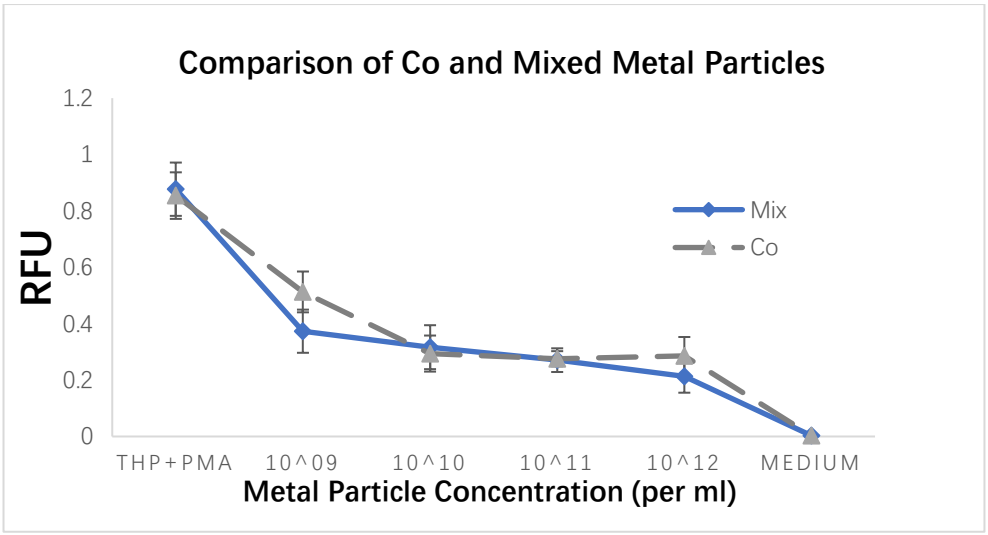

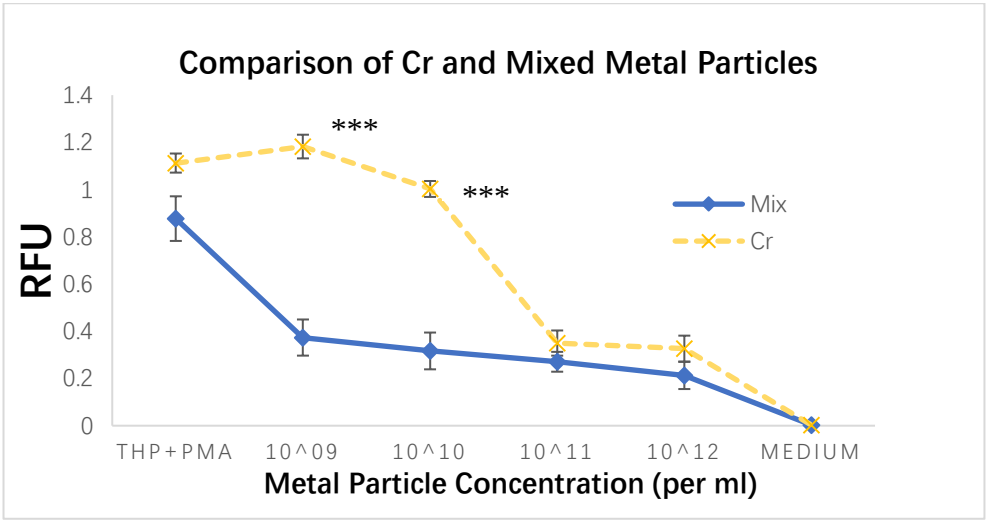

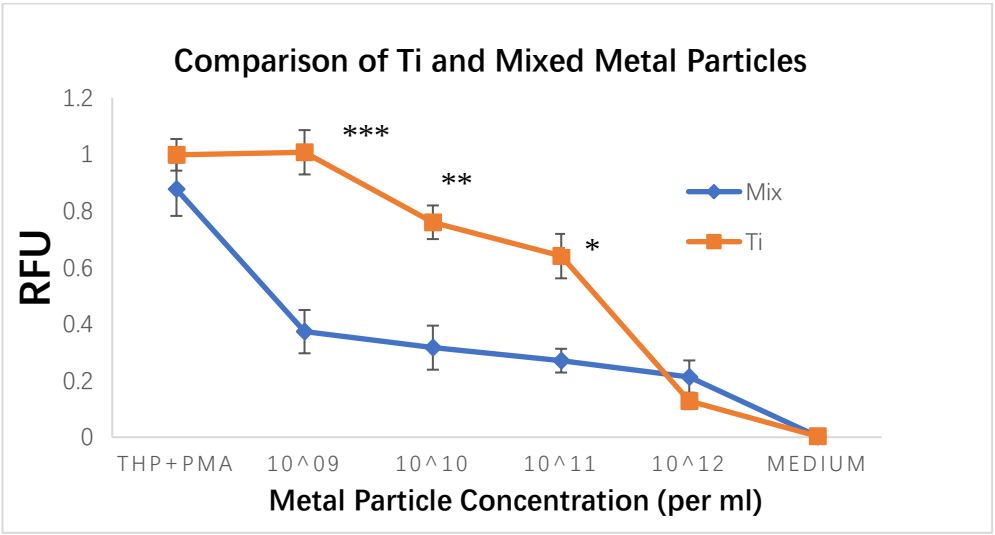

Figure 4.6 The cytotoxicity effects of different types of metal nanoparticles compared with mixed metal nanoparticles. Asterisk (*) indicates $p < 0.05$ against the 'Mix' group (added combined Co Cr and Ti nanoparticles with different concentrations). Error bar: stand deviation.

The comparison of different metallic nanoparticle groups against the mixed metal particles group with combined Co Cr and Ti nanoparticles (Mix group) are shown in Figure 4.6. Regular two-way ANOVA method was applied to compare each metal group to the 'Mix' group. Significance level was set at 0.05 (95% confidence intervals).

Compared to the 'Mix' group, the Neutral Red assay shows non-significant difference in the Co group. There was a striking difference between Mix and Cr, and Ti groups at low concentration of nanoparticles ($1x10^9$ and $1x10^{10}$ particles /ml). Whereas the significant differences are reducing with increased concentration of nanoparticles and disappeared at high concentration of nanoparticles $1x10^{12}$ particles /ml.

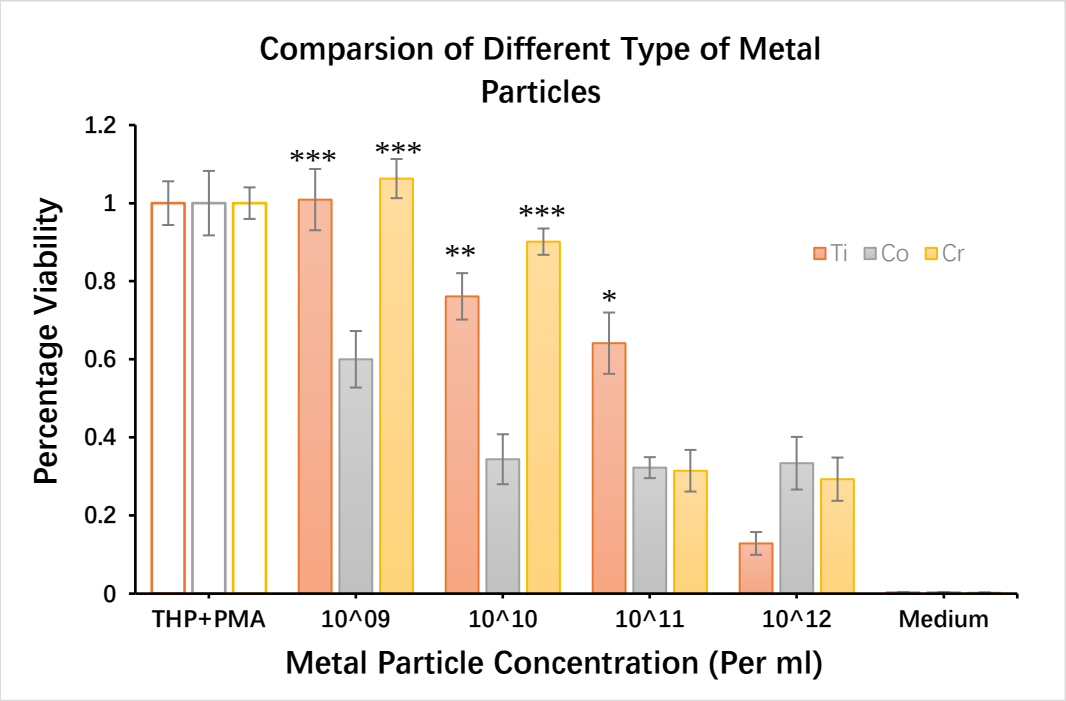

Figure 4.7. Comparison of three different types of metal nanoparticles

Asterisk '*' indicates the level of significant difference ($p<0.05$) when Ti and Cr compared with Co group respectively. And '$' indicates the level of significant difference ($p<0.05$) when Ti and Cr group compared with each other. Error bar: stand deviation.

Figure 4.7 shows the comparison of the effects of nanoparticles on the macrophages between each single type of metal particle group. Non-significant difference has been found when Ti and Cr groups compared with each other. Both Ti and Cr group indicated significant difference when comparing with the Co group at low concentration of nanoparticles ($1x10^9$ and $1x10^{10}$ particles /ml).

4.5.4. Neutral Red assay observation

In order to observe the effects of the Neutral Red solution on cells, two groups have been selected, which they are the control group (differentiated THP-1 cells without adding CoNPs) and the '10^12' group (differentiated THP-1 co-cultured with CoNPs in $1x10^{12}$ particles/ml concentration for 24 hours). Both groups were treated with the 0.33% Neutral Red solution for 2 hours in 37°C temperature with 5% CO_2. The achieved micrographs of light microscope are represented in Figure 4.8.

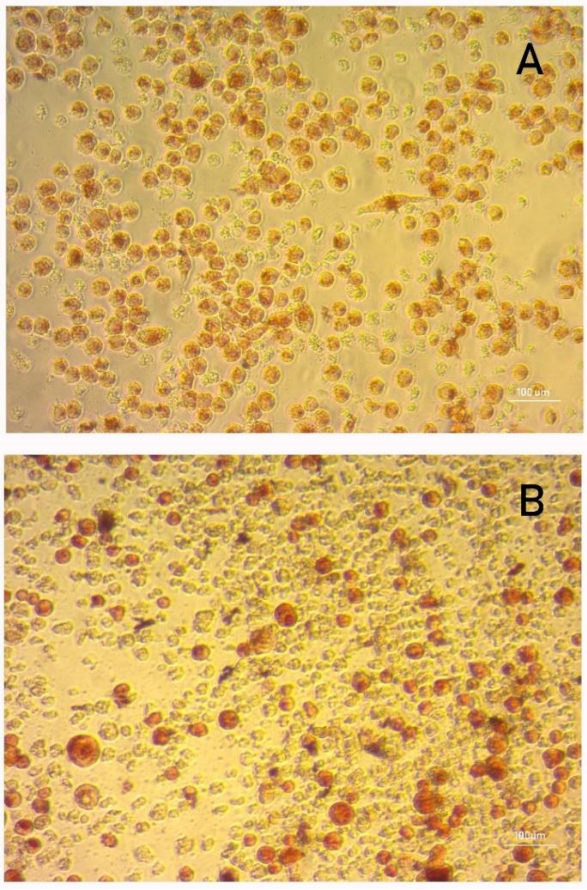

Figure 4.8. Microscopy images of Neutral Red assay

Micrographs of light microscope represent the microscopical observation after Neutral Red Treatment in two most opposite groups which are control group (A) and the highest concentration of CoNP groups ($1x10^{12}$ particles/ml) (B). Sale bar =100µm

Micrographs of light microscope in Figure 4.8. showing that most of viable cells are dyed with the Neutral Red solution. The rate of dyed cells in Figure 4.8-A are significantly higher than that in Figure 4.8-B, which means higher cells viabilities are observed in Figure 4.8-A than Figure 4.8-B. This may because high concentration of CoNPs caused adverse effects on cells and subsequent lead to cell death.

4.5.5. SEM/EDS Observation

The examinations of SEM with EDS analysis were conducted in this study to observe the distribution of CoNPs. Back-scatter electron detector (BSE) was applied to detect if CoNPs existed inside the macrophages.

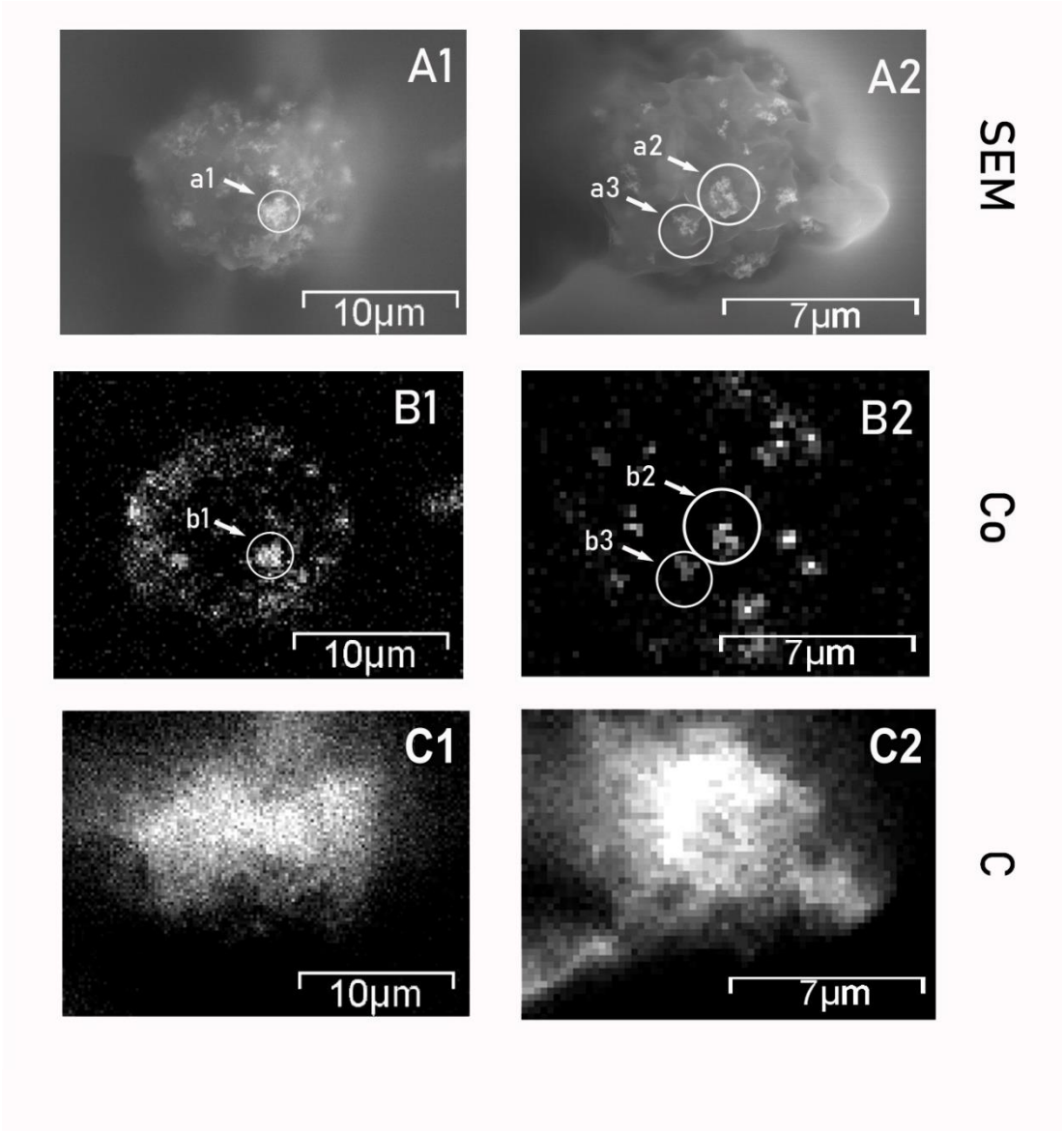

Figure 4.9. SEM/BSE Scanning with EDS analysis

Images on the first row (A1, A2) are the original SEM images with BSE detector, the remaining images are the corresponding EDS analysed images. The EDS analysis of C group (C1, C2) was used to define the outline of observed cells. Scale bar= 7μm

As is evident from Figure 4.9, Co particles have been clearly observed in the SEM/BSE images (A1, A2). The selected particles in A1 and A2 images (a1, a2 and a3) have been

detected through EDS analysis and been defined as Co element in B1 and B2 (b1, b2 and b3), which have successfully proofed the phagocytosis of metallic nanoparticles by THP-1 macrophages.

4.6. Discussion

The important histological features of pseudotumours include the occurrence of extensive necrosis and serious macrophage infiltrate (Hasegawa, Yoshida, Wakabayashi, & Sudo, 2012; Kwon et al., 2011). The facts that Co and Cr particles have been found within necrotic macrophages or in extracellular tissue have been mentioned before in reports and researches conducted (Zhidao Xia et al., 2011). According to the previous researches, it is suggested that the metallic particles involved cytotoxic effect on macrophages may be one of the key reasons of the generation of pseudotumours. However, limited previous researches have also studied the biological responses of clinically relevant metallic nanoparticles such as Co, Cr and Ti on macrophages in vitro. Moreover, the mechanisms of these metallic particles involved potential cytotoxic effects are yet to know.

In 2007, the research of detecting the cytotoxic effects of CoCr alloy nanoparticles on fibroblasts have been reported (Papageorgiou et al., 2007). The research reported that nanometre-sized metal particles caused more damage to the cells than ceramic particles and microparticles, and subsequently suggested that the wear particles involved biological responses of human cells may be fundamentally different, which depend on the particle size and materials in vitro. In this study, the biological responses of similarly-sized metallic nanoparticles with different element components have been studied, which provided more information to the understanding of the metallic particles involved biological responses to human cells.

A dose-dependent cytotoxicity study was conducted in 2009 to investigate the biological responses of clinically relevant Co nanoparticles on macrophages in vitro (Kwon et al., 2009). This research has quantified the cell viability with Alamar Blue assay and Live/Dead assay. Moreover, the dose-dependent cytotoxic effects of Co nanoparticles on macrophages have been reported. This report suggested that the

cytotoxicity was only observed with cobalt, and high concentrations of Co nanoparticles may be one of the key factors causing pseudotumours. The study in this chapter has applied a new method to quantify the cell viability which is the Neutral Red assay. The cytotoxicity of both Cr and Ti nanoparticles at high concentration (1×10^{12} particles/ml) were detected in this study which is different than previous research Figure 4.6. In addition, the mixed metal nanoparticles with the same amounts of Co Cr and Ti have shown the highest cytotoxicity effects when compared with other single-element nanoparticles. Furthermore, the cytotoxicity effects of mixed metal nanoparticles have already been observed at low concentrations ($1x10^9$ and $1x10^{10}$ particles /ml). The trend of cytotoxicity effects in the mixed metal nanoparticle group is very close to the trend of Co nanoparticle group (Figure 4.7). Therefore, it postulates that mixed metal nanoparticles cause more damages to the cells than one kind of metallic nanoparticles. In addition, Co is likely to be the key element in the mixed metal nanoparticle group that cause cytotoxicity effects.

Phagocytosis of metallic particles by macrophages from differentiated THP-1 were suggested by microscopical observation. Co particles have been detected inside the macrophages with phagocytosis according to Figure 4.2 and Figure 4.9, which are consistent with previous researches (Allen, Myer, Millett, & Rushton, 1997; Catelas, Petit, Zukor, & Huk, 2001). The hypothesise that low concentration of CoNPs ($1x10^9$ particles /ml) is likely to activate the phagocytosis by macrophages established in this study (Figure 4.5). Neutral Red is incorporated into lived cells to stain their golgi apparatus and lysosomes in histology (Seth, Yang, Choi, Sabean, & Roberts, 2004). The existence of low concentration CoNPs may cause the activation of immune reactions such as phagocytosis and antigen presentation (Revell, 2008). Therefore, the neutral red uptake is enhanced with the phagocytosis by macrophages which corresponds to higher RFU shown in the graph than control group at low concentration of CoNPs in Figure 4.5 ($1x10^9$ particles /ml).

In conclusion, metallic nanoparticles are proved to causing dose-dependent cytotoxic

effects on macrophages in vitro. The increased cytotoxic effects on macrophages in vitro are related to higher concentration of these metallic nanoparticles and longer co-culturing time. Metallic nanoparticles at low concentration such as $1x10^9$particles/ml shows a slightly higher RFU than non-nanoparticle groups in vitro, this may be because of these metallic nanoparticles are able to stimulate the phagocytosis of macrophages. In addition, single type of metallic particles causes less cytotoxic effect than multi-types of nanoparticles in vitro, which can be inferred that more serious toxic-effects occurred in patients' body with implant failures as more complicated environment in vivo. Therefore, cytotoxicity of high concentrations of metallic nanoparticles phagocytosed by macrophages located in the tissue around periprosthetic is regarded as one of the key reasons that cause series of adverse biological responses such as pseudotumours.

The study in this chapter focused on the cytotoxicity effects upon cells rather than the histological mechanism. More studies about the underlying mechanism are put forward to provide additional information regarding the metal particles involved cytotoxicity effects in future study.

Chapter 5 Hypoxia Inducible Factor 1α (HIF-1α) in Cobalt Nanoparticle Induced Cytotoxicity

5.1. Introduction

According to previous studies, it is known that some metal-on-metal (MoM) designs are results of some early failures, which may be attributed to the excessive exposure to metal debris released during wear (Samelko et al., 2013). In MoM hip replacements the body's innate immune system can react to metal debris at the bearing surfaces, which can cause an adverse reaction to metal debris (ARMD) (O Lainiala et al., 2014; D. Langton et al., 2011; Zhidao Xia et al., 2011)

Cobalt (Co) is one of the main components of metal hip prostheses (Kwon et al., 2009) and cobalt nanoparticles (CoNPs) produced from wear can be toxic to the cells (L. O. Simonsen, H. Harbak, & P. Bennekou, 2012). The produced CoNPs are associated with several adverse conditions such as inflammation, bone lyses and cytotoxicity at high concentrations as mentioned in Chapter 2. Furthermore, the released cobalt ions from hip implants during wear and tear result in macrophage infiltration, phagocytosis, necrosis and apoptosis with consequent inflammation and tissue mass formation such as pseudotumor (Catelas et al., 2005; Kwon et al., 2009; Zhidao Xia et al., 2011). It has been reported that cobalt ions act as a hypoxia mimic in cell culture and stimulates the production of hypoxic signalling by stabilising hypoxia inducible transcription factor 1α (HIF1α) (A. Vengellur & J. J. LaPres, 2004). However, the underlying mechanism and if this process plays a role in MoM THA related cytotoxicity is not fully understood.

Hypoxia is defined as a state when oxygen tension drops below normal limits (Ke & Costa, 2006), but cobalt activates HIF1α when the oxygen levels in the environment are normal (Caicedo, Samelko, McAllister, Jacobs, & Hallab, 2013). HIF1α is stabilised, translocated to the nucleus and dimerized with the constitutively expressed

HIF1α to elicit the transcription of target genes necessary for increased oxygen demand (red cell production and angiogenesis), cell survival (growth factors) and paradoxically apoptosis (proteins within cell death pathway) depending on the environment (Ke & Costa, 2006; A. Vengellur & J. LaPres, 2004).

5.2. Hypothesis

HIF1α plays an important role in CoNP-induced cellular cytotoxicity in THP-1 macrophages in vitro.

5.3. Aim of Study

The Aim of this study is to investigate that if CoNP will increase HIF 1 α accumulation and cytotoxicity; also, to knock out HIF 1 α expression in THP-1 cells will reduce CoNP induced cytotoxicity

5.4. Materials and Methods

5.4.1. Cell culture

THP-1 macrophage cell line was recovered from liquid nitrogen stock and cultured in RPMI1640 with glutamax (Gibco BRL, Invitrogen Ltd, Paisley, UK) supplemented with 10% foetal bovine serum (FBS; Labtech International, UK) and penicillin / streptomycin (Gibco, BRL, Invitrogen Ltd, Paisley, UK) at a seeding density of 3 x 10^4 cells per ml in a 10 cm diameter tissue culture dish. Cells were sub cultured at 1:10 dilution weekly twice to maintain stocks. THP-1 cells were differentiated to macrophages by incubating in the medium containing 50 nM phorbol 12-myristate 13-acetate (PMA, Sigma-Aldrich, UK) for 72 hours.

5.4.2. Cobalt Nanoparticles (CoNPs)

The same kind of CoNPs with exactly same process methods as Chapter 4 was used here.

5.4.3. RNA interference of HIF1α and detection

Three groups were set in this part of study (Control, Neg siRNA and HIF siRNA). The details of these three comparing group are shown in Table 5.1. Total HIF1α was measured in cell lysates from CoNP induced and control macrophages using the Human/Mouse Total HIF1αDuoset® IC ELISA (R&D Systems) as per manufacturer's instructions.

Table 5.1. HIF1α and Neg siRNA dilution

	Opti-MEM	SiRNAs	Lipofectamine
Lipofectamine Control	500 ul	0	7.5 ul
Neg siRNA	500 ul	5 ul	7.5 ul
HIF siRNA	500 ul	5 ul	7.5 ul

siRNAs targeting human HIF1α were used to silence HIF1α (Silencer® select siRNA from Applied Biosystems, Ambion, UK) expression. HIF1α targeted or mismatched negative siRNA (10μM) was mixed with Opti-MEM (Gibco BRL, Invitrogen Ltd, Paisley, UK) and Lipofectamine RNAiMax transfection reagent (Invitrogen™ life Technologies, UK) inside individual wells of a 6 well plate and incubated for 5 minutes at room temperature to allow the transfection reagent to complex with the siRNA. The plate design of the SiHIF-1α and Neg siRNA dilution is showing in Table 4.2.

Table 5.2. SiRNA transfection plate design

Plate 1	1	2	3
A	Control 10^{12}/ml CoNP	Neg siRNA 10^{12}/ml CoNP	HIF siRNA 10^{12}/ml CoNP
B	Control 10^{11}/ml CoNP	Neg siRNA 10^{11}/ml CoNP	HIF siRNA 10^{11}/ml CoNP
Plate 2	1	2	3
A	Control No CoNP	Neg siRNA No CoNP	HIF siRNA No CoNP
B			

Subsequently, undifferentiated THP-1 cells (9 x 10^5/ well) in RPMI containing 10%FBS and P/S were added to each well containing the siRNA complexes to a total volume of 3ml (17nM siRNA). A transfection control with no siRNA was run alongside.

Cells were incubated for 24 hours before being activated by 50 nM PMA for 24 hours. Cells were subsequently treated with 10^{12}CoNP/ml for 24 hours before being solubilised in ice-cold RLT lysis buffer (Qiagen, from RNeasy® Plus Mini Kit, UK). The lysates were homogenised using a 25G needle and syringe and centrifuged at 14,000 rpm for 10 minutes. The supernatant was removed, and the collected samples are stored at -70°C before use. Protein was quantitated using the bicinchoninic acid kit (Sigma Aldrich, BCA1-1KT, UK) assay as per manufacturer's instructions. Four groups of sample dilution were set with different dilution ratios of samples (1, 1/2, 1/5, 1/10). The plate design of protein quantitation is showing in Table 5.3. Bovine serum albumin (BSA) was used as the protein standard.

Table 5.3 Protein quantitation plate design

	1	2	3	4	5	6	7	8	9
A	1mg/ml		Control 10^{12}/ml CoNP		HIF SsiRNA No CoNP		Neg siRNA No CoNP		Cont
B	0.8mg/ml		Neg siRNA 10^{12}/ml CoNP		Control 10^{12}/ml CoNP		HIF siRNA No CoNP		Neg
C	0.6mg/ml		HIF siRNA 10^{12}/ml CoNP		Neg siRNA 10^{12}/ml CoNP		Control 10^{12}/ml CoNP		HIF si
D	0.4mg/ml		Control 10^{11}/ml CoNP		HIF siRNA 10^{12}/ml CoNP		Neg siRNA 10^{12}/ml CoNP		Cor
E	0.2mg/ml		Neg siRNA 10^{11}/ml CoNP		Control 10^{11}/ml CoNP		HIF SiRNA 10^{12}/ml CoNP		Neg s
F	0mg/ml		HIF siRNA 10^{11}/ml CoNP		Neg siRNA 10^{11}/ml CoNP		Control 10^{11}/ml CoNP		HIF s
G			Control No CoNP		HIF siRNA 10^{11}/ml CoNP		Neg siRNA 10^{11}/ml CoNP		Cor
H			Neg siRNA No CoNP		Control No CoNP		HIF siRNA 10^{11}/ml CoNP		Neg s

The first two columns are standard with different concertation. Different colours were used to distinguish these samples (blue: 1, pink 1/2, yellow 1/5, green 1/10).

The group that best fits the standard curve (in the exponential phase of the curve) was selected to set up the HIF-1α ELISA experiment after the protein quantitation, and 40ug protein was subsequently used for the ELISA.

The procedures of HIF-1α ELISA are showing below:

i. Dilute capture antibody 1:180 in PBS and add 50µl per well in the 96-well cell culture plate. Seal the late and incubate overnight in the incubator.
ii. Aspirate and wash with 150µl wash buffer three times. Bang the plate on blur towel after each wash to remove any remaining wash buffer.
iii. Add 150µl reagent diluent to each well and incubate for 1 hour.
iv. Add 50µl sample or standard (in reagent diluents) to each well using reagent diluents as the zero standard. Cover plate and incubate for 2 hours on plate shaker at room temperature.
v. After wash with wash buffer 3 times, the detection antibody was diluted 1:36 in reagent diluent and then add 50ul to each well. Cover with new plate sealer and incubate for 2 hours at room temperature.
vi. After wash 3 times, the streptavidin-HRP was diluted 1:200 in reagent diluent, and then add 50µl to each well and incubate for 20 minutes at room temperature.
vii. After wash 3 times, 50µl substrate solution was added into each well and incubate for roughly 20 minutes at room temperature with avoiding the direct light.
viii. 50µl l stop solution was added into each well and tap plate to ensure thorough mixing.
ix. The optical density of each well was determined using the POLARstar Omega plate reader with wavelength 450 nm and wavelength correction at 540 nm.

5.4.4. Cytotoxicity Studies with Neutral Red Assay

The CoNPs induced cellular cytotoxicity was assessed in THP-1 macrophages using the Neutral Red assay. Four groups have been set in this part of study, the plate design is shown in Table 5.4. After completed the transfect dilution, cells were seeded into 96 well plates at 1x 10^4 cells per well and incubated for a further 24 hours with 50nM PMA (no PMA was added in the THP-1 group). subsequently, cells were incubated with CoNP over a concentration range of 10^{11} – 10^{12}/ml for 24 hours alongside

untreated controls. After that, Neutral Rad Assy was applied with the same operation procedures as Chapter 4. A 'FLUO star Omega' plate reader was used to measure absorbance at a wavelength of 540 nm and measure the background absorbance of multi-well plates at 690 nm.

Table 5.4. Neutral Red Assay Plate Design

	1	2	3	4	5	6	7	8	9	10	11	12
A	Blank No cell						Medium Only					
B	Control No CoNP						THP-1 No CoNP					
C	Control 10^{11}/ml CoNP						THP-1 10^{11}/ml CoNP					
D	Control 10^{12}/ml CoNP						THP-1 10^{12}/ml CoNP					
E	Neg siRNA No CoNP						HIF siRNA No CoNP					
F	Neg siRNA 10^{11}/ml CoNP						HIF siRNA 10^{11}/ml CoNP					
G	Neg siRNA 10^{12}/ml CoNP						HIF siRNA 10^{12}/ml CoNP					
H												

Four groups were applied in this experiment:
Control group: differentiated THP-1 macrophages,
THP-1 group: undifferentiated THP-1,
SiRNA group: differentiated THP-1 macrophages treated with siRNAs,
Neg siRNA group: differentiated THP-1 macrophages treated with negative siRNAs.

5.4.5. Statistical analysis

Statistical comparisons were made using non-parametric statistics (Mann Whitney t-test) using Graph Pad software. Differences between groups were considered significant at $p<0.05$. Error bar =mean±standard deviation

5.5. Results

5.5.1. RNA interference of HIF1α and detection

After the protein quantitation, the 1/2 dilution group was selected to set the ELISA up as this dilution best fits the standard curve. The results of ELISA assay were processed by Excel software. A graph that shows the effects of HIF siRNA on THP-1 macrophages was plotted in Figure 5.1.

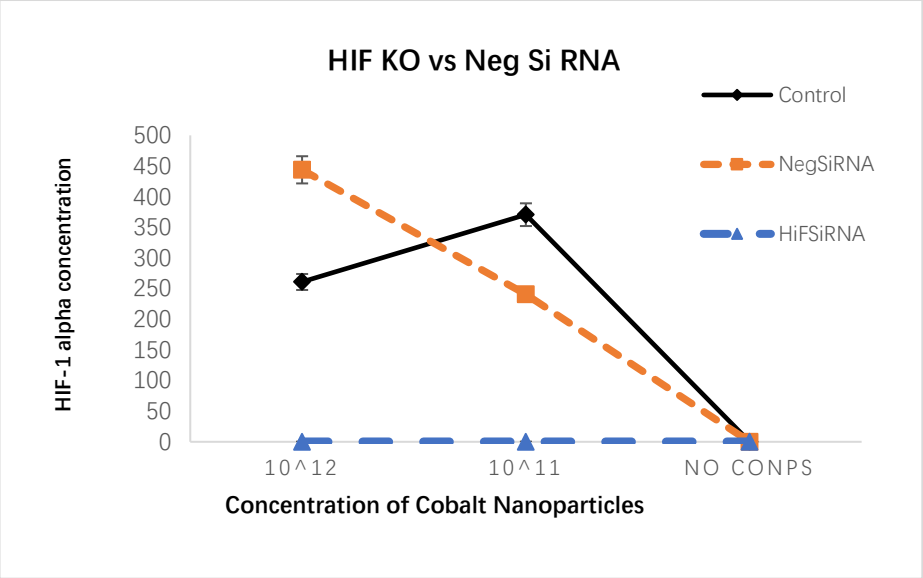

Figure 5.1. Detected HIP-1 alpha with different concentration of CoNPs

As it can be seen from Figure 5.1, no HIF α were detected in the HIF siRNA group, which indicates that the expression of HIF α was successfully silenced by siRNA. High concentration of HIF α were observed in both Control and Neg siRNA groups at high dose of CoNP treatment and disappeared without adding CoNPs. The results are consisted with previous studies that CoNPs are able to stimulates the production HIF α.

5.5.2. Cytotoxicity Studies with Neutral Red Assay

The results of the Neutral Red assay were obtained from the A 'FLUO star Omega' plate reader and subsequently been analysed with Excel software. The results are shown in Figure 5.2.

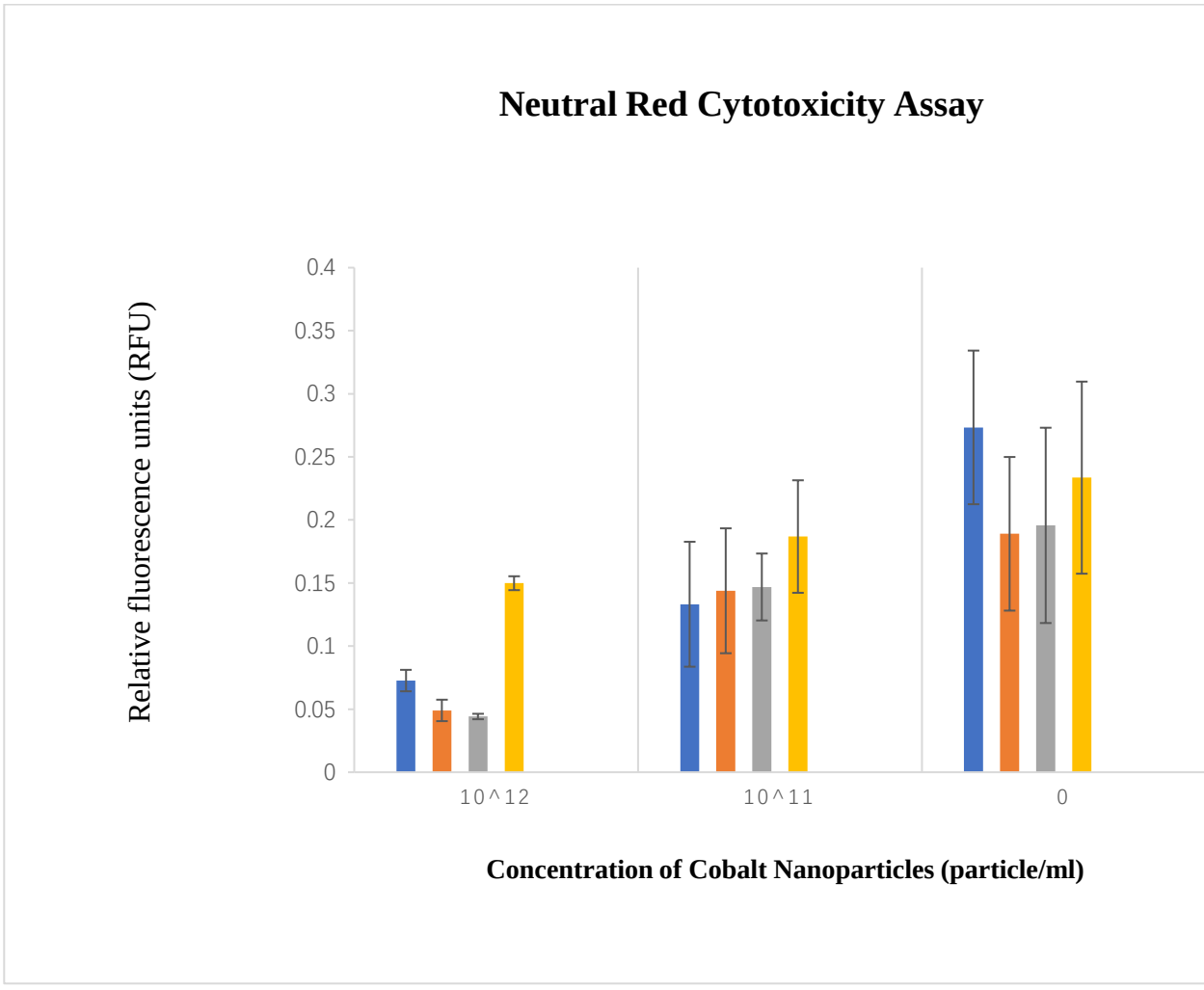

Figure 5.2. Neural Red cytotoxicity assay of different CoNPs treated grou

Figure 5.2 represents that cell viabilities are negatively affected by high concertation of CoNPs, which are consisted with previous studies. THP groups shows the most cell viability when treated with CoNP, this may because the phagocytosis of THP-1 macrophages is stronger than undifferentiated THP-1 cells. Thus, more CoNPs were phagocytized by differentiated THP-1 macrophage and subsequently leaded to more cell death. Similarly, control group represents higher cell viability than THP group without CoNP treatment as better phagocytosis of THP-1 macrophages.

In order to detect the role of HIF1α in CoNP-induced cellular cytotoxicity, further studies are needed with statistical analysis to compare the Neg siRNA, HIF siRNA and Control group. No significances were observed when three groups were treated with 10×10^{11} CoNPs or no CoPs ($p<0.05$). Whereas significances were detected when they were treated with 10×10^{12} CoNPs (Figure 5.3).

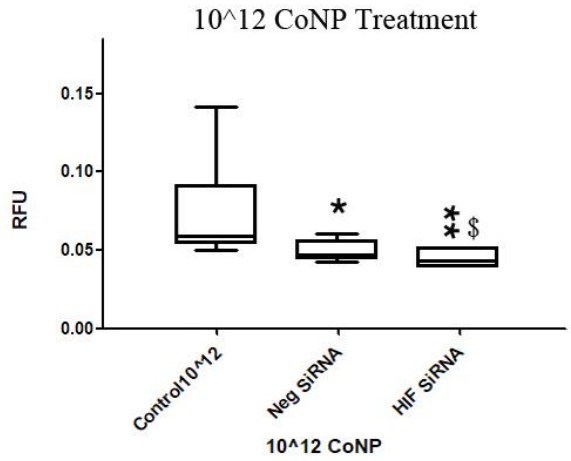

Figure 5.3. Comparison of three groups with 10×10^{12} CoNP treatment

'*' indicates the level of significant difference ($p<0.05$) when Neg siRNA and HIF siRNA compared with Control group respectively; '$' indicates the level of significant difference ($p<0.05$) when Neg siRNA and HIF siRNA compared with each other.

According to Figure 5.3, both HIF SiRNA and Neg SiRNA group present significant difference when compared with Control group (siRNA **, Neg siRNA when $p<0.05$) at high dose of CoNP treatment (10×10^{12} per ml). Also, HIF siRNA shows significant difference ($, $p<0.05$) when compared with Neg siRNA. The obtained results were

consisted with most of expected results except that no significant difference was expected to be observed when Neg siRNA compared with Control ($p<0.05$).

5.6. Discussion

It is confirmed that CoNPs are toxic to macrophages in this study, which is consist with previous reports (A. J. Hart et al., 2012). However, the mechanism of the CoNP-induced cytotoxicity is not fully understood. there is still debate as to whether CoNP or solubilised cobalt ions are the causative agent of cell toxicity.

Toxicological studies reported that metal nanoparticles inside some of the macrophages by phagocytosis are not digested by enzymes, but will be corroded by the acidic environment with the subsequent release of Co ions(Xia & Triffitt, 2006), which causes the increasing of reactive oxygen species (ROS) production and leads to induce programmed cell death or necrosis (Karlsson, Gustafsson, Cronholm, & Möller, 2009).

Cobalt ions play a key role in the HIF1α mediated pathway as shown within THP-1 macrophages during this study, which is consisted with related research (Lars Ole Simonsen, Henrik Harbak, & Poul Bennekou, 2012). The released Co (II) ions are able to increase HIF1α activity and inhibit the proteasomal degradation of HIF1α by HIF-α-prolyl-4-hydroxylases (Ziello, Jovin, & Huang, 2007). Therefore, the accumulation of HIF1α is affected by cobalt ions and subsequently cause hypoxia molecular pathway while the oxygen levels in the environment are normal, which may potentially result in pseudotumor related tissue reactions such as cell metabolism, cell proliferation, angiogenesis, inflammation and apoptosis (Saini et al., 2010).

Therefore, the potential mechanism of CoNP induced cytotoxicity is shown in Figure 5.4.

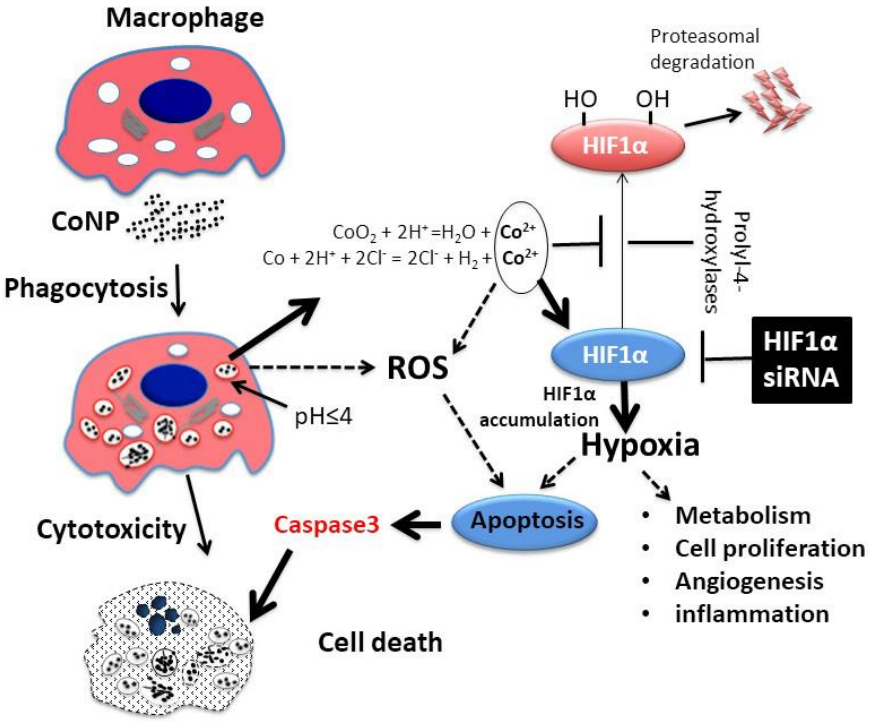

Figure 5.4. The potential mechanism of CoNP induced cytotoxicity

As the CoNP-induced cytotoxicity is increasing with HIF1 in THP-1 macrophages, we aimed to determine if the increase in HIF1α is the main reason that results in apoptosis and cell death. HIF1α has been reported that it plays a complex but important role in apoptosis by regulating the expression of genes involved in either activating or inhibiting the cell death cascade (Ke & Costa, 2006). The results showed that high dose of CoNPs correlated with a high concentration of HIF1α and low cell viabilities. The suggestion therefore would be that the CoNP-activated HIF1α may have a direct role in initiating apoptosis. However, the negative mismatched control siRNA group showed difference when compared with control although it showed difference to the HIF siRNA in this study. The exact role HIF1α plays in apoptosis is not fully confirmed. It is known that the role of HIF1α is varied depending on different environmental

factors such as resisting apoptosis in the cells of solid tumours (Greijer & Van der Wall, 2004) and resistance to hypoxia induced apoptosis in pancreatic cells (Akakura et al., 2001). In this study, HIF1α was conformed to responsible, at least in part, for the CoNP-induced cytotoxicity.

In conclusion, HIF1α accumulation is affected by cobalt treatment when oxygen levels in the environment are normal. Also, accumulation of HIF α is one of the related factors in CoNP-induced cellular cytotoxicity in THP-1 macrophages. Further investigation is suggested to detect the exact role HIF1α plays in CoNP-induced apoptosis and cell death.

Chapter 6 Assessment of THP-1 Cell Mediated Bio-Corrosion

6.1. Introduction

The results in previous chapters (chapter 4 and chapter 5) have indicated that metallic nanoparticle have dose-dependent cytotoxic effects on human macrophages in vitro. Thus, how to reduce the generation of metallic particles from implant prostheses has become an important question for the improvement of these implant prostheses. Over the last decades, researchers are looking for ideal metal alloy prostheses which contain good biocompatibility and optimal mechanical characteristics. (Long & Rack, 1998)

However increased clinical reports showed the continuously improved prostheses still tendency to corrode and produce metal nanoparticles and ions when exposed to a physiological environment.(Nadim James Hallab et al., 2005) Metallic nanoparticles have been observed in clinically retrieved tissues from patients with implant failures.(Urban et al., 2000) In addition, elevated concentrations of metal ions have been measured in the body fluids and distal organs of these patients.(Savarino et al., 2002; Urban et al., 2000) The biological mechanism behind the corrosion inside the human body and the interaction between human cells and implant prostheses is still not fully understood.

Some research mentioned that the generation of the metal wear particles are responsible for severe hypersensitivity and inflammatory responses of cells such as macrophages. (Bauer, 2002; Voggenreiter et al., 2003) Another research demonstrated that titanium metal ions can induce the osteoclast precursors differentiated into mature osteoclasts which leads to bone resorption and effective metal corrosion. (Cadosch, Chan, Gautschi, Meagher, et al., 2009) However, direct evidence of metal corrosion by human cells has been missing to date. It is suggested that the presence of electrochemical response at the cell-metal interface lead to bio-corrosion and producing metal ion. Moreover, it has been debated whether human cells such as macrophages are able to corrode metal when contact with these metal surfaces.

White-light interferometry (WLI) is one of the proven optical measurement techniques for recording 3-D structures with depth resolution in the range of nanometre. This technique is widely used in the determination of step heights on the sample surface, the characterisation of surfaces with different roughness values, and the precise measurement of curved surfaces. The measured data of surface are acquired and processed in parallel, and the information of height can be collected over a large range in a very short time. (Thomas, 2017)

6.2. Hypothesis

- THP-1 macrophages are able to directly corrode the surface of stainless steel 316L slice and produce absorbed pits on the metal surface.

- Electrochemical response exists when THP-1 macrophages interacting with metal surface (surgical titanium and stainless steel 316L) and leads to releasing metal ions and voltage changing at the cell-metal interface.

6.3. Aim of Study

The aims of this study were firstly, to investigate whether THP-1 macrophages can directly corrode biomaterials such as surgical stainless steel 316L slices. Secondly, to initiate a new method to assess biological responses of macrophage mediated metal corrosion on surgical titanium slices and SS metal slices.

6.4. Materials and methods

6.4.1. Metal Foil Process

An experiment was designed to detect the THP-1 macrophages involved metal corrosion on the stainless-steel (SS) metal foil surface. Clinically applied stainless-steel 316 foils (Cr 16.4%, Ni 10.12%, Mo 2.06% and Fe Balance) with 0.1mm thickness were purchased from Advent Research Materials (FE694608, Oxford, UK). The stainless-steel (SS) foils were cut into 1cm^2 area circular shape and subsequently been washed with detergent and sterilized in 70% ethanol and rinsed with phosphate buffered saline (PBS).

After been soaked in RPMI1640 culture medium for 30 mins, the processed metal slices were put in a 24-well cell culture plate (Greiner CELLSTAR, M8937-100EA, UK). THP-1 cells were seeded on these processed SS slices in 24-well cell culture plate (1×10^5/well) with RPMI1640 medium supplemented with 10% FBS and P/S. Cells were incubated for 24 hours before being treated by 50 nM PMA. The control group with untreated THP-1 cells was run alongside. The culture medium was changed every three days and the whole incubation period was 14 days at 37 °C, humidified, 5% CO_2 environment.

SS metal slices were removed from the 24-well cell culture plate after 14-days incubation and subsequently been soaked in 10% Triton X-100 (Sigma Aldrich, 9002-93-1, UK) distilled water for 24 hours after been washed with deionized water 3 times. After that, these metal slices were cleaned with sonication for 10 times (2minutes each time with 50% pulse). The slices were left to dry in air for SEM scanning after being washed with deionized water three times.

A developed experiment was designed to compare the difference before and after seeding THP-1 macrophages on the stainless-steel (SS) metal substrate at same area. Same 01.mm SS foiled was applied and been cut into 1cm^2 area circular shape. The 1mm x 1mm 'hash symbols' were marked on the surface of these metal slices with a carbon steel surgical blade (Zoro, ZT1197217X, UK). These SS slices were washed

and sterilized with the same method as last experiment. THP-1 cells were seed on these metal slices in 24-well cell culture plate (1×10^5/well) with RPMI1640 + 10% FBS and P/S at 37 °C temperature with 5% CO_2 environment. Cells were treated with 50 nM PMA after 24 hours incubation. Untreated cell group was set as control. The SS slices were removed from cell culture plate after 14-days incubation and been processed with same procedure as before to wash off the cells and ready for SEM observation.

6.4.2. SEM Observation

SEM analyses were performed for observing the surfacing changes on stainless-steel metal foil before and after incubation of THP-1 macrophages in Swansea University. SEM images with different magnifications ($1x10^4$, $3\ x10^4$ and $5x10^4$) were obtained for the first experiment (accelerating voltage = $5\ x10^3$ volt). In addition, the obtained SEM images for the developed experiment (accelerating voltage = $1x10^4$volt, magnification = 500) were processed with 'Photoshop' software to stitch into a completed image to show the whole area of the marked hash symbol.

6.4.3. White Light Interferometry (WLI) Roughness testing

The white light interferometry (WLI) was applied to detect the roughness changes on stainless-steel (SS) metal substrate before and after seeding THP-1 macrophages. Stainless-steel foils were cut into $1cm^2$ area circular shape. Numbers were marked at back of these slices and metal surfaces were subsequently cleaned with detergent in an ultrasonicator, rinse in deionized water 3 times then washed with 70% ethanol for three times and air dry in clean fume cabinet.

The processed SS slices were subsequently covered with 25mm 3M PTFE Film Tape (3M™ Science, 5490, UK) on the both top and bottom sides. Rolling on the surface of these slices with a pen to make them flat and eliminate bubbles between the coved tapes and SS slices. Three circular areas in the surface were punched with a 2mm biopsy punch (Thermo Fisher Scientific, 12460406, UK).

The roughness in these punched areas were examined using the white light interferometry (Wyko NT9300) in Swansea University college of engineering. The stitching diameters were set as outer: 3mm and inner 0mm. Scan length was set as

40.00 microns (1119 frames). The analysis and control of the entire measurement process is performed by the 'Vison' software. The used white light interferometry and processed samples are showing in Figure 6.1

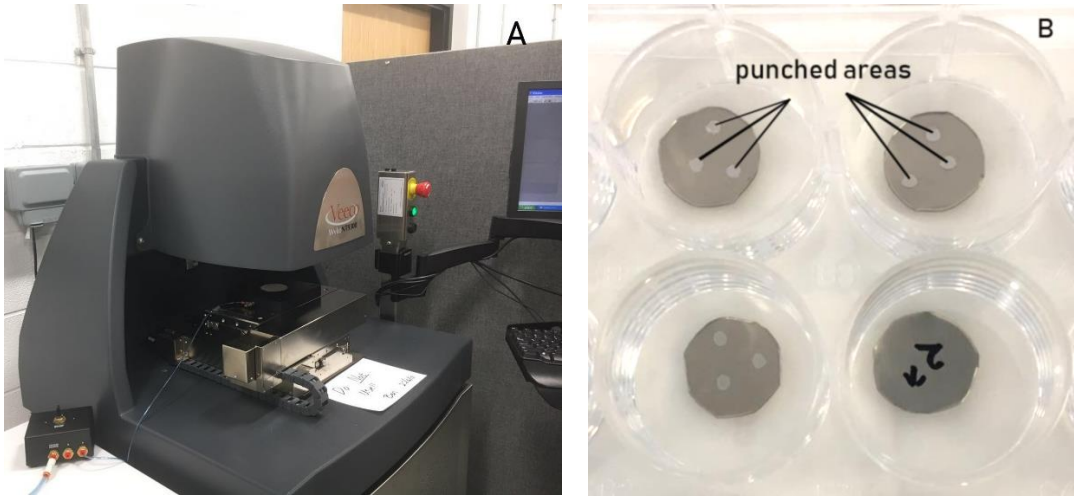

Figure 6.1-A represents the Wyko NT9300 white light interferometry
Figure 6.1-B represents the processed SS metal slices were coved with 3M film tapes. Three circular areas were punched on front surface of the metal slices.

Same THP-1 macrophage cell line was applied as before. THP-1 cells were seeded on these SS slices in 24-well cell culture plate with RPMI1640 culture medium supplemented with 10% FBS + P/S at seeding density of 1×10^5 per well. PMA was added into the RPMI medium (50nM) after 24 hour's incubation to active THP-1 cells differentiated into macrophages. Cell culture was performed in incubator for 14 days at 37°C+5% CO_2. environment. Culture medium was replaced every 3 days.

After 14-days cell culture, sample were soaked into 10% Triton X-100 for 24 hours. Then washed off the cells with sonicate 10 times (2minutes each time with 50% pulse) and subsequently put samples in fume cupboard till air dried. Roughness in these punched areas were re-tested with WLI to compare with previous roughness before seeding cells.

6.4.4. Electronical response between THP-1 macrophages and metal slices

i. Initial test

An in-house developed biosensor was designed to assess the electronical responses of macrophage mediated metal corrosion. The initial design of the in-house developed biosensor is shown as Figure 6.2 (A).

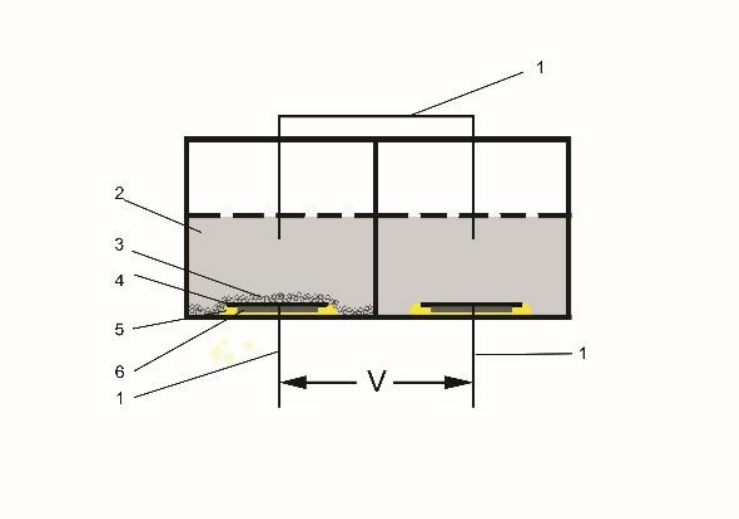

Figure 6.2. The design of the initial biosensor
1. Silver wires, 2. Culture media, 3. THP-1 cells, 4. Titanium or stainless-steel metal slice, 5. Araldite glue, 6. Silver Film

Same kind of SS foils were applied in this experiment, and 0.1mm thickness titanium foils (Advent Research Materials, TI228717, UK) with 99.6% purity were applied for comparing test. Both titanium (Ti) and stainless-steel (SS) foils were cut into 1cm x 1cm square shape. After that, the metal slices were washed with detergent and sterilized in 70% ethanol and rinsed with distilled water. A 500nm silver film was applied at the bottom of these metal slice by using physical vapour deposition (PVD) in Swansea University. A silver wire was soldered onto the silver film at the bottom of the metal slice as TI and SS metal cannot be soldered with silver wire directly.

Metal slices were fixed at the well of 24-well cell culture plate (Greiner CELLSTAR, M8812-100EA, UK) with Araldite glue (Zoro, ARA-400003, UK). The THP-1 cell cells were seeded onto only one side of the metal slice in 24-well cell culture plate

(1×10^5/ well). The cultures were incubated with 10% FBS and P/S in standard environment (37 C, humidified, 5% CO_2).

The plate design of this experiment is showing in Figure 6.3. The test includes three groups which are control, experiment group and blank. 50nm PMA was added into the experiment group after 24 hours incubation to active the differentiation of THP-1 cells.

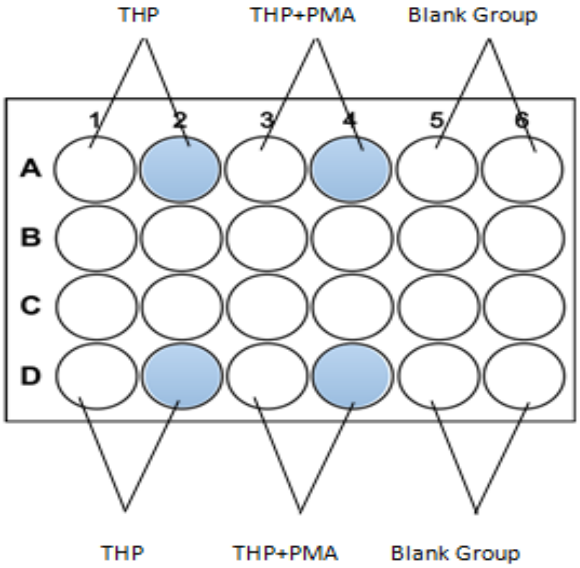

Figure 6.3. The plate design of biosensor experiment

THP-1 cell culture without adding PMA was the control (A 1-2 and D 1-2)
THP-1 cells treated with 50 nM PMA was the experiment group (A 3-4 and D 3-4)
RPMI 1640 medium without adding cells was the blank (A 5-6 and D 5-6)

The voltage changes were measured from the silver wires which connected to the metal slices with a multi-meter every 24 hours, after overnight incubation. The obtained results were processed with Excel software to observe the trend of voltage changing against time.

ii. Developed test

An improved biosensor has been developed based on previous in-house developed biosensor for more detailed measurement. Only titanium metal foils were selected for the new biosensor. The Ti slices were cut into squares of 1 x 1 cm^2 with a 'long tail' (Figure 6.4) to replace the silver films and silver wires in previous design. Therefore, the disturbance produced by silver films and silver wires have been removed.

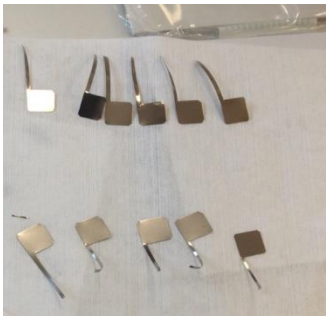

Figure 6.4. Metal slices with a 'long tail' design

The design of the developed biosensor is shown as Figure 6.5, the washed Ti slices were fixed into a sterile 24-well cell culture plate with lid (CELLSTAR).

The 'long tail' of the metal slice crossed the small holes which had been drilled at the bottom of plated. After that, the drilled holes were sealed with the Araldite glue to avoid leaking. THP-1 cells were seeded onto only on side of the Ti metal slice with same culture density, medium and environment as the initial test.

Figure 6.5. Design of the developed biosensor

1.Silver wire, 2.THP-1 cells, 3. RPMI Culture media, 4. Titanium metal slice with the 'long tail' design.

Same plate design was applied in this developed test (Figure 6.3). The voltage values at different hours (1 hours, 2 hours, 4 hours, 8 hours and 24 hours after seeding cells) were recorded from the ‘long tail’ of the metal slices with a multi-meter for the first day of incubation. The voltage changes for the remaining days were measured every 24 hours. This testing was repeated three times, and the average voltages were taken to plot the curve of voltage changing with Excel software for comparing each group.

6.5. Results

6.5.1. SEM Observation

i. SEM Observation on SS metal surface

The obtained SEM images of stainless-steel slices after14-days incubation with cells are showing in Figure 6.6. $1x10^4$, $3 x10^4$ and $5x10^4$ magnifications were applied for observation with $5 x10^3$ volt accelerating voltage.

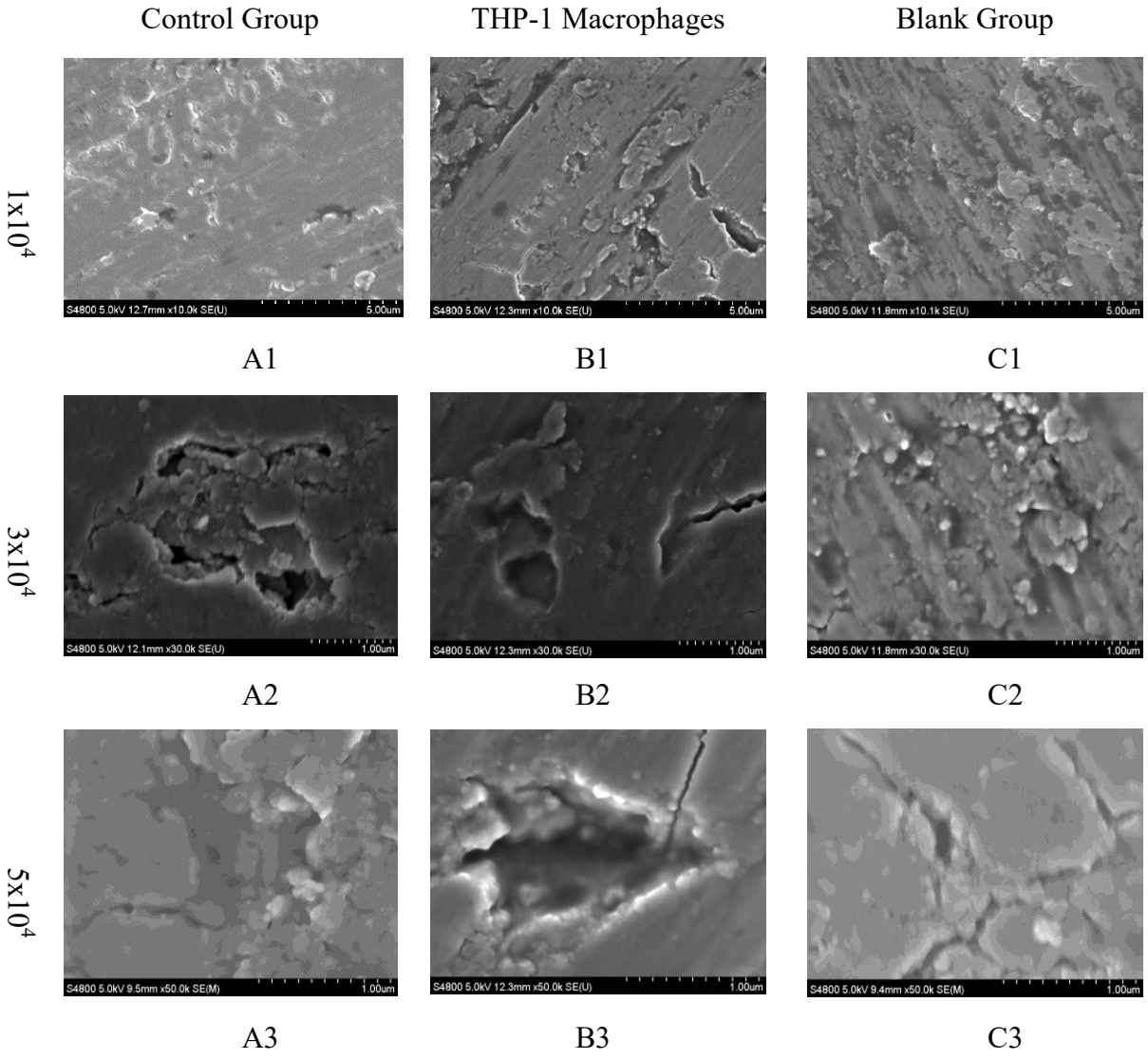

Figure 6.6. SEM images of stainless-steel metal surfaces with different magnifications ($1x10^4$, $3 x10^4$ and $5x10^4$) after 14-days incubation of THP-1cells
Scale bar in first row = 5.0µm, Scale bar in second and third row = 1.00µm

According to Figure 6.6, no obvious difference was found between each group at low magnifications ($1x10^4$). However, significant difference was observed in the THP-1 macrophages group (experiment group) at high magnifications ($5x10^4$). As can be seen from the B3 image in Figure 6.5, the observed small holes on the image are seems like macrophages related absorbed pits which are different to naturally scratches.

ii. SEM Observation of 'hash symbol' marked areas on SS metal slices

Figure 6.7 shows the comparison of the 'hash symbol' marked areas on processed metal slices. Local images of the 'hash symbol' marked areas were achieved by using SEM with 500 magnification at $1x10^4$V accelerating voltage. The obtained images (approximately 25 images for each hash symbol) subsequently been stitched into the completed regains of the hash symbol through 'Photoshop' software.

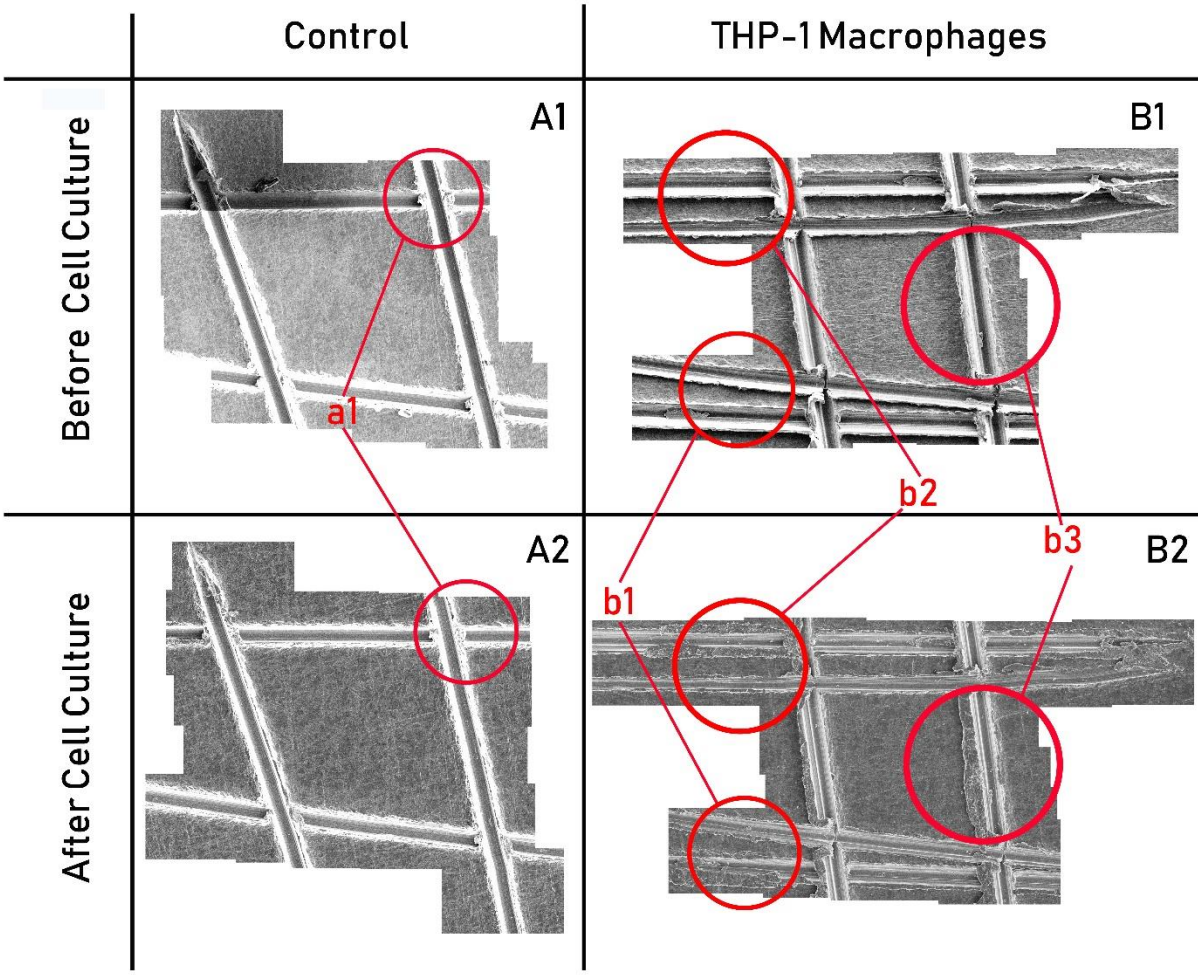

Figure 6.7. The comparison of the ‘hash symbol’ marked areas on processed metal slices before

As it can be seen from Figure 6.6, the first row represents the 'hash symbol' areas on processed metal slices before seeding cells on them, and the second row represents the changes at the 'hash symbol' areas after seeding cells on these metal slices for 14-days incubation. The control (A1) and blank (C1) groups did not show significant difference when comparing with the images after 14-days incubation (A1 and C1). Whereas, image B2 represents that 'hash symbol' area seems to be seriously corroded when comparing with the same area before seeding THP-1 macrophages. Moreover, the selected areas in the experiment groups (b1, b2 and b3) are the areas which show the biggest difference before and after cell culture.

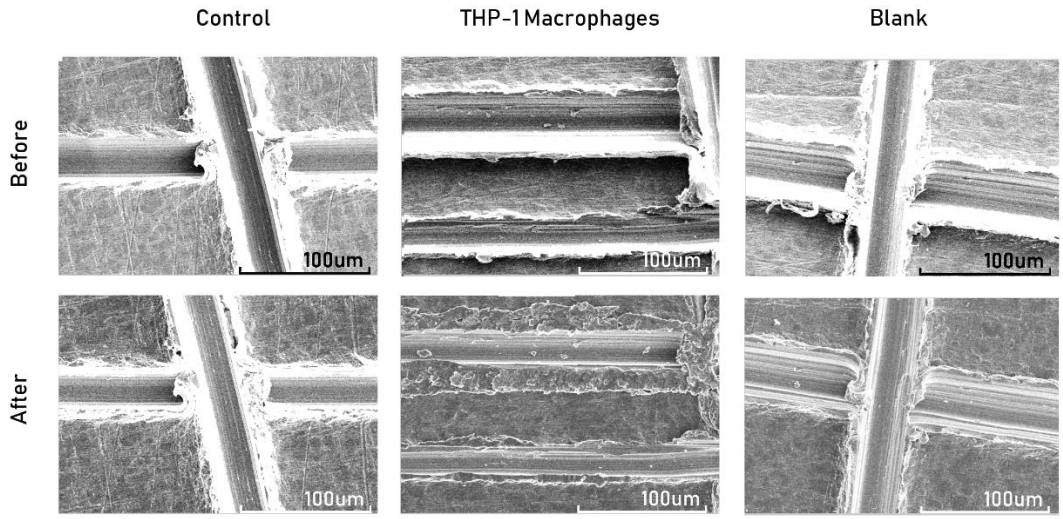

Figure 6.8 The zooming in SEM images of selected areas in figure 6.7

The first column indicates the a1 area in Figure 6.7-A, the second column indicates the b1 area in Figure 6.7-B and the third column indicates the c1 area in Figure 6.7-C. Scale bar= 100μm

Figure 6.8 represents the original SEM images of the selected areas in Figure 6.7 (accelerating voltage = $1x10^4$ Volt, magnification = 500) to provide more details for comparison between each group. The scratches in the experiment group (THP-1 macrophages) showed the trend to become flat after seeding THP-1 macrophages for 14 days, which are different to the scratches in control and blank group.

6.5.2. WLI Bio Corrosion

The examined results from the White-light interferometry were collected and processed via Vison software. The 3D images of the sample surface were simulated to provide detailed information of surface roughness. Corrosion behaviours were detected on some of metal surfaces after 14-days culture as Figure 6.9.

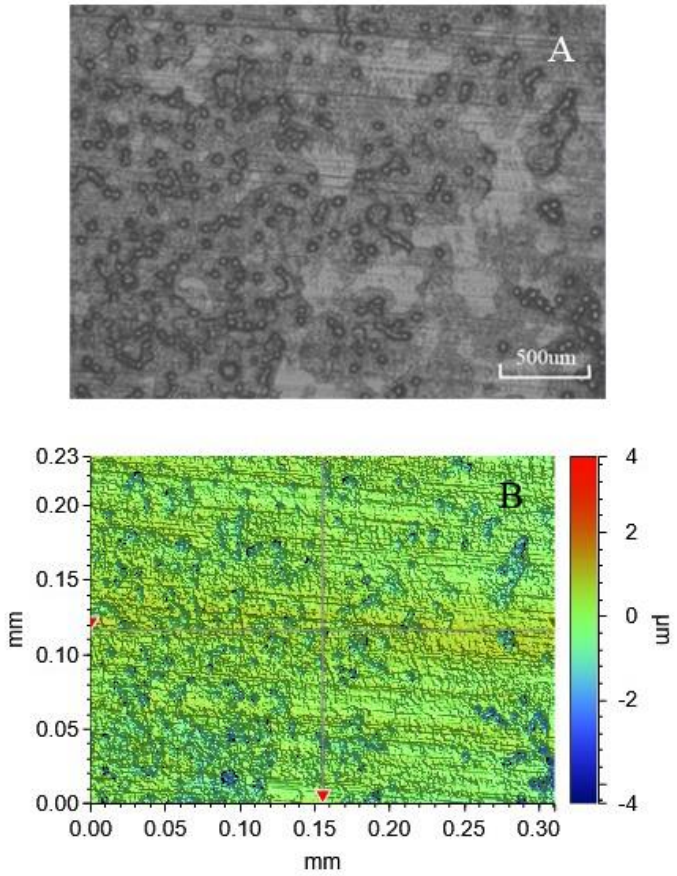

Figure 6.9 Absorbed pits on stainless steel surface

Figure 6.9-A is the observed image from WLI and Figure 6.8-B is the analysed image via Vision software. It is one of the representative images of resorption pits after 14-days incubation of THP-1 macrophages on stainless steel surface (inset shows magnified resorption pits).

More detailed analyses were conducted from the simulated 3D images of SS samples by Vison software, and the changes of surface roughness on the SS surface were compared before and after macrophages incubation. The simulated 3D images and obtained data of surface roughness from one of the representative samples were shown in Figure 6.10 and the roughness comparison of selected area were shown in Figure 6.11

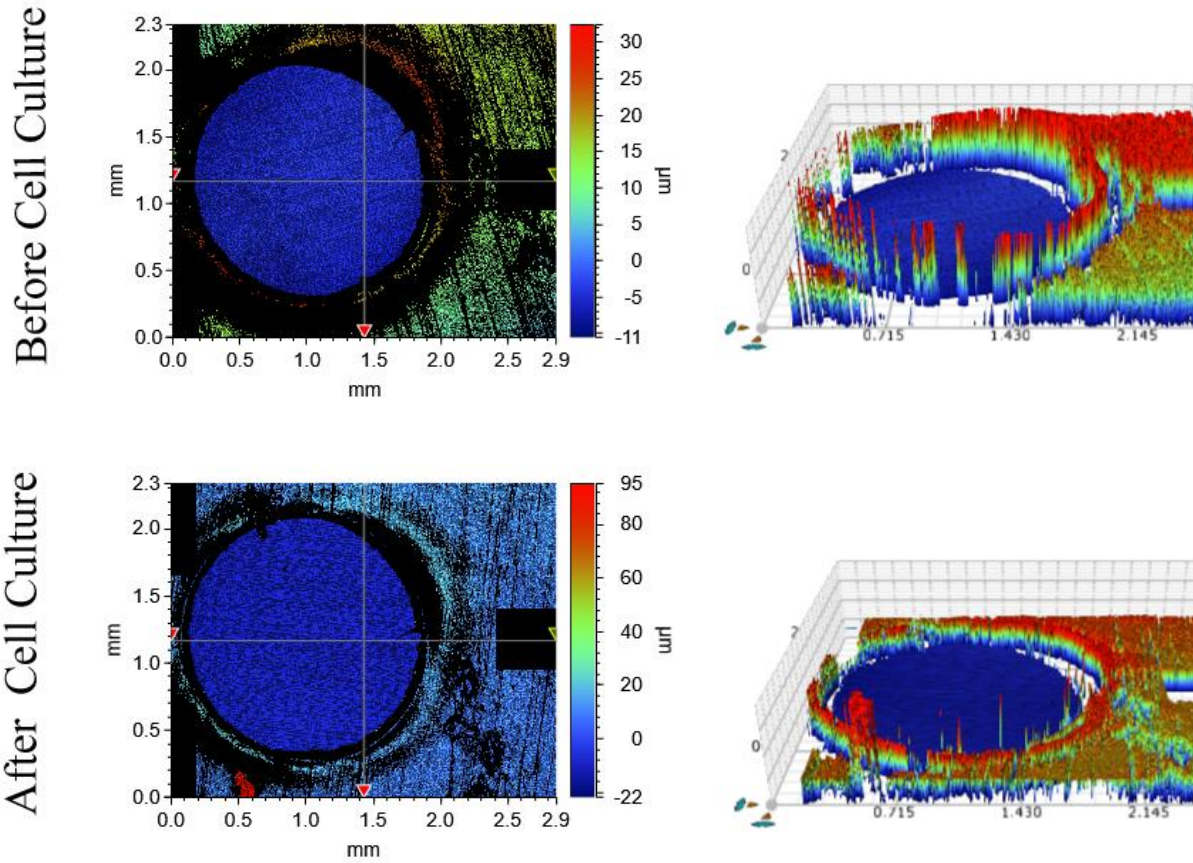

Figure 6.10 The roughness comparison of representative sample

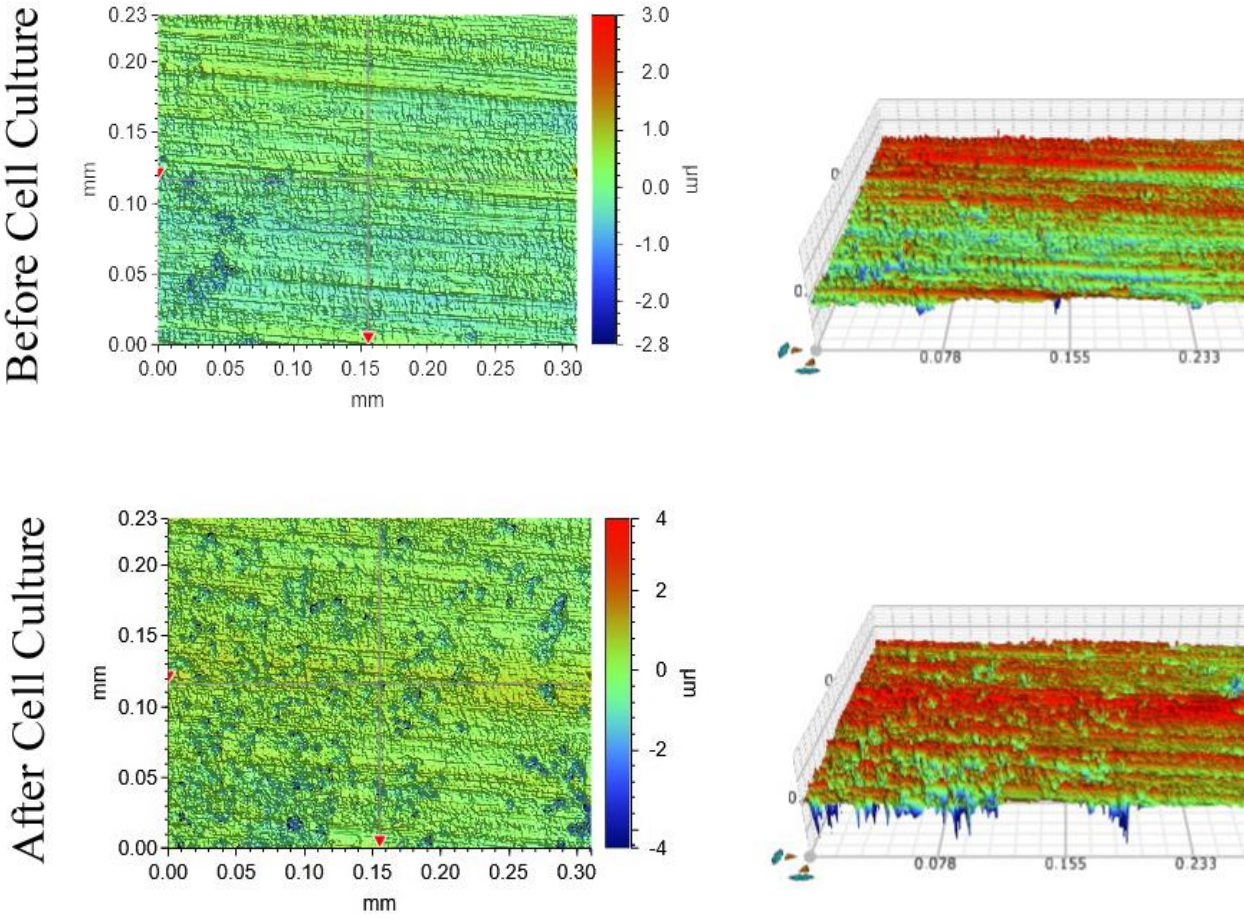

Figure 6.11 The roughness comparison of selected local surface

The parameters in Figure 6.10 and 6.11 are explained as below:

- Sa (arithmetical mean height) expresses, as an absolute value, the difference in height of each point compared to the arithmetical mean of the surface.

- Sku (Kurtosis) value is a measure of the sharpness of the roughness profile. Sku<3: Height distribution is skewed above the mean plane; Sku=3: Height distribution is normal. (Sharp portions and indented portions co-exist.); and Sku>3: Height distribution is spiked.

- Sp (Maximum peak height) is defined as the height of the highest peak within the defined area.

- Sq (Root mean square height) represents the root mean square value of ordinate values within the definition area. It is equivalent to the standard deviation of heights.

- Ssk (Skewness) values represent the degree of bias of the roughness shape (asperity). Ssk<0: Height distribution is skewed above the mean plane; Ssk=0: Height distribution (peaks and pits) is symmetrical around the mean plane; and Ssk>0: Height distribution is skewed below the mean plane.

- Sv (Maximum pit height) is defined as the absolute value of the height of the largest pit within the defined area

- Sz (Maximum height) is the sum of the largest peak height value and the largest pit depth value within the defined area.

In short, the Sa parameter is generally used to evaluate surface roughness. (Suketa et al., 2005) However, this parameter is insensitive to the “polarity” of the surface texture in that a deep valley or a high peak will result in the same Sa value. Root mean square roughness (Sq) was calculated as typical surface texture parameter (Annunziata et al., 2011).

As it can be seen from the achieved data in Figure 6.9, both Sa and Sq values of the tested sample before seeding cells (4.706 and 6.48μm) are significantly lower than after 14-days incubation (7.321 and 10.715μm). Which indicates the surface roughness of test sample has been raised after 14-days incubation.

The results in Figure 6.10 represent the Sa and Sq values of the selected area increased after 14-days incubation. Furthermore, the roughness changes of the surface can be observed from the 3D simulated images directly.

6.5.3. Electronical response between THP-1 macrophages and metal slices

i. Initial Test

The voltage changes between cells and implant-associated metal (Ti and SS) were tested by the initial in-house developed biosensor. The obtained data were processed via Excel software. The curves that represent the trend of voltage changing with time were plotted in Figure 6.12.

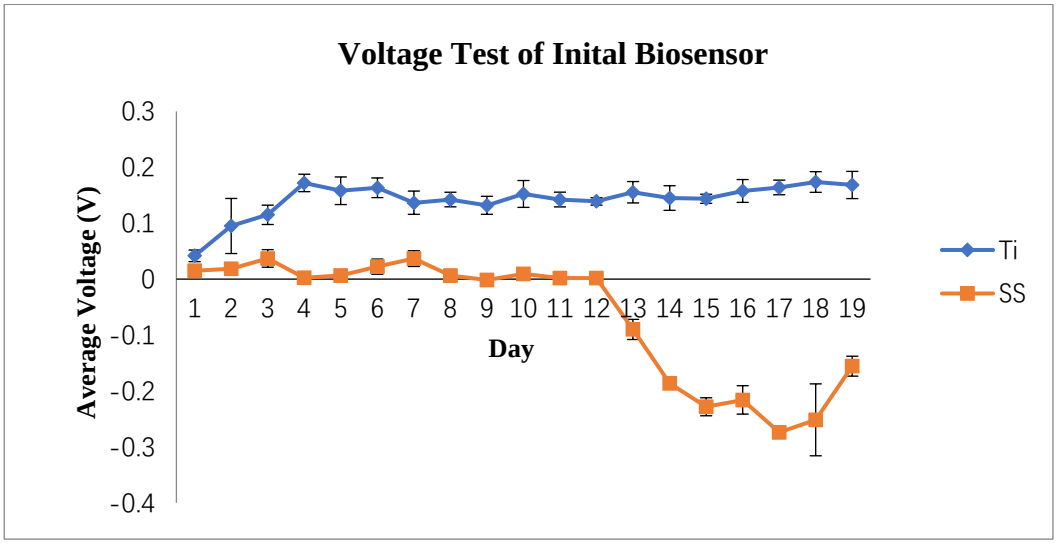

Figure 6.12. The tested voltage changing with time using the initial biosensor. Error bar: standard deviation.

According to Figure 6.12, we can find that voltage changes in titanium group kept increasing at the first 4 days and then remained stable for the rest of the days. The voltage in stainless-steel group trended to flat at first 12 days and started to grow rapidly after day 12. The trend of voltage changes in Ti group are more match to the expected theoretical results than SS group. Thus, only titanium was applied for the design of the developed biosensor.

ii. Developed Test

The improved biosensor was applied to find the interaction between THP-1 cells and implant-associated titanium metal slices. The curves that represent the trend of voltage changing in different experiment groups were plotted in Figure 6.13 and 6.14. (Error bar: standard deviation)

24 hours testing:

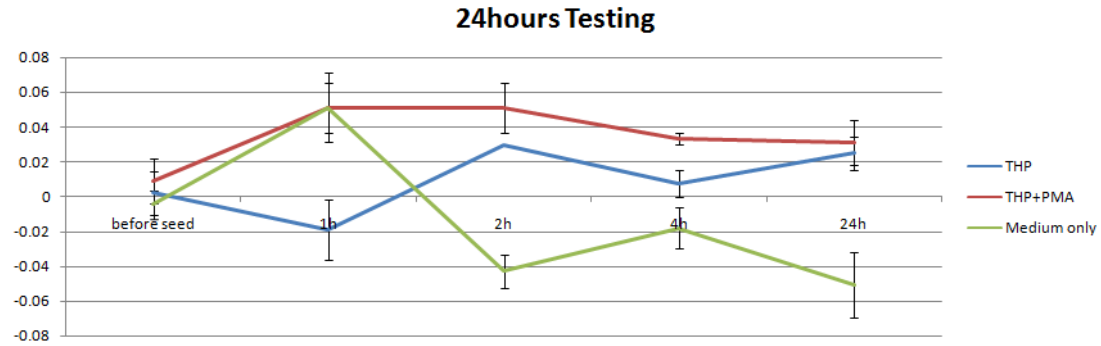

Figure 6.13. Voltage changing in the first 24 hours after seeding cells

21 days testing:

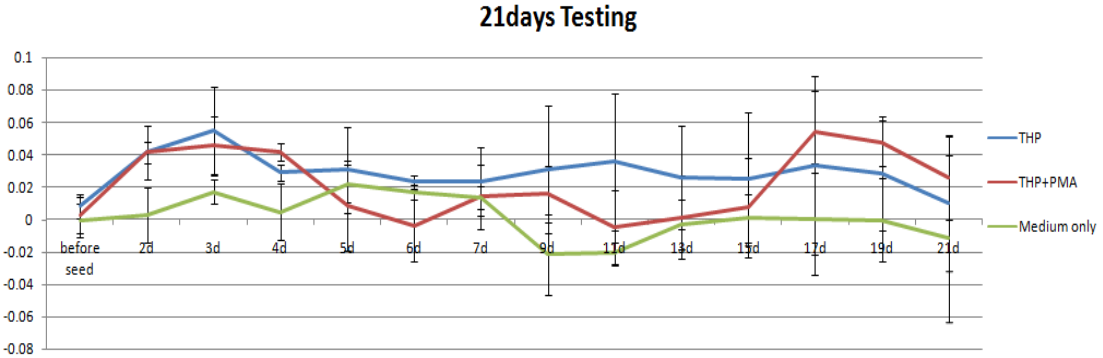

Figure 6.14. The tested voltage changing with time using the improved biosensor.

'THP' on the figure indicates the control group: THP-1 cells seeding on the Ti metal slices. 'THP+PMA' indicates the experiment group: differentiated THP-1 macrophages seeding on the Ti metal slices and 'Medium only' indicates the blank group: RPMI1640 medium only.

Figure 6.13 represents that at the first day of cell culture, the voltages kept increasing in both control and experiment groups and reduced in blank group. Figure 6.14 represents that the voltages in both control and experiment groups are significantly higher than blank group at first 4 days but became unstable from day 5 till the end.

According to the results of voltage changing, it is suggested that both THP-1 cells and differentiated THP-1 cells may produce voltages when interacting with metal slices. Small voltage may be produced as soon as seeding cells onto titanium metal slices. According to the recorded data at the first 4 days in Figure 6.14, the voltages in both control and experiment groups increased at first and trended to flat at day 4, which is close to the results in the initial testing. Whereas the data became very unstable in the remaining days. The reason may because the noise occurred during measurement leads to errors. Thus, the design of biosensor is still not precise enough and need to be improved in future study.

6.6. Discussion

Metal alloy osteosynthetic and prosthetic devices play significant roles in trauma and orthopedic surgery. (Cadosch, Chan, Gautschi, Simmen, et al., 2009) Therefore, it is important to detect the interactions between implant metal materials (such as SS and TI) and the surrounding cells or tissues. Recently, the SS metal in contact with biological systems undergo corrosion by an electrochemical process has been reported by a published research.(Cadosch, Chan, Gautschi, Simmen, et al., 2009) This study have applied human osteoclasts (OC) to grow on surgical SS surface and suggested that the matured OC can corrode SS surface directly and release corresponding metal ions with an electrochemical process at the cell-metal interface. The released metal ions are able to induce the secretion of pro-inflammatory cytokines and lead to a series of adverse bioreactions. In the current study, potential bio-corrosion investigated on a different cell type, THP-1 macrophages, with same type of SS foil. Macrophages related absorption pits have been observed in this study. Furthermore, new developed testing method showed more detailed evidence to prove the hypothesis that

macrophages are able to directly corrode stainless steel surface and not only produce absorbed pits and destroy some fragile structures on the metal surface.

However, it has been debated that the selected areas for taking SEM images are picked targeting the hypothesis. Thus, the new WLI experiment have been designed after discussing with Professor James Sullivan in College of Engineering in order to provide more convinced results. The purpose of using 3M tapes to cover SS surface is to make sure the metal surface contact cells only in the punched areas. This theoretically increases the chance of corrosion and benefit locating the same area for study. Despite the obtained positive results, more persuasive results are still required in this study. Thus, more improved attempts and more discussions with bio-metal corrosion related researchers are recommended to develop the method of this experiment and improve the rate of positive result.

The electrochemical corrosion behaviours of metal alloys implants were reported in previous research and released metal ions were detected by using potentiodynamic scan method. (Hsu, Yang, Huang, & Chen, 2005) Whereas, limited researches have recorded the whole procedure of the electrochemical behaviours. The starting point and the information of voltage changing during whole bio corrosion has been missing to date. Different attempts have been applied in this study (some attempts that didn't get ideal result can be seen in appendix) to detect the entire bio corrosion process at the cell-metal interface.

The in-house developed biosensor and the improved devices were designed via discussing with Dr Andy Wain in National Physical Laboratory (NPL) in London. These devices have recorded the voltage changes from the beginning of bio corrosion which can be inferred that the biocorrosion begins as soon as cells contact with the implant metals. However, the recorded results from day 5 represented the shortage of the applied biosensor. Excessive noises were produced during the measurement which leads to the quality of collected data have been negatively affected. Therefore, an improved design based on previous biosensor is highly suggested to reducing noises of measurement.

In conclusion, the study in this chapter initiated several new methods to investigate the mechanism of bio-metal corrosion at the cell-metal interface. The THP-1 macrophages mediated metal corrosion behaviours have been observed and the electrochemical reactions at the cell-metal interface have been detected in this experiment. However, improvements of this innovative experiment are required, and more improved experiment designs are suggested in the future to provide better evidence-based results with reduced errors.

Chapter 7 Conclusions and Future Work

7.1 Conclusions

The scope of this thesis is to determine the mechanism of metal wear nanoparticles involved clinical complication of total of hip arthroplasty. This thesis set out to examine the research question on the following manner:

- Firstly, the characterisation of nanoparticles retrieved from tissue during revision was performed to detect physicochemical properties of these nanoparticles.

- Secondly, in vitro experiments were conducted to investigate the role of metal-induced cytotoxic effects of different type of metal nanoparticles as potential biological reactions mediating the occurrence of adverse biological reactions in patients with implant failures.

- Thirdly, the functional role of HIF-1α in CoNP induced cytotoxicity was established to assess the potential mechanism of nanoparticles involved apoptosis and cell death.

- Lastly, innovative methods were initiated to detect the electrochemical reactions of macrophage mediated extra cellular metal corrosion

The main conclusions of these studies are discussed in the following section:

A review of the literature (Chapter 2) demonstrated that despite the important role of MoM THA for treating end stage osteoarthritis and long-history studies of improving MoM THA, the cases of metal wear nanoparticles involved clinical complications are increasingly being reported and the current available information is limited to a small number of descriptive studies with the interaction between human cells and these metal nanoparticles. This resulted for further studies designed to explore the potential mechanisms involved in metal wear nanoparticles related clinical complication.

The study of nanoparticles characterisation (Chapter 3) was necessary in order to get better understanding of these produced nanoparticles and assessing the mechanism of particle generation. The majority of observed nanoparticles in Non-MoM DMNTHA samples were circle or square shapes, 70 nm size with predominant Cr element. Most of the nanoparticles in retrieved MoM LHTHA samples were irregular shapes, 75nm size and consisting of two types (one type almost exclusively composed of Ti with very low Cr, another type contained Cr with minor component of Ti). Also, nanoparticles in measured MoM HRA samples were rectangular or oval shapes, 50nm size and containing high proportion of Cr without Ti element. This suggested that the physiochemical properties and the generating mechanism of metal wear nanoparticles were different due to different configuration of prostheses.

A series of in vitro experiments were conducted to investigate the local cytotoxic effects of different type of metal nanoparticles (Chapter 4) and the potential biological mechanism (Chapter 5). The results of these studies demonstrate that metal nanoparticles have dose-dependent effects on the viability of THP-1 macrophages in vitro. Co and Mixed nanoparticles showed higher cytotoxicity than Ti and Cr at high concentration. Moreover, CoNP induced accumulation of HIF-1α may be an important biological reaction involved in the occurrence of ALTR such as pseudotumours. This highlighted the cytotoxicity of metal nanoparticles and the potential biological mechanism of CoNP induced toxic effects.

Innovative experiments were then developed to determine whether biocorrosion behaviours are exist between THP-1 macrophages and clinical applied metals such as SS and Ti and subsequently produce metal nanoparticles or ions which involved in the occurrence of adverse biological reactions. The results demonstrated that THP-1 macrophages were able to corrode clinical applied metals. The structure and roughness of SS metal surface were changed, and electrochemical signals were detected on Ti metal surface. This concluded that the occurrence of biocorrosion between THP-1 macrophages and metal implants may be an important mechanism responsible for the generation of metal nanoparticles and subsequently cause implant failure.

7.2 Limitations

There are several limitations in the current study of the nano-analyses of wear particles (Chapter 3). The primary wear particles and secondary particles phagocytized after their release from apoptotic macrophages or tissue necrosis were not able to be distinguish from the achieved images. Furthermore, the morphological and elemental analysis of the particles did not provide information about their three-dimensional structure.

Ti and Cr particles are only applied when it is comparing the effect of different types metal nanoparticles with different concentration on macrophage viability at 24 hours co-culturing time in Chapter 4. The obtained SEM/EDS images in Figure 4.10 only demonstrated the relationship of CoNPs and macrophages, but the relationship of macrophages and other metallic nanoparticles, such as Cr and Ti are yet to know. Better SEM/EDS images are suggested with macrophages co-culturing with combined metallic particles to provide more information to understand the relationships between macrophages and different types of metallic nanoparticles.

In the study of Chapter 5 only investigated that HIF1α is likely to involve in cobalt nanoparticles (CoNP) induced cellular cytotoxicity. However, the direct causal factor of HIF-1 α independent apoptosis needs further study and the molecular pathway as a resultant of CoNP induced HIF-1 α increase is still not fully understood.

The major limitation in the study of bio-metal corrosion (Chapter 6) is that only few related researches that represents the mechanism of cell mediated biocorrosion are reported as the experiment methods were newly-developed. Moreover, the obtained results showed that the occurrence of metal corrosion that can be detected only in around 20% of tested samples (3 in 14 samples). More quantitative results are required to prove the hypothesis. For the biosensor experiment, the main limitation is that the unexpected interference may occur in the public tissue culture room, it is difficult to find an independent incubator to conduct the whole experiment without the interference of external factors.

7.3 Recommendations for future study

Future investigations are recommended to overcome important inherent limitations of the studies presented in this thesis. Further analysis will be necessary to focus on the underlying mechanism of metal wear nanoparticles mediated adverse effects. For the study in chapter 3, more clinical data such as the rate of occurrence of at different implantation times are suggested to be involved in the final particle analysis to provide more information about the entire metal wear and corrosion procedure.

More comparison experiments of each metal nanoparticle group are suggested to achieve more information regarding the difference of biological responses based on different types of metal nanoparticles in Chapter 4. Moreover, further research is required to develop the molecular pathways involved in the metal nanoparticle induced metal clinical complication in Chapter 5.

Future work for the study of bio-metal corrosion (Chapter 6) is suggested to polish all metal specimens to the same surface with silicon carbide abrasive papers discs before seeding cells onto metal slices. Furthermore, reproducible techniques need to be improved to increase the reliability and benefit for taking more convincible proofs. The design of future biosensor experiment is suggested to focus on the stable of measurement and it is hoped to produce continuously voltages changing to explore the interaction at cell-metal interface. A better biosensor has been designed as Figure 7.1. The continuously voltages changing will be recorded via a Hantek365 series data logger which is designed to connect with a computer and biosensor.

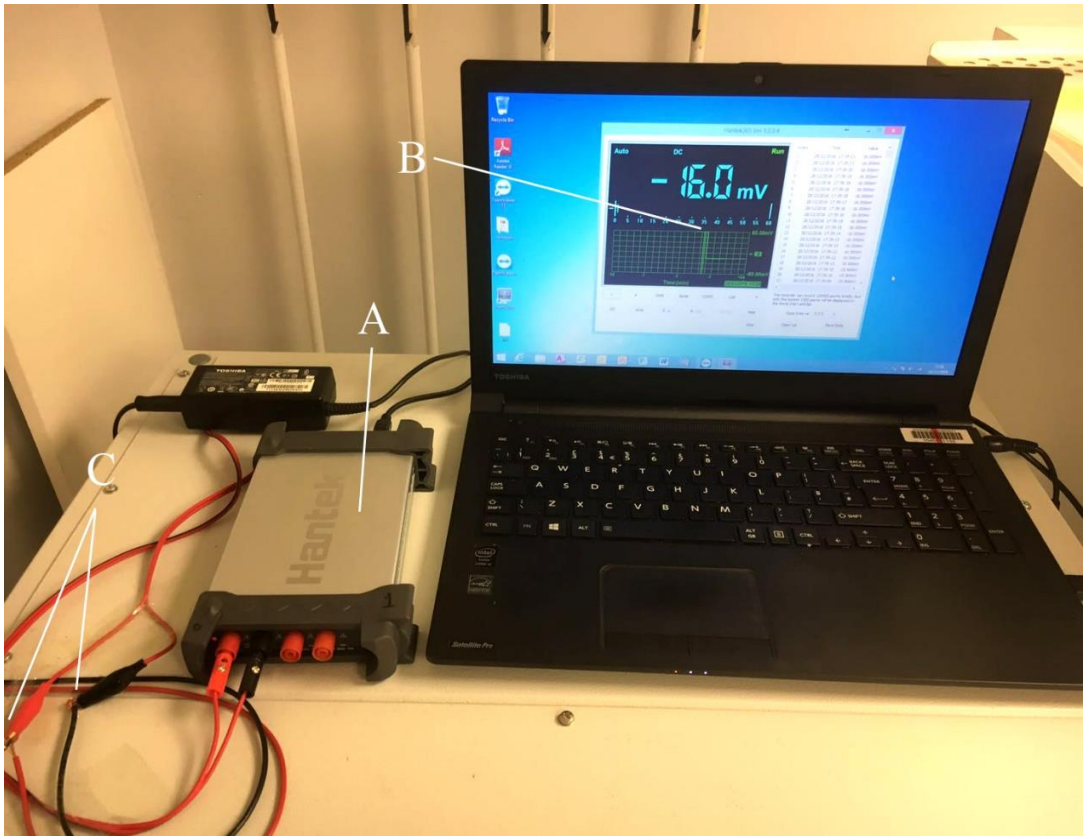

Figure 7.1. The design of new biosensor
A indicates the Hantek365 series data logger, B indicates a laptop with installing Hantek365 Ver1.0.0 software and being connected with the Hantek data logger. C indicates the datalogger are recording the continuously voltages changes from a connected biosensor which are been placed in an incubator.

All the attempts and future works aim to investigate more evidence-based information which will contribute developing total hip replacement techniques, minimising the occurrence of adverse clinical outcomes and improving the quality life.

Appendices and References

References

1. Akakura, N., Kobayashi, M., Horiuchi, I., Suzuki, A., Wang, J., Chen, J., . . . Asaka, M. (2001). Constitutive expression of hypoxia-inducible factor-1α renders pancreatic cancer cells resistant to apoptosis induced by hypoxia and nutrient deprivation. *Cancer research, 61*(17), 6548-6554.

2. Allen, M. J., Myer, B. J., Millett, P. J., & Rushton, N. (1997). The effects of particulate cobalt, chromium and cobalt-chromium alloy on human osteoblast-like cells in vitro. *The Journal of Bone and Joint Surgery. British volume, 79*(3), 475-482.

3. Anantharajah, A., Buyck, J. M., Faure, E., Glupczynski, Y., Rodriguez-Villalobos, H., De Vos, D., . . . Tulkens, P. M. (2015). Correlation between cytotoxicity induced by Pseudomonas aeruginosa clinical isolates from acute infections and IL-1β secretion in a model of human THP-1 monocytes. *Pathogens and disease, 73*(7).

4. Anissian, H. L., Stark, A., Gustafson, A., Good, V., & Clarke, I. C. (1999). Metal-on-metal bearing in hip prosthesis generates 100-fold less wear debris than metal-on-polyethylene. *Acta Orthopaedica Scandinavica, 70*(6), 578-582.

5. Annunziata, M., Oliva, A., Basile, M. A., Giordano, M., Mazzola, N., Rizzo, A., . . . Guida, L. (2011). The effects of titanium nitride-coating on the topographic and biological features of TPS implant surfaces. *Journal of dentistry, 39*(11), 720-728.

6. Ayers, D. C. (2018). How Common Is Revision for Adverse Reaction to Metal Debris After Total Hip Replacement with a Metal-on-Polyethylene Bearing Surface?: Commentary on an article by Anders Persson, MD, et al.“Revision for Symptomatic Pseudotumor Following Primary Total Hip Arthroplasty with a Standard Femoral Stem”. *JBJS, 100*(11), e82.

7. B., H. C., L., B. D., M., B., A., Y. D., E., D. R., & J., S. A. (2007). The results of primary Birmingham hip resurfacings at a mean of five years. *The Journal of Bone and Joint Surgery. British volume, 89-B*(11), 1431-1438. doi:10.1302/0301-620x.89b11.19336

8. Pollard T.C.B.; Baker R.P.; Eastaugh-Waring S.J., & Bannister G.C. (2006). Treatment of the young active patient with osteoarthritis of the hip. *The Journal of Bone and Joint Surgery. British volume, 88-B*(5), 592-600. doi:10.1302/0301-620x.88b5.17354

9. Back, D. L., Young, D., & Shimmin, A. (2005). How do serum cobalt and chromium levels change after metal-on-metal hip resurfacing? *Clinical Orthopaedics and Related Research®, 438*, 177-181.

10. Barton, J. R. (1827). On the treatment of anchylosis, by the formation of artificial joints. *The New England Medical Review and Journal, 1*(3), 309-314.

11. Bauer, T. W. (2002). Particles and periimplant bone resorption. *Clinical Orthopaedics and Related Research®, 405*, 138-143.

12. Baxmann, M., Pfaff, A. M., Schilling, C., Grupp, T. M., & Morlock, M. M. (2017). Biomechanical Evaluation of the Fatigue Performance, the Taper Corrosion and the Metal Ion Release of a Dual Taper Hip Prosthesis under Physiological Environmental Conditions. *Biotribology, 12*, 1-7. doi:https://doi.org/10.1016/j.biotri.2017.07.002

13. Beaver, W. B., Jr., & Fehring, T. K. (2012). Abductor dysfunction and related sciatic nerve palsy, a new complication of metal-on-metal arthroplasty. *J Arthroplasty, 27*(7), 1414 e1413-1415. doi:10.1016/j.arth.2011.11.002

14. Benson, M., Goodwin, P., & Brostoff, J. (1975). Metal sensitivity in patients with joint replacement arthroplasties. *Br Med J, 4*(5993), 374-375.

15. Beyond The Spotlight with Ron Noreman. (2015). *Iron Magazine*.

16. Board, T., Mohan, S., Gambhir, A., & Porter, M. (2009). *Clinical experience of revision of resurfacing hip arthroplasty for ALVAL.* Paper presented at the Procs American Academy of Orthopaedic Surgeons Annual Meeting.

17. Boardman, D., Middleton, F., & Kavanagh, T. (2006). A benign psoas mass following metal-on-metal resurfacing of the hip. *The Journal of Bone and Joint Surgery. British volume, 88*(3), 402-404.

18. Bosker, B., Ettema, H., Van Rossum, M., Boomsma, M., Kollen, B., Maas, M., & Verheyen, C. (2015). Pseudotumor formation and serum ions after large head metal-on-metal stemmed total hip replacement. Risk factors, time course and revisions in 706 hips. *Archives of orthopaedic and trauma surgery, 135*(3), 417-425.

19. Brewster, D. H., Stockton, D. L., Reekie, A., Ashcroft, G. P., Howie, C. R., Porter, D. E., & Black, R. J. (2013). Risk of cancer following primary total hip replacement or primary resurfacing arthroplasty of the hip: a retrospective cohort study in Scotland. *British journal of cancer, 108*(9), 1883-1890. doi:10.1038/bjc.2013.129

20. Brodner, W., Grohs, J. G., Bancher-Todesca, D., Dorotka, R., Meisinger, V., Gottsauner-Wolf, F., & Kotz, R. (2004). Does the placenta inhibit the passage of chromium and cobalt after metal-on-metal total hip arthroplasty? *The Journal of arthroplasty, 19*(8), 102-106.

21. Buergi, M. L., & Walter, W. L. (2007). Hip Resurfacing Arthroplasty: The Australian Experience. *The Journal of arthroplasty, 22*(7, Supplement), 61-65. doi:https://doi.org/10.1016/j.arth.2007.05.021

22. Cadosch, D., Chan, E., Gautschi, O. P., Meagher, J., Zellweger, R., & Filgueira, L. (2009). Titanium IV ions induced human osteoclast differentiation and enhanced bone resorption in vitro. *Journal of Biomedical Materials Research Part A: An Official Journal of The Society for Biomaterials, The Japanese Society for Biomaterials, and The Australian Society for Biomaterials and the Korean Society for Biomaterials, 91*(1), 29-36.

23. Cadosch, D., Chan, E., Gautschi, O. P., Simmen, H. P., & Filgueira, L. (2009). Bio-corrosion of stainless steel by osteoclasts—in vitro evidence. *Journal of orthopaedic research, 27*(7), 841-846.

24. Caicedo, M. S., Samelko, L., McAllister, K., Jacobs, J. J., & Hallab, N. J. (2013). Increasing both CoCrMo-alloy particle size and surface irregularity induces increased macrophage inflammasome activation in vitro potentially through lysosomal destabilization mechanisms. *Journal of orthopaedic research, 31*(10), 1633-1642.

25. Campbell, P., Ebramzadeh, E., Nelson, S., Takamura, K., De Smet, K., & Amstutz, H. C. (2010). Histological features of pseudotumor-like tissues from metal-on-metal hips. *Clinical Orthopaedics and Related Research®, 468*(9), 2321-2327.

26. Campbell, P., Shimmin, A., Walter, L., & Solomon, M. (2008). Metal sensitivity as a cause of groin pain in metal-on-metal hip resurfacing. *The Journal of arthroplasty, 23*(7), 1080-1085.

27. Casson, C. N., Yu, J., Reyes, V. M., Taschuk, F. O., Yadav, A., Copenhaver, A. M., . . . Shin, S. (2015). Human caspase-4 mediates noncanonical inflammasome activation against gram-negative bacterial pathogens. *Proceedings of the National Academy of Sciences*, 201421699.

28. Catelas, I., Medley, J. B., Campbell, P. A., Huk, O. L., & Bobyn, J. D. (2004). Comparison of in vitro with in vivo characteristics of wear particles from metal–metal hip implants. *Journal of Biomedical Materials Research Part B: Applied Biomaterials: An Official Journal of The Society for Biomaterials, The Japanese Society for Biomaterials, and The Australian Society for Biomaterials and the Korean Society for Biomaterials, 70*(2), 167-178.

29. Catelas, I., Petit, A., Vali, H., Fragiskatos, C., Meilleur, R., Zukor, D. J., . . . Huk, O. L. (2005). Quantitative analysis of macrophage apoptosis vs. necrosis induced by cobalt and chromium ions in vitro. *Biomaterials, 26*(15), 2441-2453.

30. Catelas, I., Petit, A., Zukor, D. J., & Huk, O. L. (2001). Cytotoxic and apoptotic effects of cobalt and chromium ions on J774 macrophages–implication of caspase-3 in the apoptotic pathway. *Journal of Materials Science: Materials in Medicine, 12*(10-12), 949-953.

31. Chanput, W., Mes, J. J., & Wichers, H. J. (2014). THP-1 cell line: an in vitro cell model for immune modulation approach. *International immunopharmacology, 23*(1), 37-45.

32. Cobb, A., & Schmalzreid, T. (2006). The clinical significance of metal ion release from cobalt-chromium metal-on-metal hip joint arthroplasty. *Proceedings of the Institution of Mechanical Engineers, Part H: Journal of Engineering in Medicine, 220*(2), 385-398.

33. Colas, S., Allalou, A., Poichotte, A., Piriou, P., Dray-Spira, R., & Zureik, M. (2017). Exchangeable Femoral Neck (Dual-Modular) THA Prostheses Have Poorer Survivorship Than Other Designs: A Nationwide Cohort of 324,108 Patients. *Clinical Orthopaedics and Related Research, 475*(8), 2046-2059. doi:10.1007/s11999-017-5260-6

34. Cooper, H. J., Urban, R. M., Wixson, R. L., Meneghini, R. M., & Jacobs, J. J. (2013). Adverse local tissue reaction arising from corrosion at the femoral neck-body junction in a dual-taper stem with a cobalt-chromium modular neck. *The Journal of bone and joint surgery. American volume, 95*(10), 865.

35. Corten, K., & MacDonald, S. J. (2010). Hip resurfacing data from national joint registries: what do they tell us? What do they not tell us? *Clinical Orthopaedics and Related Research, 468*(2), 351-357. doi:10.1007/s11999-009-1157-3

36. Daniel, J., Ziaee, H., Pradhan, C., Pynsent, P., & McMinn, D. (2007). Blood and urine metal ion levels in young and active patients after Birmingham hip resurfacing arthroplasty: four-year results of a prospective longitudinal study. *The Journal of Bone and Joint Surgery. British volume, 89*(2), 169-173.

37. Davies, A., Willert, H., Campbell, P., Learmonth, I., & Case, C. (2005). An unusual lymphocytic perivascular infiltration in tissues around contemporary metal-on-metal joint replacements. *JBJS, 87*(1), 18-27.

38. Delaunay, C. (2006). *Metasul bearings of first and second generation designs in primary THA.* Paper presented at the Orthopaedic Proceedings.

39. Delaunay, C., Petit, I., Learmonth, I. D., Oger, P., & Vendittoli, P. A. (2010). Metal-on-metal bearings total hip arthroplasty: The cobalt and chromium ions release concern. *Orthopaedics & Traumatology: Surgery & Research, 96*(8), 894-904. doi:https://doi.org/10.1016/j.otsr.2010.05.008

40. Delaunay, C. P. (2004). Metal-on-metal bearings in cementless primary total hip arthroplasty. *The Journal of arthroplasty, 19*(8), 35-40.

41. Della Valle, C. J., Nunley, R. M., Raterman, S. J., & Barrack, R. L. (2009). Initial American experience with hip resurfacing following FDA approval. *Clinical Orthopaedics and Related Research, 467*(1), 72-78.

42. Di Laura, A., Hothi, H. S., Meswania, J. M., Whittaker, R. K., de Villiers, D., Zustin, J., . . . Hart, A. J. (2017). Clinical relevance of corrosion patterns attributed to inflammatory cell-induced corrosion: A retrieval study. *Journal of Biomedical Materials Research Part B: Applied Biomaterials, 105*(1), 155-164.

43. Doorn, P. F., Campbell, P. A., Worrall, J., Benya, P. D., McKellop, H. A., & Amstutz, H. C. (1998). Metal wear particle characterization from metal on metal total hip replacements: transmission electron microscopy study of periprosthetic tissues and isolated particles. *Journal of Biomedical Materials Research: An Official Journal of The Society for Biomaterials, The Japanese Society for Biomaterials, and the Australian Society for Biomaterials, 42*(1), 103-111.

44. Doorn, P. F., Mirra, J. M., Campbell, P. A., & Amstutz, H. C. (1996). Tissue reaction to metal on metal total hip prostheses. *Clinical Orthopaedics and Related Research, 329*, S187-S205.

45. Erdfelder, E., Faul, F., & Buchner, A. (1996). GPOWER: A general power analysis program. *Behavior research methods, instruments, & computers, 28*(1), 1-11.

46. Eswaramoorthy, V., Moonot, P., Kalairajah, Y., Biant, L., & Field, R. (2008). The Metasul metal-on-metal articulation in primary total hip replacement: clinical and radiological results at ten years. *The Journal of Bone and Joint Surgery. British volume, 90*(10), 1278-1283.

47. Fang, C. S., Harvie, P., Gibbons, C. L., Whitwell, D., Athanasou, N. A., & Ostlere, S. (2008). The imaging spectrum of peri-articular inflammatory masses following metal-on-metal hip resurfacing. *Skeletal radiology, 37*(8), 715-722.

48. Felson, D. T., Lawrence, R. C., Dieppe, P. A., Hirsch, R., Helmick, C. G., Jordan, J. M., . . . Zhang, Y. (2000). Osteoarthritis: new insights. Part 1: the disease and its risk factors. *Annals of internal medicine, 133*(8), 635-646.

49. Felson, D. T., Lawrence, R. C., Hochberg, M. C., McAlindon, T., Dieppe, P. A., Minor, M. A., . . . Weinberger, M. (2000). Osteoarthritis: new insights. Part 2: treatment approaches. *Annals of internal medicine, 133*(9), 726-737.

50. Felson, D. T., Zhang, Y., Anthony, J. M., Naimark, A., & Anderson, J. J. (1992). Weight loss reduces the risk for symptomatic knee osteoarthritis in women: the Framingham Study. *Annals of internal medicine, 116*(7), 535-539.

51. Fields, W., Fowler, K., Hargreaves, V., Reeve, L., & Bombick, B. (2017). Development, qualification, validation and application of the neutral red uptake assay in Chinese Hamster Ovary (CHO) cells using a VITROCELL® VC10® smoke exposure system. *Toxicology in Vitro, 40*, 144-152. doi:https://doi.org/10.1016/j.tiv.2017.01.001

52. Ford, M. C., Hellman, M. D., Kazarian, G. S., Clohisy, J. C., Nunley, R. M., & Barrack, R. L. (2018). Five to Ten-Year Results of the Birmingham Hip Resurfacing Implant in the US: A Single Institution's Experience. *JBJS, 100*(21), 1879-1887.

53. Gamblin, A.-L., Brennan, M. A., Renaud, A., Yagita, H., Lézot, F., Heymann, D., . . . Layrolle, P. (2014). Bone tissue formation with human mesenchymal stem cells and biphasic calcium phosphate ceramics: the local implication of osteoclasts and macrophages. *Biomaterials, 35*(36), 9660-9667.

54. Germain, M., Hatton, A., Williams, S., Matthews, J., Stone, M., Fisher, J., & Ingham, E. (2003). Comparison of the cytotoxicity of clinically relevant cobalt–chromium and alumina ceramic wear particles in vitro. *Biomaterials, 24*(3), 469-479.

55. Gilbert, J. L., Sivan, S., Liu, Y., Kocagöz, S. B., Arnholt, C. M., & Kurtz, S. M. (2015). Direct in vivo inflammatory cell-induced corrosion of CoCrMo alloy orthopedic implant surfaces. *Journal of Biomedical Materials Research Part A, 103*(1), 211-223.

56. Gioe, T. J. X. Metal-on-Metal vs. Highly Linked Polyethylene: Influence on Survivorship.

57. Glyn-Jones, S., Pandit, H., Kwon, Y.-M., Doll, H., Gill, H., & Murray, D. (2009). Risk factors for inflammatory pseudotumour formation following hip resurfacing. *The Journal of Bone and Joint Surgery. British volume, 91*(12), 1566-1574.

58. Gofton, W. T., Illical, E. M., Feibel, R. J., Kim, P. R., & Beaulé, P. E. (2017). A Single-Center Experience With a Titanium Modular Neck Total Hip Arthroplasty. *The Journal of arthroplasty, 32*(8), 2450-2456. doi:https://doi.org/10.1016/j.arth.2017.03.025

59. Goldstein, J. I., Newbury, D. E., Echlin, P., Joy, D. C., Fiori, C., & Lifshin, E. (1981). *Scanning electron microscopy and X-ray microanalysis. A text for biologists, materials scientists, and geologists*: Plenum Publishing Corporation.

60. Gomez, P. F., & Morcuende, J. A. (2005). Early Attempts at Hip Arthroplasty: 1700s to 1950s. *Iowa Orthop J, 25*, 25-29.

61. Gomez, P. F., & Morcuende, J. A. (2005). Early attempts at hip arthroplasty: 1700s to 1950s. *Iowa Orthop J, 25*, 25.

62. Goodman, S. B., Ma, T., Chiu, R., Ramachandran, R., & Smith, R. L. (2006). Effects of orthopaedic wear particles on osteoprogenitor cells. *Biomaterials, 27*(36), 6096-6101.

63. Grammatopolous, G., Pandit, H., Kwon, Y.-M., Gundle, R., McLardy-Smith, P., Beard, D., . . . Gill, H. (2009). Hip resurfacings revised for inflammatory pseudotumour have a poor outcome. *The Journal of Bone and Joint Surgery. British volume, 91*(8), 1019-1024.

64. Greijer, A., & Van der Wall, E. (2004). The role of hypoxia inducible factor 1 (HIF-1) in hypoxia induced apoptosis. *Journal of clinical pathology, 57*(10), 1009-1014.

65. Gruber, F. W., Böck, A., Trattnig, S., Lintner, F., & Ritschl, P. (2007). Cystic lesion of the groin due to metallosis: a rare long-term complication of metal-on-metal total hip arthroplasty. *The Journal of arthroplasty, 22*(6), 923-927.

66. Haddad, F. S., Thakrar, R. R., Hart, A. J., Skinner, J. A., Nargol, A. V., Nolan, J. F., . . . Case, C. P. (2011). Metal-on-metal bearings: the evidence so far. *J Bone Joint Surg Br, 93*(5), 572-579. doi:10.1302/0301-620X.93B4.26429

67. Halawi, M. J., Brigati, D., Messner, W., & Brooks, P. J. (2017). Birmingham hip resurfacing in patients 55 years or younger: risk factors for poor midterm outcomes. *The Journal of arthroplasty, 32*(6), 1880-1883.

68. Hallab, N., Merritt, K., & Jacobs, J. J. (2001). Metal sensitivity in patients with orthopaedic implants. *JBJS, 83*(3), 428-436.

69. Hallab, N. J., Anderson, S., Stafford, T., Glant, T., & Jacobs, J. J. (2005). Lymphocyte responses in patients with total hip arthroplasty. *Journal of orthopaedic research, 23*(2), 384-391. doi:doi:10.1016/j.orthres.2004.09.001

70. Hallab, N. J., Mikecz, K., & Jacobs, J. J. (2000). A triple assay technique for the evaluation of metal-induced, delayed-type hypersensitivity responses in patients with or receiving total joint arthroplasty. *Journal of Biomedical Materials Research: An Official Journal of The Society for Biomaterials, The Japanese Society for Biomaterials, and The Australian Society for Biomaterials and the Korean Society for Biomaterials, 53*(5), 480-489.

71. Hart, A., Sabah, S., Henckel, J., Lewis, A., Cobb, J., Sampson, B., . . . Skinner, J. (2009). The painful metal-on-metal hip resurfacing. *The Journal of Bone and Joint Surgery. British volume, 91*(6), 738-744.

72. Hart, A. J., Quinn, P. D., Lali, F., Sampson, B., Skinner, J. A., Powell, J. J., . . . Flanagan, A. (2012). Cobalt from metal-on-metal hip replacements may be the clinically relevant active agent responsible for periprosthetic tissue reactions. *Acta biomaterialia, 8*(10), 3865-3873.

73. Hart, A. J., Quinn, P. D., Sampson, B., Sandison, A., Atkinson, K. D., Skinner, J. A., . . . Mosselmans, J. F. W. (2010). The chemical form of metallic debris in tissues surrounding metal-on-metal hips with unexplained failure. *Acta biomaterialia, 6*(11), 4439-4446.

74. Hasegawa, M., Yoshida, K., Wakabayashi, H., & Sudo, A. (2012). Pseudotumor with dominant B-lymphocyte infiltration after metal-on-metal total hip arthroplasty with a modular cup. *The Journal of arthroplasty, 27*(3), 493. e495-493. e497.

75. Heath, J., Freeman, M., & Swanson, S. (1971). Carcinogenic properties of wear particles from prostheses made in cobalt-chromium alloy. *The Lancet, 297*(7699), 564-566.

76. Hjorth, M. H., Mechlenburg, I., Soballe, K., Jakobsen, S. S., Roemer, L., & Stilling, M. (2018). Physical Activity Is Associated With the Level of Chromium but Not With Changes in Pseudotumor Size in Patients With Metal-on-Metal Hip Arthroplasty. *The Journal of arthroplasty*.

77. Hsu, R. W.-W., Yang, C.-C., Huang, C.-A., & Chen, Y.-S. (2005). Electrochemical corrosion studies on Co–Cr–Mo implant alloy in biological solutions. *Materials Chemistry and Physics, 93*(2), 531-538. doi:https://doi.org/10.1016/j.matchemphys.2005.04.007

78. Hu, W., Culloty, S., Darmody, G., Lynch, S., Davenport, J., Ramirez-Garcia, S., . . . Sheehan, D. (2015). Neutral red retention time assay in determination of toxicity of nanoparticles. *Marine Environmental Research, 111*, 158-161. doi:https://doi.org/10.1016/j.marenvres.2015.05.007

79. J., D., B., P. P., & W., M. D. J. (2004). Metal-on-metal resurfacing of the hip in patients under the age of 55 years with osteoarthritis. *The Journal of Bone and Joint Surgery. British volume, 86-B*(2), 177-184. doi:10.1302/0301-620x.86b2.14600

80. Jiang, Q., Li, X., Cheng, S., Gu, Y., Chen, G., Shen, Y., . . . Cao, Y. (2016). Combined effects of low levels of palmitate on toxicity of ZnO nanoparticles to THP-1 macrophages. *Environmental Toxicology and Pharmacology, 48*, 103-109. doi:https://doi.org/10.1016/j.etap.2016.10.014

81. Junnila, M., Seppanen, M., Mokka, J., Virolainen, P., Polonen, T., Vahlberg, T., . . . Makela, K. T. (2015). Adverse reaction to metal debris after Birmingham hip resurfacing arthroplasty. *Acta Orthop, 86*(3), 345-350. doi:10.3109/17453674.2014.1004015

82. Karas, S. (2012). Outcomes of birmingham hip resurfacing: a systematic review. *Asian journal of sports medicine, 3*(1), 1-7.

83. Karlsson, H. L., Gustafsson, J., Cronholm, P., & Möller, L. (2009). Size-dependent toxicity of metal oxide particles—a comparison between nano-and micrometer size. *Toxicology letters, 188*(2), 112-118.

84. Kayani, B., Rahman, J., Hanna, S. A., Cannon, S. R., Aston, W. J., & Miles, J. (2012). Delayed sciatic nerve palsy following resurfacing hip arthroplasty caused by metal debris. *BMJ Case Rep, 2012*. doi:10.1136/bcr-2012-006856

85. Ke, Q., & Costa, M. (2006). Hypoxia-inducible factor-1 (HIF-1). *Molecular pharmacology, 70*(5), 1469-1480.

86. Keegan, G., Learmonth, I., & Case, C. (2007). Orthopaedic metals and their potential toxicity in the arthroplasty patient: a review of current knowledge and future strategies. *The Journal of Bone and Joint Surgery. British volume, 89*(5), 567-573.

87. Keegan, G. M., Learmonth, I. D., & Case, C. (2008). A systematic comparison of the actual, potential, and theoretical health effects of cobalt and chromium exposures from industry and surgical implants. *Critical reviews in toxicology, 38*(8), 645-674.

88. Khanna, A. S. (2016). *High Temperature Corrosion*: World Scientific.

89. Kim, K. W., Han, J. W., Cho, H. J., Chang, C. B., Park, J. H., Lee, J. J., . . . Kim, T. K. (2011). Association between comorbid depression and osteoarthritis symptom severity in patients with knee osteoarthritis. *The Journal of Bone & Joint Surgery, 93*(6), 556-563.

90. Kolatat, K., Perino, G., Wilner, G., Kaplowitz, E., Ricciardi, B. F., Boettner, F., . . . Purdue, P. E. (2015). Adverse local tissue reaction (ALTR) associated with corrosion products in metal-on-metal and dual modular neck total hip replacements is associated with upregulation of interferon gamma-mediated chemokine signaling. *Journal of orthopaedic research, 33*(10), 1487-1497.

91. Korovessis, P., Petsinis, G., Repanti, M., & Repantis, T. (2006). Metallosis after contemporary metal-on-metal total hip arthroplasty: five to nine-year follow-up. *JBJS, 88*(6), 1183-1191.

92. Kwon, Y.-M., Ostlere, S. J., McLardy-Smith, P., Athanasou, N. A., Gill, H. S., & Murray, D. W. (2011). "Asymptomatic" pseudotumors after metal-on-metal hip resurfacing arthroplasty: prevalence and metal ion study. *The Journal of arthroplasty, 26*(4), 511-518.

93. Kwon, Y.-M., Xia, Z., Glyn-Jones, S., Beard, D., Gill, H. S., & Murray, D. W. (2009). Dose-dependent cytotoxicity of clinically relevant cobalt nanoparticles and ions on macrophages in vitro. *Biomedical Materials, 4*(2), 025018.

94. Laaksonen, I., Donahue, G. S., Madanat, R., Makela, K. T., & Malchau, H. (2017). Outcomes of the recalled articular surface replacement metal-on-metal hip implant system: a systematic review. *The Journal of arthroplasty, 32*(1), 341-346.

95. Lainiala, O., Eskelinen, A., Elo, P., Puolakka, T., Korhonen, J., & Moilanen, T. (2014). Adverse reaction to metal debris is more common in patients following MoM total hip replacement with a 36 mm femoral head than previously thought: results from a modern MoM follow-up programme. *Bone Joint J, 96-B*(12), 1610-1617. doi:10.1302/0301-620X.96B12.33742

96. Lainiala, O., Eskelinen, A., Elo, P., Puolakka, T., Korhonen, J., & Moilanen, T. (2014). Adverse reaction to metal debris is more common in patients following MoM total hip replacement with a 36 mm femoral head than previously thought: results from a modern MoM follow-up programme. *The bone & joint journal, 96*(12), 1610-1617.

97. Langton, D., Joyce, T., Jameson, S., Lord, J., Van Orsouw, M., Holland, J., . . . De Smet, K. (2011). Adverse reaction to metal debris following hip resurfacing: the influence of component type, orientation and volumetric wear. *The Journal of Bone and Joint Surgery. British volume, 93*(2), 164-171.

98. Langton, D. J., Joyce, T. J., Jameson, S. S., Lord, J., Van Orsouw, M., Holland, J. P., . . . De Smet, K. A. (2011). Adverse reaction to metal debris following hip resurfacing: the influence of component type, orientation and volumetric wear. *J Bone Joint Surg Br, 93*(2), 164-171. doi:10.1302/0301-620X.93B2.25099

99. Laughton, D., Jameson, S., Joyce, T., Natu, S., Logishetty, R., Tulloch, C., & Nargol, A. (2009). *Adverse reactions to metal debris following large bearing metal-on-metal arthroplasty.* Paper presented at the annual scientific meeting British Hip Society, Manchester.

100. Learmonth, I. D., Young, C., & Rorabeck, C. (2007). The operation of the century: total hip replacement. *Lancet, 370*(9597), 1508-1519. doi:S0140-6736(07)60457-7 [pii]

101. Lehil, M. S., & Bozic, K. J. (2014). Trends in total hip arthroplasty implant utilization in the United States. *J Arthroplasty, 29*(10), 1915-1918. doi:10.1016/j.arth.2014.05.017

102. Leonardo, R. A. (1943). *History of surgery*: Froben Press.

103. Liao, Y., Pourzal, R., Wimmer, M., Jacobs, J., Fischer, A., & Marks, L. (2011). Graphitic tribological layers in metal-on-metal hip replacements. *Science, 334*(6063), 1687-1690.

104. Lie, S. A., Engesæter, L. B., Havelin, L. I., Gjessing, H. K., & Vollset, S. E. (2004). Dependency issues in survival analyses of 55 782 primary hip replacements from 47 355 patients. *Statistics in medicine, 23*(20), 3227-3240.

105. Lombardi, A. V., Jr., Barrack, R. L., Berend, K. R., Cuckler, J. M., Jacobs, J. J., Mont, M. A., & Schmalzried, T. P. (2012). The Hip Society: algorithmic approach to diagnosis and management of metal-on-metal arthroplasty. *J Bone Joint Surg Br, 94*(11 Suppl A), 14-18. doi:10.1302/0301-620X.94B11.30680

106. Lombardi, A. V., Jr., Berend, K. R., Morris, M. J., Adams, J. B., & Sneller, M. A. (2015). Large-diameter metal-on-metal total hip arthroplasty: dislocation infrequent but survivorship poor. *Clinical Orthopaedics and Related Research, 473*(2), 509-520. doi:10.1007/s11999-014-3976-0

107. Lombardi, J., AV, Barrack, R., Berend, K., Cuckler, J., Jacobs, J., Mont, M., & Schmalzried, T. (2012). The Hip Society: algorithmic approach to diagnosis and management of metal-on-metal arthroplasty. *The Journal of Bone and Joint Surgery. British volume, 94*(11_Supple_A), 14-18.

108. Long, M., & Rack, H. (1998). Titanium alloys in total joint replacement—a materials science perspective. *Biomaterials, 19*(18), 1621-1639.

109. Lund, M. E., To, J., O'Brien, B. A., & Donnelly, S. (2016). The choice of phorbol 12-myristate 13-acetate differentiation protocol influences the response of THP-1 macrophages to a pro-inflammatory stimulus. *Journal of Immunological Methods, 430*, 64-70. doi:https://doi.org/10.1016/j.jim.2016.01.012

110. Mabilleau, G., Bourdon, S., Joly-Guillou, M., Filmon, R., Baslé, M., & Chappard, D. (2006). Influence of fluoride, hydrogen peroxide and lactic acid on the corrosion resistance of commercially pure titanium. *Acta biomaterialia, 2*(1), 121-129.

111. Mabilleau, G., Kwon, Y.-M., Pandit, H., Murray, D. W., & Sabokbar, A. (2008). Metal-on-metal hip resurfacing arthroplasty: a review of periprosthetic biological reactions. *Acta orthopaedica, 79*(6), 734-747.

112. MacLennan, W. (1999). History of arthritis and bone rarefaction evidence from paleopathology onwards. *Scottish medical journal, 44*(1), 18-20.

113. Mallory, T. H. (2003). Total hip replacement: Google Patents.

114. Mao, X., Tay, G. H., Godbolt, D. B., & Crawford, R. W. (2012). Pseudotumor in a well-fixed metal-on-polyethylene uncemented hip arthroplasty. *The Journal of arthroplasty, 27*(3), 493. e413-493. e417.

115. Matharu, G. S., Mellon, S. J., Murray, D. W., & Pandit, H. G. (2015). Follow-up of metal-on-metal hip arthroplasty patients is currently not evidence based or cost effective. *The Journal of arthroplasty, 30*(8), 1317-1323.

116. Matthies, A. K., Skinner, J. A., Osmani, H., Henckel, J., & Hart, A. J. (2012). Pseudotumors are common in well-positioned low-wearing metal-on-metal hips. *Clinical Orthopaedics and Related Research®, 470*(7), 1895-1906.

117. Mazzoli, A., & Favoni, O. (2012). Particle size, size distribution and morphological evaluation of airborne dust particles of diverse woods by Scanning Electron Microscopy and image processing program. *Powder Technology, 225*, 65-71.

118. McKee, G., & Watson-Farrar, J. (1966). Replacement of arthritic hips by the McKee-Farrar prosthesis. *Journal of Bone & Joint Surgery, British Volume, 48*(2), 245-259.

119. McMinn, D., Daniel, J., Ziaee, H., & Pradhan, C. (2011). Indications and results of hip resurfacing. *International orthopaedics, 35*(2), 231-237.

120. Mediero, A., Ramkhelawon, B., Wilder, T., Purdue, P. E., Goldring, S. R., Dewan, M. Z., . . . Cronstein, B. N. (2015). Netrin-1 is highly expressed and required in inflammatory infiltrates in wear particle-induced osteolysis. *Ann Rheum Dis*, annrheumdis-2015-207593.

121. Mendez, E. P., Lipton, R., Ramsey-Goldman, R., Roettcher, P., Bowyer, S., Dyer, A., & Pachman, L. M. (2003). US incidence of juvenile dermatomyositis, 1995–1998: results from the National Institute of Arthritis and Musculoskeletal and Skin Diseases Registry. *Arthritis Care & Research, 49*(3), 300-305.

122. Mertl, P., Boughebri, O., Havet, E., Triclot, P., Lardanchet, J. F., & Gabrion, A. (2010). Large diameter head metal-on-metal bearings total hip arthroplasty: Preliminary results. *Orthopaedics & Traumatology: Surgery & Research, 96*(1), 14-20. doi:https://doi.org/10.1016/j.otsr.2009.09.013

123. Meyer, H., Mueller, T., Goldau, G., Chamaon, K., Ruetschi, M., & Lohmann, C. H. (2012). Corrosion at the cone/taper interface leads to failure of large-diameter metal-on-metal total hip arthroplasties. *Clinical Orthopaedics and Related Research®, 470*(11), 3101-3108.

124. Middleton, M. (2013). Meet a Fly Girl. *growing bolder*.

125. Milošev, I., Trebše, R., Kovac, S., Cör, A., & Pišot, V. (2006). Survivorship and retrieval analysis of Sikomet metal-on-metal total hip replacements at a mean of seven years. *JBJS, 88*(6), 1173-1182.

126. Mont, M. A., Ragland, P. S., Etienne, G., Seyler, T. M., & Schmalzried, T. P. (2006). Hip resurfacing arthroplasty. *JAAOS-Journal of the American Academy of Orthopaedic Surgeons, 14*(8), 454-463.

127. Moore, A. T., & Bohlman, H. R. (2006). THE CLASSIC: Metal Hip Joint: A Case Report. *Clinical Orthopaedics and Related Research, 453*, 22-24.

128. Munro, J. T., Masri, B. A., Duncan, C. P., & Garbuz, D. S. (2014). High complication rate after revision of large-head metal-on-metal total hip arthroplasty. *Clinical Orthopaedics and Related Research®, 472*(2), 523-528.

129. Munro, J. T., Masri, B. A., Duncan, C. P., & Garbuz, D. S. (2014). High complication rate after revision of large-head metal-on-metal total hip arthroplasty. *Clin Orthop Relat Res, 472*(2), 523-528. doi:10.1007/s11999-013-2979-6

130. Murphy, L., & Helmick, C. G. (2012). The impact of osteoarthritis in the United States: a population-health perspective. *AJN The American Journal of Nursing, 112*(3), S13-S19.

131. Murray, D., Carr, A., & Bulstrode, C. (1993). Survival analysis of joint replacements. *The Journal of Bone and Joint Surgery. British volume, 75*(5), 697-704.

132. Narvani, A., Tsiridis, E., Nwaboku, H., & Bajekal, R. (2006). Sporting activity following Birmingham hip resurfacing. *International journal of sports medicine, 27*(06), 505-507.

133. Nawabi, D. H., Do, H. T., Ruel, A., Lurie, B., Elpers, M. E., Wright, T., . . . Westrich, G. H. (2016). Comprehensive Analysis of a Recalled Modular Total Hip System and Recommendations for Management. *JBJS, 98*(1), 40-47. doi:10.2106/jbjs.n.01121

134. Nüesch, E., Dieppe, P., Reichenbach, S., Williams, S., Iff, S., & Jüni, P. (2011). All cause and disease specific mortality in patients with knee or hip osteoarthritis: population based cohort study. *BMJ, 342*.

135. Oldfield, J. W. (1988). Electrochemical theory of galvanic corrosion *Galvanic Corrosion*: ASTM International.

136. Pabinger, C., & Geissler, A. (2014). Utilization rates of hip arthroplasty in OECD countries. *Osteoarthritis and Cartilage, 22*(6), 734-741. doi:https://doi.org/10.1016/j.joca.2014.04.009

137. Pandit, H., Glyn-Jones, S., McLardy-Smith, P., Gundle, R., Whitwell, D., Gibbons, C.,Murray, D. (2008). Pseudotumours associated with metal-on-metal hip resurfacings. *The Journal of Bone and Joint Surgery. British volume, 90*(7), 847-851.

138. Papageorgiou, I., Brown, C., Schins, R., Singh, S., Newson, R., Davis, S., . . . Case, C. (2007). The effect of nano-and micron-sized particles of cobalt–chromium alloy on human fibroblasts in vitro. *Biomaterials, 28*(19), 2946-2958.

139. Paradowski, P. T., Bergman, S., Sundén-Lundius, A., Lohmander, L. S., & Roos, E. M. (2006). Knee complaints vary with age and gender in the adult population. Population-based reference data for the Knee injury and Osteoarthritis Outcome Score (KOOS). *BMC musculoskeletal disorders, 7*(1), 38.

140. Park, H. (1733). *An account of a new method of treating diseases of the joints of the knee and elbow: in a letter to Mr. Percival Pott*: printed for J. Johnson.

141. Perino, G., Ricciardi, B. F., Jerabek, S. A., Martignoni, G., Wilner, G., Maass, D., . . . Purdue, P. E. (2014). Implant based differences in adverse local tissue reaction in failed total hip arthroplasties: a morphological and immunohistochemical study. *BMC clinical pathology, 14*(1), 39.

142. Rang, M. (1966). Anthology of Orthopaedics E & S Livingstone. *Edinburgh and London*.

143. Reito, A., Puolakka, T., & Pajamäki, J. (2011). Birmingham hip resurfacing: five to eight year results. *International orthopaedics, 35*(8), 1119-1124.

144. Revell, P. A. (2008). The combined role of wear particles, macrophages and lymphocytes in the loosening of total joint prostheses. *Journal of the Royal Society Interface, 5*(28), 1263.

145. Revie, R. W. (2008). *Corrosion and corrosion control*: John Wiley & Sons.

146. Ricciardi, B. F., Nocon, A. A., Jerabek, S. A., Wilner, G., Kaplowitz, E., Goldring, S. R., . . . Perino, G. (2016). Histopathological characterization of corrosion product associated adverse local tissue reaction in hip implants: a study of 285 cases. *BMC clinical pathology, 16*(1), 3.

147. Ring, P. (1971). Replacement of the hip joint. *Annals of the Royal College of Surgeons of England, 48*(6), 344.

148. Rogers, J., Watt, I., & Dieppe, P. (1981). Medical History: Arthritis in Saxon and mediaeval skeletons. *BMJ, 283*(6307), 1668-1670.

149. Rouder, J. N., Speckman, P. L., Sun, D., Morey, R. D., & Iverson, G. (2009). Bayesian t tests for accepting and rejecting the null hypothesis. *Psychonomic bulletin & review, 16*(2), 225-237.

150. Saini, Y., Greenwood, K. K., Merrill, C., Kim, K. Y., Patial, S., Parameswaran, N., . . . LaPres, J. J. (2010). Acute cobalt-induced lung injury and the role of hypoxia-inducible factor 1α in modulating inflammation. *Toxicological sciences, 116*(2), 673-681.

151. Samelko, L., Caicedo, M. S., Lim, S. J., Della-Valle, C., Jacobs, J., & Hallab, N. J. (2013). Cobalt-alloy implant debris induce HIF-1alpha hypoxia associated responses: a mechanism for metal-specific orthopedic implant failure. *PLoS One, 8*(6), e67127. doi:10.1371/journal.pone.0067127

152. Sansone, V., Pagani, D., & Melato, M. (2013). The effects on bone cells of metal ions released from orthopaedic implants. A review. *Clinical cases in mineral and bone metabolism, 10*(1), 34-40.

153. Savarino, L., Granchi, D., Ciapetti, G., Cenni, E., Nardi Pantoli, A., Rotini, R., . . . Giunti, A. (2002). Ion release in patients with metal-on-metal hip bearings in total joint replacement: A comparison with metal-on-polyethylene bearings. *Journal of Biomedical Materials Research: An Official Journal of The Society for Biomaterials, The Japanese Society for Biomaterials, and The Australian Society for Biomaterials and the Korean Society for Biomaterials, 63*(5), 467-474.

154. Schätzle, M., Männchen, R., Zwahlen, M., & Lang, N. P. (2009). Survival and failure rates of orthodontic temporary anchorage devices: a systematic review. *Clinical oral implants research, 20*(12), 1351-1359.

155. Scully, W. F., & Teeny, S. M. (2013). Pseudotumor associated with metal-on-polyethylene total hip arthroplasty. *Orthopedics, 36*(5), e666-e670.

156. Seppänen, M., Laaksonen, I., Pulkkinen, P., Eskelinen, A., Puhto, A.-P., Kettunen, J., . . . Mäkelä, K. (2018). High Revision Rate for Large-head Metal-on-metal THA at a Mean of 7.1 Years: A Registry Study. *Clinical Orthopaedics and Related Research®, 476*(6), 1223-1230. doi:10.1007/s11999.0000000000000159

157. Seth, R., Yang, S., Choi, S., Sabean, M., & Roberts, E. (2004). In vitro assessment of copper-induced toxicity in the human hepatoma line, Hep G2. *Toxicology in Vitro, 18*(4), 501-509.

158. Shahrdar, C., Campbell, P., Mirra, J., & Dorr, L. D. (2006). Painful metal-on-metal total hip arthroplasty. *The Journal of arthroplasty, 21*(2), 289-293.

159. Shimmin, A., Beaulé, P. E., & Campbell, P. (2008). Metal-on-Metal Hip Resurfacing Arthroplasty. *JBJS, 90*(3), 637-654. doi:10.2106/jbjs.g.01012

160. Sieber, H.-P., Rieker, C., & Köttig, P. (1999). Analysis of 118 second-generation metal-on-metal retrieved hip implants. *The Journal of Bone and Joint Surgery. British volume, 81*(1), 46-50.

161. Simonsen, L. O., Harbak, H., & Bennekou, P. (2012). Cobalt metabolism and toxicology--a brief update. *Sci Total Environ, 432*, 210-215. doi:10.1016/j.scitotenv.2012.06.009

162. Simonsen, L. O., Harbak, H., & Bennekou, P. (2012). Cobalt metabolism and toxicology—a brief update. *Science of the Total Environment, 432*, 210-215.

163. Singh, R., & Dahotre, N. B. (2007). Corrosion degradation and prevention by surface modification of biometallic materials. *Journal of Materials Science: Materials in Medicine, 18*(5), 725-751. doi:10.1007/s10856-006-0016-y

164. Smith, A. J., Dieppe, P., Vernon, K., Porter, M., & Blom, A. W. (2012). Failure rates of stemmed metal-on-metal hip replacements: analysis of data from the National Joint Registry of England and Wales. *The Lancet, 379*(9822), 1199-1204. doi:https://doi.org/10.1016/S0140-6736(12)60353-5

165. Stanley, P. (2003). *For fear of pain, British surgery, 1790-1850* (Vol. 70): Rodopi.

166. Suketa, N., Sawase, T., Kitaura, H., Naito, M., Baba, K., Nakayama, K., . . . Atsuta, M. (2005). An antibacterial surface on dental implants, based on the photocatalytic bactericidal effect. *Clinical implant dentistry and related research, 7*(2), 105-111.

167. THe surgical clinics of john b. murphy, m.d., at mercy hospital, chicago. (1912). *Journal of the American Medical Association, LVIII*(8), 584-584. doi:10.1001/jama.1912.04260020268038

168. Tamaki, Y., Goto, T., Tsutsui, T., Takasago, T., Wada, K., & Sairyo, K. (2017). Compression of the Femoral Vessels by a Pseudotumor after Metal-on-Metal Total Hip Arthroplasty. *Case reports in orthopedics, 2017*.

169. Teo, W. Z. W., & Schalock, P. C. (2016). Metal Hypersensitivity Reactions to Orthopedic Implants. *Dermatology and therapy, 7*(1), 53-64. doi:10.1007/s13555-016-0162-1

170. Tharani, R., Dorey, F. J., & Schmalzried, T. P. (2001). The risk of cancer following total hip or knee arthroplasty. *JBJS, 83*(5), 774-780.

171. Thomas, D. J. (2017). 3D white light interferometry assessment of robotic laser scalpel assisted surgery to minimise scar tissue formation. *International Journal of Surgery, 38*, 117-118. doi:https://doi.org/10.1016/j.ijsu.2016.12.037

172. Thompson, F. (1952). Vitallium intramedullary hip prosthesis, preliminary report. *New York state journal of medicine, 52*(24), 3011-3020.

173. Thould, A., & Thould, B. (1983). Arthritis in Roman Britain. *BMJ, 287*(6409), 1909-1911.

174. Tibor, L. M., & Ganz, R. (2015). Hip Osteoarthritis: Definition and Etiology Osteoarthritis Hip OA See Osteoarthritis *Hip Arthroscopy and Hip Joint Preservation Surgery* (pp. 177-188): Springer.

175. Toms, A. P., Marshall, T. J., Cahir, J., Darrah, C., Nolan, J., Donell, S. T., . . . Tucker, J. K. (2008). MRI of early symptomatic metal-on-metal total hip arthroplasty: a retrospective review of radiological findings in 20 hips. *Clinical Radiology, 63*(1), 49-58. doi:https://doi.org/10.1016/j.crad.2007.07.012

176. Tortorella, M. D., & Malfait, A. M. (2003). The usual suspects: verdict not guilty? *Arthritis & Rheumatism, 48*(12), 3304-3307.

177. Traina, F., Fine, M. D., Tassinari, E., Sudanese, A., Calderoni, P. P., & Toni, A. (2011). Modular neck prostheses in DDH patients: 11-year results. *Journal of Orthopaedic Science, 16*(1), 14-20. doi:https://doi.org/10.1007/s00776-010-0018-y

178. Trinkaus, E. (1985). Pathology and the posture of the La Chapelle-aux-Saints Neandertal. *American journal of physical anthropology, 67*(1), 19-41.

179. Tsuchiya, S., Yamabe, M., Yamaguchi, Y., Kobayashi, Y., Konno, T., & Tada, K. (1980). Establishment and characterization of a human acute monocytic leukemia cell line (THP-1). *International journal of cancer, 26*(2), 171-176.

180. UK, Arthritis Research. (2013). Osteoarthritis in general practice-data and perspectives. https://www.arthritisresearchuk.org/~/media/Files/Policy%20files/Policy%20pages%20files/Osteoarthritis%20in%20general%20practice%20%20July%202013%20%20Arthritis%20Research%20UK%20PDF%20421%20MB.ashx.

181. Urban, R. M., Jacobs, J. J., Tomlinson, M. J., Gavrilovic, J., Black, J., & Peoc'h, M. (2000). Dissemination of wear particles to the liver, spleen, and abdominal lymph nodes of patients with hip or knee replacement. *JBJS, 82*(4), 457-477.

182. van Dijk, J. D., Groothuis-Oudshoorn, C. G., Marshall, D. A., & IJzerman, M. J. (2016). An empirical comparison of discrete choice experiment and best-worst scaling to estimate stakeholders' risk tolerance for hip replacement surgery. *Value in health, 19*(4), 316-322.

183. Vengellur, A., & LaPres, J. (2004). The role of hypoxia inducible factor 1α in cobalt chloride induced cell death in mouse embryonic fibroblasts. *Toxicological Sciences, 82*(2), 638-646.

184. Vengellur, A., & LaPres, J. J. (2004). The role of hypoxia inducible factor 1alpha in cobalt chloride induced cell death in mouse embryonic fibroblasts. *Toxicol Sci, 82*(2), 638-646. doi:10.1093/toxsci/kfh278

185. Videla, H., & Herrera, L. (2004). Biocorrosion. *Studies in Surface Science and Catalysis, 151*, 193-218.

186. Visuri, T., Pukkala, E., Paavolainen, P., Pulkkinen, P., & Riska, E. B. (1996). Cancer risk after metal on metal and polyethylene on metal total hip arthroplasty. *Clinical Orthopaedics and Related Research, 329*, S280-S289.

187. Vogel, D. W. T., Steinbach, L. S., Hertel, R., Bernhard, J., Stauffer, E., & Anderson, S. E. (2005). Acromioclavicular joint cyst: nine cases of a pseudotumor of the shoulder. *Skeletal radiology, 34*(5), 260-265.

188. Voggenreiter, G., Leiting, S., Brauer, H., Leiting, P., Majetschak, M., Bardenheuer, M., & Obertacke, U. (2003). Immuno-inflammatory tissue reaction to stainless-steel and titanium plates used for internal fixation of long bones. *Biomaterials,*

24(2), 247-254.

189. Wang, J. Y., Wicklund, B. H., Gustilo, R. B., & Tsukayama, D. T. (1997). Prosthetic metals impair murine immune response and cytokine release in vivo and in vitro. *Journal of orthopaedic research, 15*(5), 688-699.

190. Warchomicka, F., Stockinger, M., & Degischer, H.-P. (2006). Quantitative analysis of the microstructure of near β titanium alloy during compression tests. *Journal of Materials Processing Technology, 177*(1-3), 473-477.

191. Waugh, W. (1990). *John Charnley*: Springer Science & Business Media.

192. Wedemeyer, C., Xu, J., Neuerburg, C., Landgraeber, S., Malyar, N. M., von Knoch, F., . . . Saxler, G. (2007). Particle-induced osteolysis in three-dimensional micro-computed tomography. *Calcified tissue international, 81*(5), 394-402.

193. Wiles, P. (1958). The surgery of the osteo-arthritic hip. *British Journal of Surgery, 45*(193), 488-497.

194. Willert, H.-G., Buchhorn, G. H., Fayyazi, A., Flury, R., Windler, M., Köster, G., & Lohmann, C. H. (2005). Metal-on-metal bearings and hypersensitivity in patients with artificial hip joints: a clinical and histomorphological study. *JBJS, 87*(1), 28-36.

195. Witt, F., Bosker, B., Bishop, N., Ettema, H., Verheyen, C., & Morlock, M. (2014). The relation between titanium taper corrosion and cobalt-chromium bearing wear in large-head metal-on-metal total hip prostheses: a retrieval study. *JBJS, 96*(18), e157.

196. Witzleb, W.-C., Hanisch, U., Kolar, N., Krummenauer, F., & Guenther, K.-P. (2007). Neo-capsule tissue reactions in metal-on-metal hip arthroplasty. *Acta orthopaedica, 78*(2), 211-220.

197. Wyles, C. C., Van Demark, R. E., 3rd, Sierra, R. J., & Trousdale, R. T. (2014). High rate of infection after aseptic revision of failed metal-on-metal total hip arthroplasty. *Clin Orthop Relat Res, 472*(2), 509-516. doi:10.1007/s11999-013-3157-6

198. Xia, Z., Kwon, Y.-M., Mehmood, S., Downing, C., Jurkschat, K., & Murray, D. W. (2011). Characterization of metal-wear nanoparticles in pseudotumor following metal-on-metal hip resurfacing. *Nanomedicine: Nanotechnology, Biology and Medicine, 7*(6), 674-681.

199. Xia, Z., Kwon, Y. M., Mehmood, S., Downing, C., Jurkschat, K., & Murray, D. W. (2011). Characterization of metal-wear nanoparticles in pseudotumor following metal-on-metal hip resurfacing. *Nanomedicine, 7*(6), 674-681. doi:10.1016/j.nano.2011.08.002

200. Xia, Z., Ricciardi, B. F., Liu, Z., von Ruhland, C., Ward, M., Lord, A., . . . Murray, D. (2017). Nano-analyses of wear particles from metal-on-metal and non-metal-on-metal dual modular neck hip arthroplasty. *Nanomedicine: Nanotechnology, Biology and Medicine, 13*(3), 1205-1217.

201. Xia, Z., & Triffitt, J. T. (2006). A review on macrophage responses to biomaterials. *Biomedical Materials, 1*(1), R1.

202. Ziaee, H., Daniel, J., Datta, A., Blunt, S., & McMinn, D. (2007). Transplacental transfer of cobalt and chromium in patients with metal-on-metal hip arthroplasty: a controlled study. *The Journal of Bone and Joint Surgery. British volume, 89*(3), 301-305.

203. Ziello, J. E., Jovin, I. S., & Huang, Y. (2007). Hypoxia-Inducible Factor (HIF)-1 regulatory pathway and its potential for therapeutic intervention in malignancy and ischemia. *The Yale journal of biology and medicine, 80*(2), 51.

Appendix 1 Publications and Conference Proceedings

Publications

Nano-analyses of wear particles from metal-on-metal and non-metal-on-metal dual modular neck hip arthroplasty

Z. Xia, B.F. Ricciardi, Z. Liu, C.V. Ruhland, M. Ward, A. Lord, L. Hughes, S. R. Golding, E. Purdue, D. Murray, G. Perino.
Nanomedicine: Nanotechnology, Biology and Medicine. 2017 13(3) 1205-1217

The role of Hypoxia Inducible Factor 1α in Cobalt Nanoparticle induced cytotoxicity of human THP-1 macrophages

W.R. Francis, X. Wang, Z. Liu, S.E. Owens, H. Intabli, A. Lord, V. Kanamarlapudi, H. Xue, Z. Xia
Manuscript in preparation

Conference Proceedings

Nano-analytic Characterisation of Co/Cr Nanoparticles Retrieved from Metal-on-metal Total Hip-replacement

Z. Liu
Oral Presentation, *Post Graduate Research Students Bi-Annual Conference, Swansea University. 12th December 2016*

TEM Image Analysis with 'Image J' (Image Processing and Analysis in Java)

Z. Liu, Z. Xia
Oral Presentation, *Scientia Research Group, Swansea University, 12th June 2015*

Nano-analytic Characterisation of Tissue Morphology Particles Retrieved from Total Hip-replacement

Z. Liu
Oral Presentation, *Scientia Research Group, Swansea University, 15th April 2016*

Appendix 2: Suppliers of Materials

Araldite 2-Tubes Standard Epoxy	Zoro, ARA-400003, UK
Bicinchoninic Acid Kit	Sigma Aldrich, BCA1-1KT, UK
Carbon Steel Surgical Blade	Zoro, ZT1197217X, UK
Foetal Bovine Serum	Labtech International, UK
Hexamethyldisilazane	Fluka, 52619, UK
Glutaraldehyde Solution	Fisher Scientific BP2548-1, USA
Lipofectamine RNAiMax Transfection Reagent	Invitrogen™ life Technologies, UK
Metal Nanoparticles (Co, Cr, Ti)	American Elements, Merelex Corp, Los Angeles, USA
Neutral Red Solution 0.33% in DPBS	Sigma-Aldrich, N-2889, UK
Neutral Red Assay Solubilization Solution	Sigma-Aldrich, N-4395, UK
Opti-MEM	Gibco BRL, Invitrogen Ltd, Paisley, UK
PBS pH7.4 (1X)	Thermo Fisher, 10010023, UK
PMA	Sigma Aldrich, 79346, UK
Penicillin / Streptomycin	Gibco, BRL, Invitrogen Ltd, Paisley, UK
RPMI medium 1640 (1X) + L-glutamine	Thermo Fisher, 11875093, UK
Silencer® Select siRNA	Applied Biosystems, Ambion, UK
Stainless Steel AISI 316 Foil	Advent Research Materials, FE694608,

	UK
THP-1 Cell Line	Sigma Aldrich, 88081201, UK
Titanium Foil 99.6+%	Advent Research Materials, TI228717, UK
Triton X100	Sigma Aldrich, 9002-93-1, UK
3M PTFE Film Tape	3M™ Science, 5490, UK
3MM Biopsy Punch	Thermo Fisher Scientific, 12460406, UK
Greiner CELLSTAR® 6-Well Cell Culture Plate	Greiner CELLSTAR, M8562-100EA, UK
Greiner CELLSTAR® 24-Well Cell Culture Plate	Greiner CELLSTAR, M8812-100EA, UK
Greiner CELLSTAR® 48-Well Cell Culture Plate	Greiner CELLSTAR, M8937-100EA, UK
Greiner CELLSTAR® 96-Well Cell Culture Plate	Greiner CELLSTAR, M0812-100EA, UK

Appendix 3: Preparation of Metal Nanoparticles Stock Solutions

Prepare a $1x10^{13}$ particles/ml stock concentration of metal nanoparticles:

i. Cobalt Nanoparticles

Density = 8900 kg/m^3 = mass in kg/volume in m^3

Mass of 1 particle = densityxvolume of 1 particle

Assume a metal nanoparticle as a sphere:

Volume of 1 particle = $4/3 \times \pi \times r^3$

Average particles diameter = 28nm, radius (r) = 14nm

Thus, volume of 1 particle (nm^3) = 11494.04

Mass of 1 particle (mg) = [8.90×10^9 mg / $1 \times 10^{27} nm^3$]x11494.04 nm^2

= 102296.96x10-18 = 1.02×10^{-13} mg

Therefore, mass of particles (mg)/ml = number of particle required/ml

$\times 1.02 \times 10^{-13}$ mg

Thus, 1×10^{13} particles/ml = 1.02 mg/ml

ii. Chromium Nanoparticles

Density = 7140 kg/m^3

Average particles diameter =30 nm, radius (r) = 15nm

Volume of 1 particle (nm^3) = 14137.16

Therefore, mass of 1 particle (mg) = [7.14×10^9 mg / $1 \times 10^{27} nm^3$] x 14137.16 nm^2

= $100939.32 \times 10^{-18} = 1.10 \times 10^{-13}$ mg

Thus, 1×10^{13} particles/ml = 1.1 mg/ml

iii. Titanium Nanoparticles

Density = 4507 kg/m^3

Average particles diameter =35 nm, radius (r) = 17.5 nm

Volume of 1 particle (nm^3) = 22449.30

Therefore, mass of 1 particle (mg) = [4.51×10^9 mg / $1 \times 10^{27} nm^3$] x 2249.30 nm^2

$= 101246.34 \times 10^{-18} = 1.10 \times 10^{-13}$ mg

Thus, $1x10^{13}$ particles/ml = 1.01 mg/ml

Appendix 4: Part of Selected TEM Images for Particles Analysis

Figure 8.1-3 represent parts of TEM Images which have been selected for characterization of nanoparticles and the Feret Ratio distribution of three classes of configuration (MoM HRA, MoM LHTHA and Non-MoM DMNTHA)

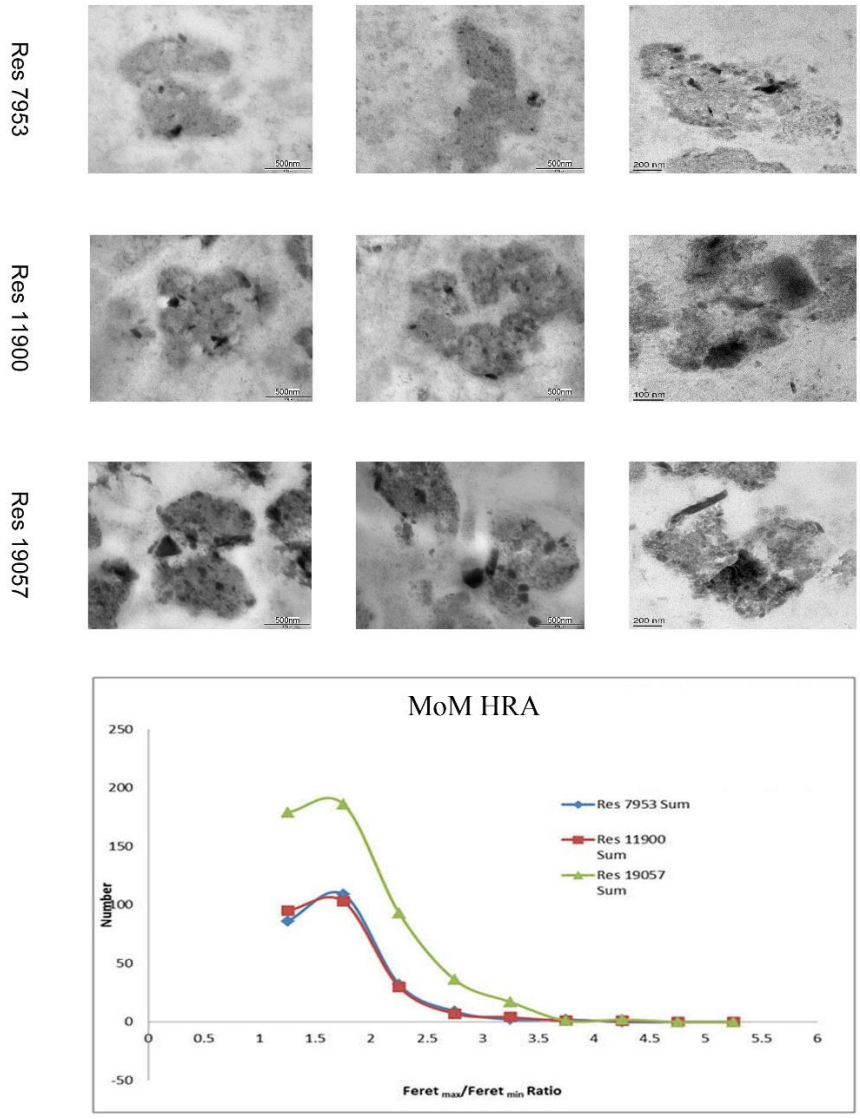

Figure 8.1. The Feret Ratio distribution of Nanoparticles in MoM HRA
The X-axis indicates the values of Feret Ratio ($Feret_{max}/Feret_{min,}$), Y-axis indicates the total number of metal nanoparticles. Three colours were used to distinguish three samples for each hip replacement.

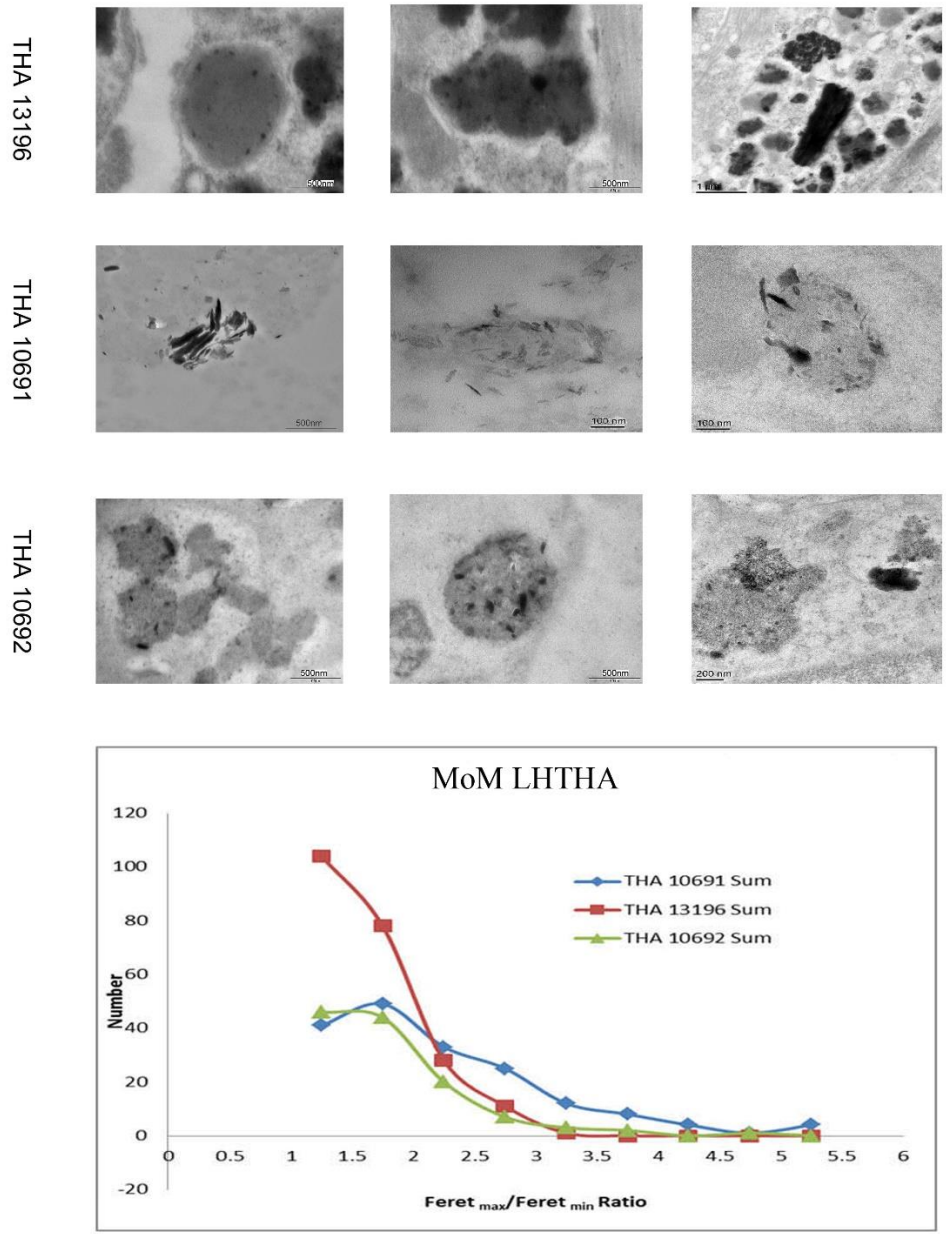

Figure 8.2. The Feret Ratio distribution of Nanoparticles in MoM LHTHA

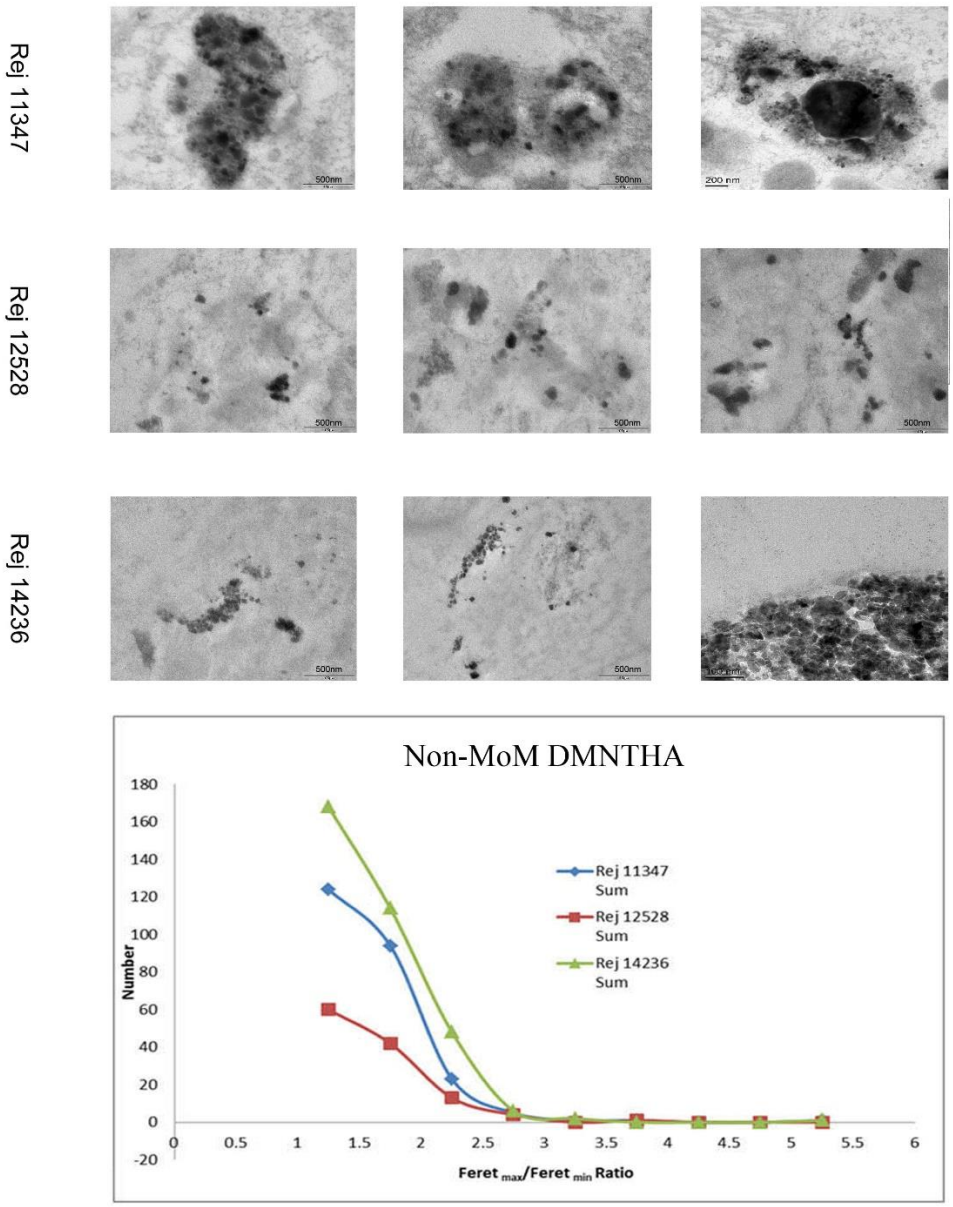

Figure 8.3. The Feret Ratio distribution of nanoparticles in Non-MoM DMNTHA